DISSERTATIONES
MEDICINAE
UNIVERSITATIS
TARTUENSIS
260

ANNE-MARI ANTON WILLMORE

Silver nanoparticles for cancer research

DISSERTATIONES MEDICINAE UNIVERSITATIS TARTUENSIS
260

DISSERTATIONES MEDICINAE UNIVERSITATIS TARTUENSIS
260

ANNE-MARI ANTON WILLMORE

Silver nanoparticles for cancer research

UNIVERSITY OF TARTU
Press

Cancer Biology Research Group, Institute of Biomedicine and Translational Medicine, University of Tartu.

The dissertation is accepted for the commencement of the degree of Doctor of Philosophy in Medicine on September 20, 2017 by the Council of the Faculty of Medicine, University of Tartu, Estonia.

Supervisors:	Professor Tambet Teesalu, PhD Lab of Cancer Biology, Institute of Biomedicine and Translational Medicine, Faculty of Medicine, University of Tartu, Estonia
	Dr. Gary Braun, PhD Cancer Research Center, Sanford-Burnham Medical Research Institute, La Jolla, California and the Center for Nanomedicine and the Department of Chemistry and Biochemistry, University of California, Santa Barbara, California, USA
Reviewers:	Professor Ursel Soomets, PhD Institute of Biomedicine and Translational Medicine, Faculty of Medicine, University of Tartu, Estonia
	Dr. Kaido Kurrikoff, PhD Institute of Technology, Faculty of Science and Technology, University of Tartu, Estonia
Opponent:	Associate Professor Hélder A. Santos, D.Sc. Tech. Drug Research Program, Division of Pharmaceutical Chemistry and Technology, Faculty of Pharmacy and Helsinki Institute of Life Science, University of Helsinki, Finland
Commencement:	November 17, 2017

Publication of this dissertation is granted by the University of Tartu.

ISSN 1024-395X
ISBN 978-9949-77-572-9 (print)
ISBN 978-9949-77-573-6 (pdf)

University of Tartu Press
www.tyk.ee

Contents

List of Original Publications

(I) Braun, G. B., Friman, T., Pang, H.-B., Pallaoro, A., de Mendoza, T. H., **Willmore, A.-M. A.**, Kotamraju, V. R., Mann, A. P., She, Z.-G., Sugahara, K. N., Reich, N. O., Teesalu, T. and Ruoslahti, E. [2014]. Etchable plasmonic nanoparticle probes to image and quantify cellular internalization, *Nature Materials*, **13**(9): 904–911.

(II) **Willmore, A.-M. A.**, Simón Gracia, L., Toome, K., Paiste, P., Kotamraju, V. R., Mölder, T., Sugahara, K. N., Ruoslahti, E., Braun, G. B. and Teesalu, T. [2016]. Targeted silver nanoparticles for ratiometric cell phenotyping, *Nanoscale* **8**: 9096–9101.

(III) Toome, K., **Willmore, A.-M. A.**, Paiste, P., Tobi, A., Sugahara, K. N., Kirsimäe, K., Ruoslahti, E., Braun, G. B. and Teesalu, T. [2017]. Ratiometric in vivo auditioning of targeted silver nanoparticles, *Nanoscale* **9**: 10094–10100.

(IV) Ikemoto, H., Lingasamy, P., **Willmore, A.-M. A.**, Hunt, H., Kurm, K., Tammik, O., Scodeller, P., Simón Gracia, L., Kotamraju, V. R., Lowy, A. M., Sugahara, K. N. and Teesalu, T. [2017]. Hyaluronan-binding peptide for targeting peritoneal carcinomatosis, *Tumor biology* **39**(5).

My contribution to the above papers is as follows:

Paper I: synthesized and functionalized nanoparticles, performed experiments.

Paper II: synthesized and functionalized nanoparticles, performed most of the experiments, developed analytical methods, conducted data analysis, wrote most of the paper.

Paper III: synthesized and functionalized nanoparticles, performed experiments, developed methods, conducted data analysis.

Paper IV: synthesized and functionalized nanoparticles, performed experiments.

Other publications:

(V) Simón Gracia, L., Hunt, H., Scodeller, P. D., Gaitzsch, J., Braun, G. B., **Willmore, A.-M. A.**, Ruoslahti, E., Battaglia, G. and Teesalu, T. [2016]. Paclitaxel-loaded polymersomes for enhanced intraperitoneal chemotherapy, *Molecular Cancer Therapeutics* **15**(4): 670–679.

Abbreviations

AgNP	silver nanoparticle
B /biot	biotin
CendR	C -end Rule
EPR	enhanced permeability and retention
HA	hyaluronic acid
ICP-MS	inductively coupled plasma mass spectrometry
IONW	iron oxide nanoworms
IP3	peptide sequence [CKRDLSRRC]
iRGD	peptide sequence [CRGDKGPDC]
K	peptide sequence [SGKRK]
FAM	fluorescein fluorescent dye
Lyp-1	peptide sequence [CGNKRTRGC]
MPS	mononuclear phagocyte system
NA	neutravidin
NP	nanoparticle
NRP-1	neuropilin-1
p32	protein p32
PEG	polyethylene glycol
PVP	polyvinylpyrrolidone
RPAR /R	peptide sequence [RPARPAR]
TEM	transmission electron microscopy

1. Introduction

Peptides show promise as tumor affinity targeting agents due to their specificity as well as small size enabling tissue penetration and the possibility for large scale production [Liu et al., 2017]. Peptide phage display, where multiple copies of a peptide are displayed on a bacteriophage surface, is used to screen for tumor homing peptides [Pasqualini and Ruoslahti, 1996]. This method uncovers peptides that home to tumor blood vessels. Knowing what receptors are available through systemic circulation is clinically relevant since all chemotherapeutics are currently administered intravenously. In finding new peptides, it is important to know which peptides can bind cells and get into cells for therapeutic effect on the *in vitro* level as well as which peptides can home to tumors and penetrate deeper into tumors for anti-cancer activity. Nanoparticles (NPs) provide many advantages for understanding these mechanisms.

Nanoparticle cancer therapeutics such as Doxil™ [*Doxil website*, 2017] and Abraxane™ [*Abraxane website*, 2017] are already in clinical use. These drugs use established chemotherapeutics and formulate them as a liposomal or albumin nanoparticle, respectively. The NPs have longer blood half-lives than free drug and accumulate at tumor sites owing to aberrant tumor vasculature [Matsumura and Maeda, 1986], even without targeting ligands, thus reducing systemic toxicity [Green et al., 2006, O'Brien et al., 2004]. The natural next step towards nanoparticle therapy is to improve this system further by active targeting. Indeed many targeted nanotherapeutics are in clinical trials for breast, prostate, and gastric cancer as well as solid tumors [Shi et al., 2017]. Phage display discovery of peptides is particularly well suited for the discovery of NP targeting ligands since the phages are themselves biological nanoparticles. When the peptides are coated onto synthetic nanoparticles they take advantage of the NPs' characteristics as well. NPs can carry multiple copies of targeting ligands, enabling multivalent, higher avidity, activity. They can comprise not only targeting ligands and drugs, but also tracking features like fluorescent dyes or isotopic markers.

The work presented in this thesis describes the development of a silver nanoparticle (AgNP) platform as a research tool in studying cancer. Phage display homing peptides can be tested for *in vitro* binding and *in vivo* targeting by coupling to the readily trackable AgNPs. AgNPs can enhance fluorescent dyes that are attached to them, and be visualized by silver enhancement and microscopy in histological sections. Exposed AgNPs can be dissolved in a biocompatible way to enable distinction between extracellular and internalized particles. They can be used in dye-free assays due to their high extinction coefficients and isotopic labeling.

Isotopic multiplexing allows for the quantification of more than one AgNP type at a time by mass spectrometry from cell or tissue lysate and spatial analysis of tissue sections. As opposed to optical techniques, this provides a critical tool for evaluating peptide efficacy in an internally controlled and quantitative manner.

2. Literature Review

2.1 Nanoparticles in cancer treatment

The first nanoparticle formulation for cancer treatment, Doxil™, was approved by the FDA in 1995 [Shi et al., 2017]. The nanoformulation took the chemotherapeutic doxorubicin and encapsulated it inside a polyethylene glycol-coated (PEGylated) liposome. This change in formulation reduced cardiotoxicity without impacting efficacy and increased circulation time and accumulation of drug at the cancer site [Gabizon et al., 1994, O'Brien et al., 2004]. The next big development in cancer nanomedicine was the approval of Abraxane™ ten years later. This albumin bound nanoformulation of paclitaxel, made it possible to avoid the toxic cremophor oil that is normally used to solubilize the drug, resulting in improved patient tolerance and better therapeutic index for the drug [Gradishar et al., 2005 Green et al., 2006]. Despite the high hopes for NP cancer therapeutics, they have yet to fully deliver. A recent meta-analysis of clinical studies revealed that liposomal chemotherapeutic formulations have not been able to increase overall survival in patients *versus* standard treatment [Petersen et al., 2016]. The number of approved NP cancer drugs remains low, although over 30 are undergoing clinical trials. The primary focus is on liposome-based formulations, although polymer and metal nanoparticles, especially for heat activated treatment, are also being tested. There is a growing interest in treatments based on gene therapy or RNA interference as well as immunomodulatory treatments [Shi et al., 2017].

2.1.1 Passive targeting

Current clinically approved nanotherapeutics are all intravenously administered and untargeted. If NPs have no targeting ligands, *e.g.* antibodies or peptides, then the main mode by which they reach the tumor is the so called enhanced permeability and retention effect (EPR) [Matsumura and Maeda, 1986]. EPR describes the passive targeting that allows nanoparticles to accumulate at tumor sites due to tumors' faulty vasculature: leaky, tortuous, and with poor lymphatics [Ruoslahti, 2002]. The concept of EPR has gained greater attention as a focus of research. EPR is not universal, and with great heterogeneity existing in tumors, different individuals will experience varying levels of this effect leading to uneven success of treatment. First assessing how well EPR works in a particular patient, *e.g.* with imaging NPs such as iron oxide particles, can help predict how well untargeted NP-chemotherapeutics will perform [Ramanathan et al., 2014].

Another option is to pre-screen patients for blood markers known to affect EPR [Yokoi et al., 2014]. Theranostic nanoparticles, that encompass both treatment and diagnostic characteristics, are another possible tool to assess treatment effectiveness in real time [Choi et al., 2012]. However, theranostic particles involve added complexity in manufacturing and regulatory approval.

2.1.2 NP characteristics

Aside from targeting ligands, nanoparticle characteristics such as size, shape, charge, surface coating, and rigidity determine NP uptake by tumors and by the rest of the organism [Albanese et al., 2012]. Very small NPs, ∼5 nm, will be cleared quickly by the kidneys, whereas large NPs will not be able to penetrate tissues effectively [Longmire et al., 2008]. NP shape has a large impact on how particles behave, for example rod- or worm-shaped particles adhere better to endothelial cells and home better to tumors than equivalent spherical particles [Chauhan et al., 2011, Park et al., 2008].

2.1.3 Protein corona

When a nanoparticle enters a biological environment it develops a coating of proteins called a corona [Lynch and Dawson, 2008]. Therefore the NP that interacts with the organism *in vivo* is not the same exact particle as that which was first injected. This protein binding can take the form of opsonization, which marks the NPs for removal by the mononuclear phagocyte system (MPS) [Mahmoudi et al., 2011]. Not all corona building is necessarily negative. Peptides with a free cysteine can piggy-back on albumin molecules, thus increasing their circulation time and improving tumor homing [Pang et al., 2014a]; the same principle may apply to NPs.

2.1.4 Stealth NPs

Often nanoparticles are preferred to be as “stealth" as possible, that is not recognized by the immune system. The standard way this is done is by covering the nanoparticle in PEG molecules [van Vlerken et al., 2007]. PEGs are hydrophilic, chemically inert, do not participate in electrostatic interactions, and also sterically hinder the binding of opsonin proteins. PEGylation reduces clearance by the MPS and increases circulation time [van Vlerken et al., 2007]. PEGylation can be optimized for many parameters including the molecular weight of PEG, terminal groups, and packing density. Whether the polymer is sparsely packed on a surface and assumes a coiled, mushroom configuration or is tightly packed, and stretched out in a brush configuration, will impact particle behavior [Jokerst et al., 2011]. While PEG is clinically approved and generally regarded as non-immunogenic, it is possible to develop anti-PEG antibodies [Garay et al., 2012]. Other strategies

for stealth particles include: labeling NPs with "self markers and coating NPs in cell membranes of erythrocytes or leukocytes [Hu et al., 2011, Parodi et al., 2013].

2.1.5 Active targeting

Therapeutic nanoparticles that incorporate targeting ligands on their surface have yet to be clinically approved. The four NPs that are currently in clinical trials are lipid or polymer-based NPs with encapsulated chemotherapeutic that are coated with affinity ligands recognizing human epidermal growth factor receptor 2 (HER2), prostate-specific membrane antigen (PSMA), epidermal growth factor receptor (EGFR), or transferrin receptor (TfR) [Shi et al., 2017]. In mouse tumor models there are many successful examples of peptide-targeted NPs including iron oxide nanoworms (IONW) [Agemy et al., 2011, 2013, Hunt et al., 2017, Sugahara et al., 2009], spherical iron oxide particles [Simberg et al., 2007], and polymersomes [Simón Gracia et al., 2016b].

2.2 Tumor homing peptide discovery

2.2.1 Vascular ZIP codes

One way to discover targeting ligands, homing peptides, is through *in vivo* phage display. This technique relies on the variations in blood vessels depending on their state. Endothelial cells that line the vessels have different molecular structures and systemically accessible molecular landscape based on their location. Such molecular variability in vasculature also exists as part of disease presence or absence. These molecular markers, or ZIP codes, can be taken advantage of to target specific tissues or pathologies. Tumor vasculature will display different ZIP codes from healthy vasculature [Ruoslahti, 2004, Teesalu et al., 2012]. Using *in vivo* phage display to target these ZIP codes, homing peptides have been found for normal brain [Fan et al., 2007], heart [Teesalu et al., 2009, Zhang et al., 2005], lung [Brown and Ruoslahti, 2004, Teesalu et al., 2009], prostate [Arap et al., 2002], angiogenic vessels [Arap et al., 1998, Simberg et al., 2007], blood clots [Pilch et al., 2006], and for various tumors [Hoffman et al., 2003, Laakkonen et al., 2002, Sugahara et al., 2009, Zhang et al., 2006] to name some examples.

2.2.2 Phage display

Phage display involves using a bacteriophage, *e.g.* T7 coliphage, that displays engineered peptides on its coat protein. Bacteriophages are viruses that infect bacteria. They use the bacteria's cellular machinery to replicate themselves and in so doing also replicate the recombinant DNA they carry. For phage display the phages' DNA has been modified to add a random peptide genetically tuned to its

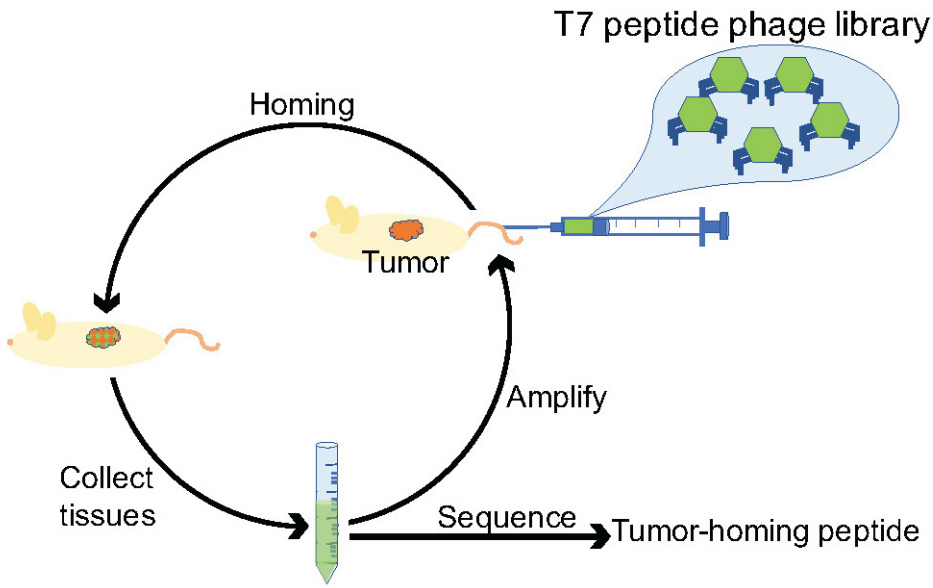

FIGURE 1: Schematic of *in vivo* phage display biopanning. A phage library is injected into circulation. As a result of specific interactions of some displayed peptides with the signature molecules expressed on the blood vessels, some phages will home to the target, *e.g.* tumor. The target organ or tumor is isolated and homogenized and the bound phage pool is amplified and injected again for another round of selection. After several rounds of biopanning, the peptide-encoding region of the phage genome is sequenced and enriched peptides are identified and analyzed.

coat protein. The diversity of such peptide-phage libraries can be enormous, in the billions. The phages that are recovered from a target tissue, are rescued by replication in fresh bacterial culture. Thus homing phages are amplified and non-homing phages are removed. During peptide phage biopanning there is a balance to be found between stringency and yield. Stringency sets higher standards for which peptides are good enough homers or target binders. However, if conditions are too stringent then good peptide-phages might be left out as overall yield of phages is too low [Smith and Petrenko, 1997].

In vivo phage display [Pasqualini and Ruoslahti, 1996] uses the vast number of peptides that can be tested on phage particles to find homing peptides to biological targets like tumors. The phages are injected into systemic circulation and, after some time, target organs, control organs, and tumors are collected (Figure 1). The tissues are homogenized and the bound phages are either sequenced immediately or amplified and applied to another round of selection. Phage display has been used to find many homing peptides, see Table 1 for examples.

TABLE 1: Homing peptides and their targets. Some listed peptides have a cryptic CendR motif (see Section 2.2.4.3): they initially bind to one receptor and after proteolytic cleavage develop an a nity for NRP-1. This dual binding is designated with (receptor/NRP-1). Adapted from [Teesalu et al., 2012].

	Sequence (Abbrev.)	***In vivo* target site (Receptor, if known)**	**Reference**
1	AKRGARSTA (linTT1)	Peritoneal carcinomatosis (p32/NRP-1)	[Hunt et al., 2017]
2	CKRGARSTC (TT1)	Breast tumors (p32/NRP-1)	[Paasonen et al., 2016]
3	RPARSGRSAGGSVA (uCendR)	Breast tumors (NRP-1)	[Braun et al., 2016]
4	CNGRC (NGR)	Angiogenic vessels (CD13)	[Arap et al., 1998]
5	CRNGRGPDC (iNGR)	Breast tumors (CD13/NRP-1)	[Alberici et al., 2013]
6	CAQK	Brain injury (proteoglycan complex)	[Mann et al., 2016]
7	RPARPAR	Prototypic CendR peptide Heart, lung (NRP-1)	[Teesalu et al., 2009]
8	CRGDKGPDC (iRGD)	Different tumors prototypic tissue-penetrating peptide ($\alpha v\beta_{3/5}$ integrins/NRP-1)	[Sugahara et al., 2009]
9	CAGALCY	Brain microvessels	[Fan et al., 2007]
10	CGKRK	Squamos cell carcinoma (p32, calreticulin)	[Hoffman et al., 2003]
11	gSMSIARL	Normal prostate	[Arap et al., 2002]
12	gVSFLEYR	Normal prostate	[Arap et al., 2002]
13	CREAGRKAC	TRAMP[0] lymphatics	[Zhang et al., 2006]
14	CAGRRSAYC	TRAMP premalignant lymphatics	[Zhang et al., 2006]
15	CRAKSKVAC	Pan-endothelial homer	[Zhang et al., 2006]
16	CRRETAWAC	($\alpha_5\beta_1$ integrins)	[Koivunen et al., 1994]
17	CRPPR	Heart (NRP-1)	[Zhang et al., 2005]
18	CGLIIQKNEC (CLT1)	Blood clot	[Pilch et al., 2006]
19	CNAGESSKNC (CLT2)	Blood clot	[Pilch et al., 2006]
20	CARSKNKDC (CAR)	Wound (heparan sulfate proteoglycans)	[Järvinen and Ruoslahti, 2007]
21	CRKDKC (CRK)	Wound	[Järvinen and Ruoslahti, 2007]

[0]TRAMP = transgenic adenocarcinoma of the mouse prostate

	Sequence (Abbrev.)	***In vivo* target site (Receptor, if known)**	**Reference**
22	GLNGLSSADPSSD WNAPAEEWGNW VDEDRASLLKSQE PISNDQKVSDDDK EKGEGALPTGKSK	Lung homing domain of metadherin	[Brown and Ruoslahti, 2004]
23	CGNKRTRGC (LyP-1)	Tumor lymphatics, tumor macrophages, and tumor cells in hypoxic areas (p32/NRP-1)	[Laakkonen et al., 2002]
24	CREKA	Angiogenic vessels (fibrin clots)	[Simberg et al., 2007]
25	CTTHWGFTLC	Angiogenic vessels (gelatinases A and B)	[Koivunen et al., 1999]
26	CSRPRRSEC	Dysplastic skin	[Hoffman et al., 2003]
27	CLSDGKRKC	Lymphatics in C8161 melanoma	[Zhang et al., 2006]
28	CNRRTKAGC (LyP-2)	K14HPV16 dysplastic skin lesions	[Zhang et al., 2006]

2.2.3 Target proteins

2.2.3.1 Neuropilin-1

One target for homing peptides is neuropilin-1 (NRP-1). NRP-1 is a transmembrane receptor, which interacts with many growth factors, such as vascular endothelial growth factor, integrins [Yaqoob et al., 2012], and semaphorins [Prud'homme and Glinka, 2012]. NRP-1 has roles in the immune system; it is expressed by T-cells and dendritic cells [Prud'homme and Glinka, 2012]. Whereas NRP-1 is expressed in endothelial cells and some other normal cells, it is overexpressed in many cancers, such as prostate [Latil et al., 2000] (including cultured PPC-1 prostate cancer cells [Teesalu et al., 2009]), and breast cancer [Stephenson et al., 2002], carcinoma, melanoma [Straume and Akslen, 2003], leukemia [Karjalainen et al., 2011], glioblastoma [Nasarre et al., 2010], and others. Upregulation of NRP-1 has been correlated with cancer progression and poor prognosis [Chaudhary et al., 2014, Hong et al., 2007, Prud'homme and Glinka, 2012]. In tumors NRP-1 has many roles from tumor initiation [Yaqoob et al., 2012] to angiogenesis and modulating invasiveness [Hong et al., 2007]. NRP-1 affects the tumor microenvironment by facilitating communication between myofibroblasts and fibronectin, thus triggering the integrin-dependent assembly of fibronectin fibril and extracellular matrix and tumor growth [Yaqoob et al., 2012]. In lung cancer models, NRP-1-targeting CendR peptides were found to inhibit cell invasion *in vitro* and to reduce angiogenesis and tumor development *in vivo* [Hong et al., 2007].

2.2.3.2 p32 protein

Another protein of interest for cancer targeting is p32. p32, also known as gC1q-R and p33, is a highly acidic, trimeric protein that is primarily associated with the mitochondria [Ghebrehiwet and Peerschke, 2004]. p32 is one of the receptors for C1q as part of the C1 complement pathway. These receptors are involved in release of adhesion molecules, autoimmune diseases, infections, and inflammation as in the case of vascular lesions or artherosclerosis [Ghebrehiwet and Peerschke, 2004]. p32 is involved in regulating kinase activity [Storz et al., 2000], transcription factors, and has a role in regulating metabolism between oxidative phosphorylation and glycolysis [Fogal et al., 2010]. Whereas p32 is normally moderately expressed by many types of cells, when under stress, the level of expression and ligand affinity has been found to increase [Guo et al., 1999]. Surface-expression of p32 has been found for breast cancer (MCF7, 4T1, MDA-MB-231, MCF10-CA1a) [Fogal et al., 2008], melanoma (MDA-MB-435) [Fogal et al., 2008], prostate cancer (PC3) [Amamoto et al., 2011], glioblastoma (005) [Agemy et al., 2013], and lymphoma cells (Raji Burkitt) [Fogal et al., 2008, Ghebrehiwet et al., 1994]. High expression of p32 has been correlated with a poor prognosis in prostate cancer patients [Amamoto et al., 2011].

2.2.4 Homing peptides

2.2.4.1 p32 targeting peptides

In vivo phage display on squamous cell carcinoma (K14-HPV16) in mice identified the peptide CGKRK [Hoffman et al., 2003]. The fluorescein labeled peptide was found to home to subcutaneous squamous cell carcinoma (PDSC5)[Hoffman et al., 2003], melanoma (MMDA-MB-435, C8161) tumors [Agemy et al., 2013, Hoffman et al., 2003], glioblastoma (H-RasV12-shp53 lentivirus-induced GBM) [Agemy et al., 2011], and also to breast cancer xenografts (MCF10CA1a, Tg (c3-1-TAg) Jeg transgenic model) [Agemy et al., 2013]. CGKRK is internalized and localizes to the cell nucleus [Hoffman et al., 2003] and to the mitochondria [Agemy et al., 2011]. For use with nanoparticles, the peptide has been coupled using the thiol side chain of the N-terminal cysteine [Agemy et al., 2011]. CGKRK iron oxide nanoworms, combined with a proapoptotic peptide, homed successfully to GBM and breast cancer and improved survival or inhibited tumor growth [Agemy et al., 2011, 2013]. The primary receptor for CGKRK was identified as p32 through affinity chromatography and mass spectrometry and verified through immunoblotting assay [Agemy et al., 2013]. Because CGKRK is a positively charged peptide (+3), its homing and binding may be not only through p32, but also through other negatively charged targets in the tumor milieu, such as phosphatydilserines or heparan sulfate proteoglycans [Hoffman et al., 2003]. In recent work, calreticulin, which is often co-expressed with p32 [Ghebrehiwet and Peerschke, 2004], has been identified as another receptor for CGKRK peptide [King et al., 2016].

2.2.4.2 NRP-1 targeting: CendR peptides

A class of NRP-1-binding peptides, dubbed CendR peptides, have an arginine or lysine followed by any two amino acids and another arginine or lysine at their C-terminus (R/KXXR/K), *e.g.* RPARPAR [Teesalu et al., 2009]. CendR peptides are not active when the C-terminal arginine or lysine is blocked by another amino acid, or the terminus is amidated [Teesalu et al., 2009]. The peptides not only bind to but are internalized by the NRP-1-expressing cells using a newly described endocytotic pathway, possibly involved in nutrient transport [Pang et al., 2014b]. Binding of CendR peptides causes vessel leakiness and the endocytosis of other material, *e.g.* cancer drugs, that are coadministered with the peptide [Roth et al., 2016, Sugahara et al., 2010, Teesalu et al., 2009]. NRP-1-mediated cell penetration has also been found for viruses [Lambert et al., 2009].

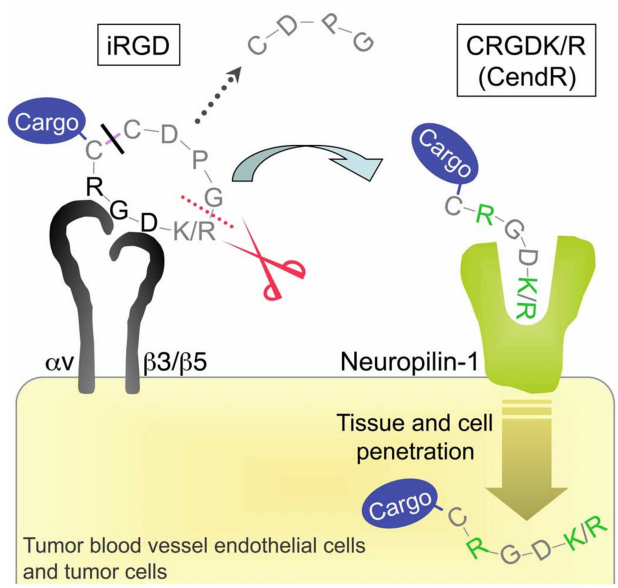

FIGURE 2: Multistep binding and penetration mechanism of iRGD peptide. The iRGD peptide accumulates at the surface of αv integrin-expressing endothelial and other cells in tumors. The RGD motif mediates the integrin binding. The peptide is cleaved by a cell surface-associated protease(s) to expose the cryptic CendR element, RXXK/R, at the C-terminus (red dotted line). The CendR element then mediates binding to neuropilin-1, with resulting penetration of cells and tissues. The peptide can penetrate into tumor cells and tissues with a cargo, such as a simple chemical or a nanoparticle, provided that the cargo is attached to the N-terminus of the iRGD peptide because the disulfide bond apparently breaks before the peptide is internalized (black line). Reprinted with permission from T. Teesalu [Sugahara et al., 2009].

2.2.4.3 Dual targeting: cryptic CendR peptides

The CendR motif can also be in the middle of a peptide sequence, and be activated after proteolytic cleavage exposes the sequence. An example of these cryptic CendR peptides is iRGD, sequence [CRGDKGPDC]. iRGD makes use of two motifs: RGD integrin binding motif [Pierschbacher and Ruoslahti, 1984] and RGDK cryptic CendR motif, that after proteolytic cleavage, acquires the ability to bind NRP-1 and to penetrate into tumors (Figure 2) [Sugahara et al., 2009]. Administering iRGD can enhance uptake of a small molecule, antibody, nanoparticle, or cancer drug and increase their therapeutic efficacy [Sugahara et al., 2010]. Another cryptic CendR peptide is LyP-1 [Laakkonen et al., 2002], sequence [CGNKRTRGC], which targets p32 and then internalizes via NRP-1 after cleavage [Roth et al., 2012]. LyP-1 has been found to home to and penetrate artherosclerotic plaques [Hamzah et al., 2011, Uchida et al., 2011], home to tumor macrophages, tumor cells, and tumor lymphatics [Fogal et al., 2008, Laakkonen et al., 2002], as well as to penetrate into tumors [Karmali et al., 2009, Laakkonen et al., 2002, von Maltzahn et al., 2008]. Like iRGD, LyP-1 peptide triggers the coadministration effect of improved uptake of nanoparticles administered together with the peptide [Roth et al., 2012]. Recently a new peptide, similar to LyP-1, but with higher p32 affinity was identified [Paasonen et al., 2016]. *De novo* design of a proteolytically activated CendR peptide has also been demonstrated [Braun et al., 2016].

2.2.4.4 Brain targeting peptide

Fan *et al.* used T7 *in vivo* phage display to identify a brain homing peptide with the sequence CAGALCY [Fan et al., 2007]. The sequence was optimized using structural analysis whereby amino acid substitutions were tested. The peptide has affinity for brain microvasculature with no homing to other organs. CAGALCY was found to inhibit platelet adhesion in mice with induced sepsis [Fan et al., 2007]. This observation supported the hypothesis that the peptide may target integrin binding sites on circulating cells, thus interfering with cellular adhesion. The free C-terminal tyrosine and hydrophobic pockets of CAGALCY are features of known integrin antagonists [Dubree et al., 2002, Gurrath et al., 1992]. However, the receptor for CAGALCY peptide has not yet been determined.

2.3 Silver nanoparticles

T7 phages display multiple copies of a peptide on their spherical, biological nanoparticle surface. While phage display libraries are powerful for new peptide discovery, once a homing peptide is identified it is often synthesized and conjugated to a synthetic nanoparticle which mimics the bacteriophage. These NPs transition the peptide towards clinical use as they can be made of biocompatible, stealth, or clinically approved materials. They also have properties which aid in the continuing

research and evaluation of the peptide such as the inclusion of fluorescent dyes for detection. Metal NPs are already used clinically for MRI contrast (iron oxide NPs) and for surgical instrument coatings (silver NPs), while other metal NPs are being evaluated as nanotherapeutic carriers in animal models [Shi et al., 2017].

2.3.1 Commercial use and toxicology

Silver nanoparticles (AgNPs) are widely used for their antibacterial properties. They are used in consumer goods such as textiles, appliances, and toys. They are present in dressings for burns and wounds, and have been found to aid wound healing [Tian et al., 2007]. Medical instruments and implants have also been coated with AgNPs for sterility purposes. The wide use of AgNPs has caused concern about their environmental impact because toxicity has been demonstrated in *in vitro* and *in vivo* studies (reviewed in [Ahamed et al., 2010, Ong et al., 2013]). The antibacterial function of AgNPs, which is the goal of commercial applications, stems primarily from particle dissolution and the release of Ag^+ ions [Beer et al., 2012, Caballero-Díaz et al., 2013]. The AgNPs tested in most toxicology experiments do not have surface coatings [Ahamed et al., 2010]. Coated, passivated surfaces help prevent oxidation and ion release, which would impact toxicity. The PEGylation of AgNPs has been found to reduce cytotoxic effects in some cases [Bastos et al., 2016, Caballero-Díaz et al., 2013], possibly by reducing uptake, while found to make no difference in other studies [Bastos et al., 2017]. Nanoparticle toxicity is not easily attributable and is determined by particle size, shape, and surface chemistry. Regulatory guidance suggests that each type of nanoparticle be assessed on its own for its cytotoxic impact rather than making generalizations [Commissioner of Food and Drugs, 2007].

2.3.2 AgNP optical properties

AgNPs have size- and shape-dependent optical properties; their absorbance maximum in solution is based on their diameter. In response to an external electrical field the electrons of metal nanoparticles oscillate collectively, referred to as plasmon resonance [Zhang et al., 2015]. The coupling of plasmon resonances of the particle and attached dye molecules leads to a distance-dependent enhancement of the signal of the attached fluorophore [Lakowicz, 2005, Zhang et al., 2010]. AgNPs in the 40–100 nm size range provide the best enhancement [Lakowicz, 2005]. AgNP coupling can also reduce photobleaching of dyes, an important feature for live cell imaging [Lakowicz, 2005]. The same feature enables the use of AgNPs for surface-enhanced Raman spectroscopy (SERS) [Braun et al., 2009, Lee and Meisel, 1982, Sun and Xia, 2003, Zhang et al., 2010].

2.3.3 AgNP synthesis

AgNPs can be synthesized in many different shapes: cubes, spheres, plates, disks, and rods [Sun and Xia, 2003, Wiley et al., 2005]. Polyol synthesis, with ethylene glycol, using polyvinylpyrrolidone (PVP) is a versatile techinque able to generate several shapes and sizes based on varying ratios between PVP and silver salt, $AgNO_3$ [Skrabalak et al., 2007, Wiley et al., 2005]. The ethylene glycol serves to reduce the Ag^+ ions to Ag^0, thus triggering nanoparticle nucleation, while PVP serves as a capping agent and stabilizer. Lee and Meisel published a citrate-based AgNP synthesis carried out in water [Lee and Meisel, 1982], which was modified by Dadosh to make a monodisperse, spherical product, with the addition of tannic acid [Dadosh, 2009].

2.3.4 AgNP functionalization

The functionalization of AgNP surfaces with molecules is primarily done through thiol-metal bonds, which are almost as strong as covalent bonds [Sperling and Parak, 2010]. For example, PEG molecules with terminal thiols will displace the weakly bound citrate molecules that are adsorbed on the AgNPs' surface from a citrate-based synthesis. The binding of ligands to the surface is a dynamic on/off process, and ligands can be displaced by those with stronger binding, or removed by excessive washing because the principle of critical micelle concentration applies. The surface ligands stabilize the particles electrostatically and sterically. Generally, strongly bound, tightly packed, charged ligands provide the most stability. Additionally, they enable the further conjugation of desired molecules such as fluorophores and peptides. Often PEG molecules with heterobifunctional terminal groups are used, *e.g.* maleimides to react with cysteines, and amines to react with N-hydroxysuccinimide esters. Other possible conjugating groups are listed in Table 2. For biological use, the AgNPs are covered with PEG molecules for stealth, biocompatible properties and conjugated further with fluorophores and targeting peptides.

Table 2: Functionalization chemistries.

Reactant 1	**Reactant 2**
Imidoester	amine
N-hydroxysuccinimide ester	amine
Carboxylic acid	amine (via carbodiimide)
Maleimide	thiol
Haloacetyl	thiol
Pyridyl disulfide	thiol
Neutravidin	biotin
Hydrazide	aldehyde
Alkoxyamine	aldehyde

3. Aims of the Study

This doctoral work was focused on the development of a silver nanoparticle (AgNP) platform to be used as a tool in cancer research. While cancer treatments continue to improve, the development of nanotherapeutics has not been as successful as hoped. As a way to improve nanotherapeutics, conjugated targeting molecules such as peptides are being explored. Homing peptides have been discovered through the phage display targeting of tumor vasculature. AgNPs were tested for their applicability to function as synthetic carriers of these peptides. The AgNPs were tested as cellular probes as well as functioning as trackable and quantitative tools for assessing homing peptide performance *in vivo.*

The specific aims were:

1. To synthesize and functionalize silver nanoparticles (AgNPs) **(I, II, III, IV)**
2. To develop isotopically distinguishable AgNPs **(II)**
3. To use etchable AgNPs conjugated with fluorescent dyes and targeting peptides as cellular probes for determining internalized *versus* extracellular NPs **(I, II)**
4. To use AgNPs conjugated with fluorescent dyes and homing peptides to target organs and tumors *in vivo* **(I, III, IV)**
5. To use multiplexed, isotopic AgNPs conjugated with targeting peptides to phenotype cancer cells **(II)**
6. To use isotopic AgNPs conjugated with targeting peptides in internally controlled, *in vivo* peptide validation studies **(III)**

4. Materials and Methods

Detailed methods can be found in the listed publications. Below is a summary of the methods used.

4.1 Materials (I, II, III, IV)

$AgNO_3$ wt (Sigma-Aldrich #209139); $AgNO_3$ 107Ag and 109Ag >99% pure isotopes (Isoflex); sodium citrate tribasic dihydrate (Sigma-Aldrich #S4641); tannic acid (Sigma-Aldrich #403040); PVP (polyvinylpyrrolidone, Sigma #856568-500G MW ∼55000); ethylene glycol (BDH #BDH1125-1LP >99.99%); D-biotin (Sigma-Aldrich #B4501); $Pd(NO_3)_2$ (Aldrich #76070); NeutrAvidin (Thermo Scientific #31055); Lipoic acid-PEG(1k)-NHS (Nanocs #PG2-AMLA-1k); CF555-NHS dye (Biotium #92130); tripotassium hexacyanoferrate $Fe(III)(CN)_6^{3-}$ (Sigma, CAS# 13746-66-2); sodium thiosulphate $Na_2S_2O_3$:$5H_2O$ (Sigma, CAS# 10102-17-7); HNO_3 (Fluka #84385); HCl (Fluka #84415); NH_4OH (Fluka #09857); Peptides were synthesized in-house at SBPMDI or ordered from TAG Copenhagen.

4.2 AgNP synthesis

In the work conducted for this thesis, particles were synthesized in the 20–70 nm size range, based on Ag core size; functionalization with polymers and proteins leading to a larger hydrodynamic diameter for the finished product. AgNPs were synthesized by two primary methods: citrate and polyvinylpyrrolidone (PVP) method.

4.2.1 AgPVP synthesis (I)

The PVP-based synthesis of AgNPs involves dissolving PVP in ethylene glycol, followed by addition of $AgNO_3$ and heating. The synthesized particles are purified by acetone precipitation and water washes with repeated centrifugation and sonication for particle suspension. The PVP method has the advantage of producing monodisperse spherical nanonparticles. With some modifications, such as polymer MW, this method can be used to produce 20 nm or 70 nm, or even larger AgNPs for maximum plasmonic enhancement.

4.2.2 Ag-citrate and tannic acid synthesis (II, III, IV)

The citrate method, developed by Lee and Meisel [Lee and Meisel, 1982], is done in a piranha-cleaned Erlenmeyer flask. *Caution! Piranha (H_2SO_4 and H_2O_2) is a highly oxidizing acid solution.* $AgNO_3$ is dissolved in ultra pure water and brought to a boil, then citrate is added. The advantage of citrate synthesis is that it is done in an aqueous environment and particle precipitation and phase transfer is not needed. The downside is that the synthesis produces a polydisperse, 20–60 nm, product that in addition to spheres contains some other shapes such as rods. The diversity of the product makes it harder to attribute nanoparticle effects to size and shape, but at the same time the variety of particles provides opportunity for finding some particles that work especially well in a given situation. A modification of this synthesis, developed by Dadosh [Dadosh, 2009], includes tannic acid in addition to the citrate and produces a monodisperse 20–25 nm product. This synthesis was chosen for the isotopic particles, while the larger citrate particles were best for visualization.

4.2.3 Ag-Pd and isotopic synthesis (II, III)

The AgNP platform was developed further for multiplexing by using isotopic barcoding. Since silver naturally only has two isotopes, 107 and 109, AgNPs on their own can only be used in duplex not multiplexed format. That is why palladium, Pd, doping was employed to create a third variety of particle. Choosing how much Pd and by which synthesis to incorporate it took a lot of testing. At first PVP synthesis was tried for Pd percentages ranging from 0.3 to 11%. Large amounts of Pd were found to change the AgNPs' shape and dispersity, so the smallest possible detectable amount (1%) was needed. One option that was tested was a PVP-style synthesis whereby Pd seeds were grown first and then coated with additional Ag. Finally, the simpler tannic acid/citrate method with 1% Pd was chosen. The particles produced in this way are slightly irregular – compared to the monodisperse spheres produced by pure Ag – but still mostly round and monodisperse.

4.2.4 AgNP size characterization (I, II, III, IV)

The main ways to characterize AgNPs were analyzing the ultraviolet-visible (UV-vis) absorption spectrum and by transmission electron microscopy (TEM). The UV-vis spectrum is based on the plasmon resonance peak of the particles. It is determined by the size of the particles; smaller particles are more towards the blue end of the spectrum and larger particles, or aggregates, are more towards the red end. The number of peaks is based on the number of axes for plasmon resonance, in the case of spheres there is one axis. Spherical particles with a size of ~ 20 nm have an absorbance maximum at about 400 nm. The measured optical density can also be used to quantify the molarity of particles by Beer's Law, using extinction coefficients (see Table 3). TEM visualization was conducted for every

batch of AgNPs. Images were analyzed by ImageJ to get a size distribution for the particles. Dynamic Light Scattering (DLS) was used sometimes, to determine the hydrodynamic radius of the particles after functionalization.

TABLE 3: Extinction coe cients for spherical AgNPs based on diameter.

AgNP diameter (nm)	**Extinction coe cient (ϵ, $M^{-1}cm^{-1}$)**
7	1.74×10^{8}
20	4.12×10^{9}
30	8.83×10^{9}
40	3.45×10^{10}
50	5.40×10^{10}
60	6.65×10^{10}
70	1.09×10^{11}
80	1.28×10^{11}

4.3 AgNA functionalization (I, II, III, IV)

For most of the thesis work AgNPs with neutravidin (NA) and polyethylene glycol (PEG) molecules were used, dubbed AgNA (Figure 3). This chemistry was chosen because NA molecules are a convenient way to attach biotinylated peptides by one of the highest affinity bonds in nature, $K_d \sim 10^{-15}$ M [Pierce Biotechnology, 2013]. Neutravidin is a deglycosylated version of avidin, making it relatively neutral in charge with low non-specific binding. The NA adsorbs to the silver surface, but is also attached by two PEG linkers per NA. These 5 kDa PEG legs were capped with orthopyridil disulfide leaving groups which come off to allow for sulfur–Ag binding, a strong if not covalent bond. In addition to the NA molecules, any remaining free space on the AgNA particles was filled with 1 kDa PEG molecules. PEG is a clinically established, bio-compatible material that helps reduce non-specific binding [van Vlerken et al., 2007]. The PEGs were also attached by sulfur–Ag bonds, via lipoic acid, a molecule with two exposed sulfur groups. The free end of the PEGs had an amine, NH_2, group that was used for dye coupling via N-hydroxysuccinimide ester (NHS) chemistry. The advantage of AgNA particles is that they can be stored in a finished state. The dye and peptide can be conjugated quickly prior to use with incubation and centrifugation to wash. Biotinylated peptides can be stored in solution and any NHS-dye can be used. Additionally, other biotinylated compounds, such as small molecules and peptide analogues [Paasonen et al., 2016], can be conjugated in the same way as the peptides.

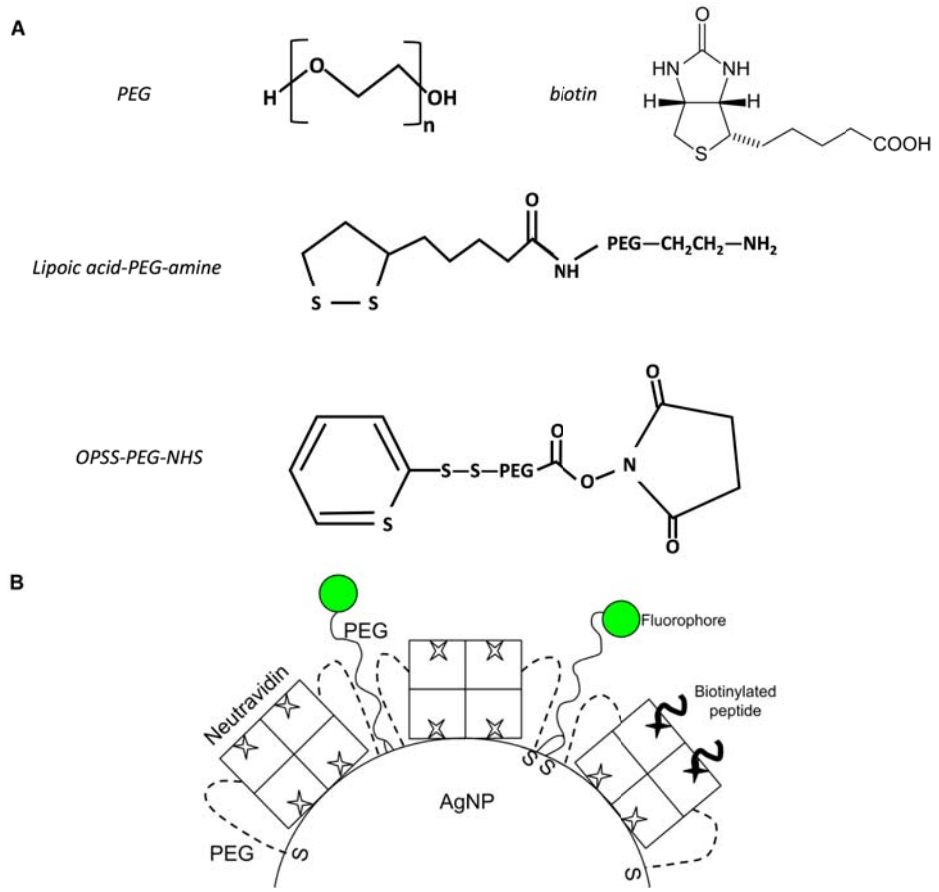

FIGURE 3: AgNP with Neutravidin and PEG functionalization (AgNA). (A) Some of the molecules for AgNA functionalization: polyethylene glycol, biotin (biotinylated peptides), lipoic acid-PEG-amine for PEGylation, and orthopyridil disulfide-PEG-NHS for anchoring NAs (B) Schematic of AgNA particle. NAs are conjugated with biotinylated peptides. PEGs are linked with lipoic acid molecules and their terminal amines are further conjugated with NHS-fluorophores.

4.3.1 Number of biotinylated peptides per AgNA (I, II, III, IV)

To determine the number of peptides per AgNA, biotinylated CF488A dye was used. Since AgNPs enhance the fluorescence of attached dyes, an accurate measurement cannot be achieved without dissolving the nanoparticles. Therefore after conjugation and washes, the AgNPs were dissolved by etching and CF488A concentration was calculated based on a standard curve. When the AgNPs are dissolved, the dyes remain attached to NA molecules due to the very strong bond. This binding reduces the fluorescence intensity of the dyes, therefore a correction factor of 1.89 is applied [Mutch and University of Washington, 2009]. The amount of

biotinylated peptides per particle was found to be $\sim$ 100 for the most commonly used citrate AgNA particles.

4.3.2 Number of dyes per AgNA (I, II, III, IV)

Dyes were conjugated to AgNPs through NHS-amine chemistry. Reactive amine groups include the terminal amines on PEG groups, as well as amines that are available on NA molecules (ϵ-amino groups of lysine residues). Sometimes it is useful to know the number of NHS-dyes that attach to nanoparticles. This was determined similarly to the method for peptide quantification, by etching particles and measuring fluorescence against a standard curve. The amount of dyes per AgNP was found to be 10–20 for the most commonly used citrate particles. The same method is relevant for quantifying AgNP drug loading when using an NHS-drug coupling strategy.

4.3.3 PEG functionalization (I)

Although mostly AgNA particles were used, due to the convenience of NA/biotin chemistry, particles were also made without NA. NA is more immunogenic and likely to trigger more AgNP clearance than a pure PEG coating would. The particles were coated with longer PEG molecules, 3.4 kDa, with terminal amines, conjugated with NHS-PEG molecules with a maleimide group on the free end, and the maleimide was then used to react to cys-peptides (Figure 4). These particles would carry a fluorescent label on the peptide, rather than conjugating an NHS-dye, limiting the choice to the dye which is attached to the synthesized peptide (most commonly fluorescein). The other downside of these particles is that since NHS and maleimide groups are unstable, the particles can be stored only with PEG-amine attached and the second PEG and peptide must be added before each use. The peptide is also unstable in solution since cys-peptides in solution form dithiol dimers, and must be weighed out before each use. For these reasons the AgNA platform was the preferred option, especially for *in vitro* work.

4.4 Peptides (I, II, III, IV)

The aim of this thesis was to establish a model nanoparticle platform and to perform proof-of-concept experiments. Therefore established peptide/ target protein combinations were used most of the time. Biotinylated RPARPAR-OH was the peptide used most often for experiments and was always used for quality control purposes. The RPARPAR/NRP-1 binding combination is robust to minor deviations in experimental conditions. GKRK-NH_2/p32 is another established combination that was used for multiplexing experiments. As a control peptide, CendR function was blocked on RPARPAR by adding a C-terminal alanine or by

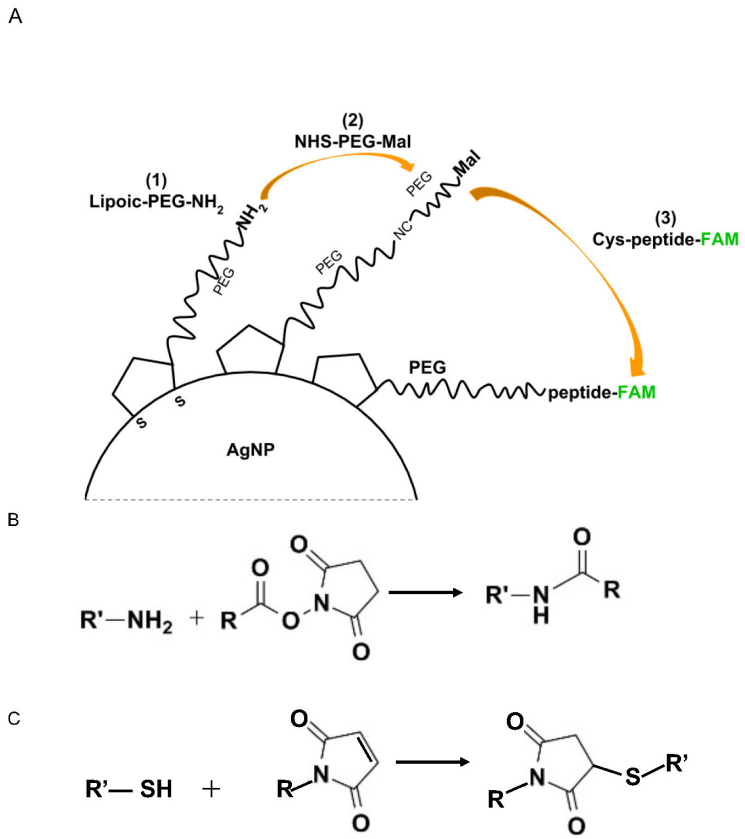

FIGURE 4: PEG-AgNP functionalization scheme. (A) AgNPs are first functionalized with lipoic acid-PEG-NH_2 (1); followed by NHS-PEG-maleimide (2); and lastly with a FAM-cys-peptide (3). (B) A primary amine reacting with an N-hydroxysuccinimide group as in step 2. (C) A thiol group reacting with a maleimide as in step 3, (reactions B and C adapted from [CovaChem, 2017]).

amidating the C-terminus, sometimes simply free biotin was used as a control. CAGALCY peptide was used for brain homing experiments. Peptides, $\geq$ 95% purity, were either ordered or synthesized by other lab members using Fmoc/*t*-Bu chemistry on a microwave assisted automated peptide synthesizer; followed by HPLC purification and validation by Q-TOF mass spectral analysis.

4.5 Protein binding assay (II)

To show specific binding of peptide-AgNPs, recombinant his-tagged proteins were used: p32, NRP-1, and NRP-1 with mutated CendR binding pocket as control. p32 is mainly an intracellular protein found in the mitochondria, however it is found on the surface of some cancer cells, making it of therapeutic interest [Fogal

et al., 2008]. Peptides, *e.g.* GKRK, have been successfully used to target p32-expressing tumors [Agemy et al., 2011, 2013]. NRP-1 is overexpressed in tumors and is involved in vessel leakiness. NRP-1 binding triggers internalization; it is the target of CendR peptides, *e.g.* RPARPAR peptide [Teesalu et al., 2009]. The CendR binding pocket is essential for endocytosis to occur and mutation at this site stops the binding and internalization of CendR peptides [Teesalu et al., 2009].

To study receptor interactions of peptide AgNPs, at first an ELISA-style assay was considered. 96-well plates were coated with protein, exposed to peptide-AgNPs, washed, and quantified. However, the plate method had a high background; possibly due to AgNPs settling onto the plate. Ni-NTA magnetic agarose beads were tested next for protein immobilization. This method worked well, and had a low background, with the magnetic beads and AgNPs kept in suspension by constant motion. The beads were loaded with protein, incubated with peptide-AgNPs, washed; the AgNPs were eluted with 400 mM imidazole. In addition to fluorescence measurement, eluted AgNPs can be detected and quantified by UV-vis spectroscopy. Using AgNP absorbance as a read-out was found to be more reliable than fluorescence measurement.

4.6 *In vitro* experiments (I, II)

Experiments with cultured cells used primarily two cell lines: PPC-1 prostate carcinoma and M21 melanoma cells. The cell lines were chosen since both are well studied cancer cell lines with published work to compare to [Sugahara et al., 2009, 2010, Teesalu et al., 2009]. Both are fast growing, adherent cells grown in Dulbecco modified Eagle's minimal essential medium (DMEM) with serum and antibiotics. PPC-1 are strongly NRP-1 expressing, whereas M21 lack cell surface NRP-1 expression [Teesalu et al., 2009]. This makes the combination of the two ideal for quality control testing with RPARPAR peptide conjugated AgNPs. The PPC-1 bind and internalize the AgNPs strongly whereas the M21 cells do not bind or take up any, aside from background non-specific pinocytosis. We found that both cell lines express some p32 on the cell surface and take up AgNPs conjugated with GKRK peptide.

4.7 Microscopy (I, II, III, IV)

Both epifluorescent and confocal microscopes were used to assess cellular uptake of AgNPs. An epifluorescent microscope with dark field condenser is able to distinguish AgNPs in cells by their effective scattering of light. This technique was also used with tissue sections. Both types of microscopes were used to assess binding of fluorescently-tagged AgNPs as well as for immunofluorescence imaging. The large, over 40 nm, AgNPs plasmonically enhance attached dyes, easing detection; smaller ∼20 nm AgNPs are detectable as well. For imaging of tissue sections,

excised tumors and organs were snap-frozen in liquid nitrogen, cryosectioned at 10 μm, fixed with 4% paraformaldehyde, immunostained, and imaged.

4.8 Flow cytometry (I, II)

Cellular uptake of AgNPs was assessed by flow cytometry. When AgNPs are fluorescently labeled, they can enhance the dye's intensity and make the AgNPs sensitive probes for cellular uptake. In fact when uptake is very high, the fluorescence can be so intense that it is out of the range of the flow cytometer's capabilities. An interesting discovery was that AgNPs change cells' side scatter (SSC) so much that this can be used as a dye-free read out of uptake.

4.9 Etching (I, II, III)

Dissolving or etching of AgNPs is a novel technique first published in [Braun et al., 2014] **(I)**. It is based on silver destaining solutions commonly used on polyacrylamide gels. Etchable AgNPs provide an important tool for distinguishing surface-bound nanoparticles from internalized ones. This is a translationally relevant feature since therapeutic cargo must be internalized into the cell to have an effect. Even high-resolution microscopy cannot absolutely determine whether a nanoparticle is inside a cell or outside. Most cellular probes cannot be turned off, and those that can be, often do so using harsh chemicals making them not biocompatible. The silver etch solutions' mildness and ease of use are key features. A side effect of dissolving extracellular AgNPs is that background is reduced. *In vivo* etching can identify peptide-AgNPs that penetrate into tumors and tumor cells.

The etch solution contains two components: hexacyanoferrate (HCF), $Fe(III)(CN)_6^{3-}$, and thiosulphate (TS), ${S_2O_3}^{2}$. The HCF oxidizes the solid silver Ag^0 to Ag^+ ions and the TS ligates the ions and carries them away. Figure 5 shows the optimization of etch component concentrations. The etch components do not pass through cell membranes due to their charged nature. Because only extracellular AgNPs are dissolved and internalized AgNPs are protected, it is possible to tell them apart with before and after etch imaging or quantification, *e.g.* by ICP-MS. The two components are used at a 1:1 ratio and are stored separately, with HCF protected from light; the components are mixed before use. The etch works diluted with PBS, cell culture medium, or injected as part of a perfusion solution in animal experiments. Its function can be stopped by the addition of the reducing agent sodium ascorbate. *Caution! HCF should not be dissolved in strong acids as toxic cyanide gas can be released!*

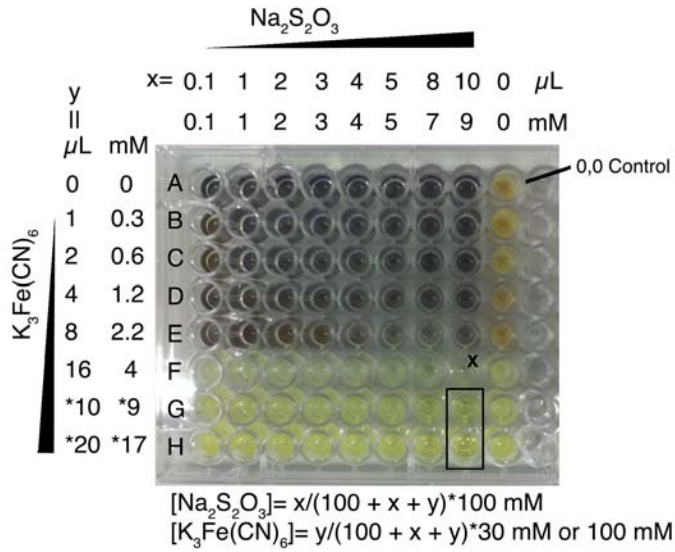

FIGURE 5: Plate optimization of etch components. Concentration of the two reagents was optimized in a plate format. Complete etching of a high concentration of AgNPs was judged by visual inspection of the color and reduced scattering, and darkfield microscopy. AgNP-PVP (80 nm diam, 200 optical density at 450 nm) were diluted 10-fold in PBST (PBS with 0.005% Tween-20 (Sigma)). 100 μL was added per well, comprising a variable amount of sodium thiosulfate solution (100 mM in water) and potassium HCF (30mM, or (*) 100 mM for rows G and H, in water). Tan color in "0,0 Control" is the unetched Ag color, and brown to black is from aggregates, induced primarily by thiosulfate. Clear colorless wells are in the farthest right column. Concentrations are provided on the axes and formulae below. A bluish hue in the well indicates conversion of the Fe(III) metal center to Fe(II), *e.g.* 16 μL HCF 30 mM, 10 μL thiosulfate 100 mM. Boxed wells show the clarified solution at minimum of 8 mM HCF and 8 mM thiosulfate. The lack of particles was verified by depositing solution onto a glass slide for darkfield analysis. Working concentration of 10 mM was chosen for each component. A stoichiometry of 1:1 HCF:thiosulfate was chosen so that the solution would have a constant clear yellow appearance during use, as the limiting reagent is predicted to be thiosulfate until 1:2 is reached. A deviation from a yellow color when combined with an otherwise colorless solution could indicate that undissolved particles remain, presence of dyes, or that there are competing reduction reactions. Since the reaction with silver is stoichiometric in Fe:Ag, it is possible to reduce the working concentration when etching fewer particles than used in this example plate **(I)**.

4.10 ICP-MS experiments (II, III)

Inductively coupled plasma mass spectrometry (ICP-MS) is a very sensitive technique for quantifying elements, including telling apart isotopes of the same material [Agilent, 2015]. The samples, completely dissolved in acidic solution, are turned

into an ionized gas or plasma by inductive heating, then fired at a detector that can distinguish the mass to charge ratio of the incoming atoms. For our experiments, the detection limit for Ag and Pd was 1 pg/g or 1 part per trillion on average, but sometimes as sensitive as 0.1 pg/g. The detection limit was determined for each set of samples that are analyzed and is based on the background level of the analyte. The purity of reagents and cleanliness of the ICP-MS instrument itself have an effect on the detection limit.

In order to analyze AgNP samples – either AgNPs alone, cell culture, or tissue lysates – dissolution protocols were developed. Unfortunately, using etch solution to dissolve AgNPs caused interference during analysis, so another method was needed. Dissolving AgNPs in HNO_3 alone, was sufficient for purely Ag samples, but not for Pd-doped samples which required HCl as well. The introduction of HCl caused a new problem of AgCl precipitate formation, which was mitigated by the addition of NH_4OH. The above mentioned chemicals were of a very high purity to avoid contaminating elements. Aside from the dissolution chemicals other components were kept to a minimum to avoid interference.

For laser ablation ICP-MS (LA-ICP-MS), a laser passes over a tissue sample to ionize the silver atoms. For this technique 30 μm thick tissue sections were used. While ICP-MS of whole tissue lysates gives and average amount of homing for the entire tissue, LA-ICP-MS is able to give an idea of the heterogeneous binding and accumulation of targeted AgNP probes.

4.10.1 ICP-MS calculations (II)

The quantity of wtAg-Pd particles taken up by cells was calculated based on measurement of the 105 isotope of Pd, and using that quantity to determine biotin-AgNPs' contribution to the 107Ag and 109Ag signals (brackets indicate concentration of analyte in ng/g):

$$[107]_{biotin} = 51.3 * [Pd] \tag{4.1}$$

$$[109]_{biotin} = 47.7 * [Pd] \tag{4.2}$$

$$\text{Total biotin} = [Pd] + [107]_{biotin} + [109]_{biotin} = 100 * [Pd] \tag{4.3}$$

$$\text{Total RPARPAR} = [107]_{total} - [107]_{biotin} \tag{4.4}$$

$$\text{Total SGKRK} = [109]_{total} - [109]_{biotin} \tag{4.5}$$

The use of palladium (Pd) doping in order to make multiplexing with AgNPs possible, brings with it a deconvolution challenge. Since two particles are either pure 107Ag or 109Ag they are easily distinguished by ICP-MS. However, the third particle is made of natural silver, 107Ag and 109Ag, and Pd. This means that the contribution of the Pd particles to the total signal for the other two types of AgNPs must be accounted for. While it is possible to calculate and deconvolute this signal overlap, (Equations 4.1–4.5) it is not ideal. Ideally the three, or more, particles

would not have any overlap. This problem was avoided in *in vivo* experiments **(III)** by using only two particle types: targeted and control with the two Ag isotopes. One potential future expansion of this platform would be to use different isotopes of Pd – there are six – doped into natural silver.

4.11 T7 phage display (IV)

A T7 peptide phage library was used for biopanning to identify IP3 peptide. The peptide library was cyclic with seven random amino acids, CX_7C, and a diversity of 10^8. Both *in vivo* screens, with MKN-45 tumor mice, and *ex vivo* screens with excised tumors were conducted. Emphasis was placed on finding peptides that had a high tumor to kidney ratio since intraperitoneal screens have problems with high background. High-throughput sequencing, with Ion Torrent, and bioinformatics data mining were utilized to identify homing phage peptide sequences.

4.12 *In vivo* experiments (I, III, IV)

All animal work was approved by the Estonian Ministry of Agriculture, Committee of Animal Experimentation (permit #42) or by the Institutional Animal Care Committee of the Sanford Burnham Prebys Medical Discovery Institute.

Healthy balb/c mice were used for lung and brain homing experiments with RPARPAR and CAGALCY isotopic AgNPs.

The MMTV-PyMT transgenic mouse model [Guy et al., 1992] was used for *in vivo* etching experiments. This model is considered useful for its similarity to human breast cancer and how the disease progresses. 4T1 tumors [Pulaski and Ostrand-Rosenberg, 2001] were also studied for the effectiveness of etch at removing background from tissue sections.

MKN-45P [Miyagi et al., 2007] and CT-26 [Brattain et al., 1980] cells were grown on cell culture flasks in DMEM with antibiotics and 10% heat-inactivated serum. The MKN-45P human gastric cancer model was induced in athymic nude mice while CT-26 tumors were induced in balb/c mice, both by injecting 2×10^6 cells intraperitoneally. MKN-45P tumors were grown for two weeks and CT-26 for one week.

5. Results and Discussion

5.1 Properties of AgNPs (I, II, III, IV)

Figure 6 summarizes the various types of silver nanoparticles that were used to carry out the doctoral research. AgNPs were synthesized with 20–70 nm metallic cores and were covered with a polyethylene glycol (PEG) coating, and usually also with neutravidin (NA) molecules (Figure 7). Large metal cores, over 40 nm, have the property of plasmonic enhancement of any dye coupled within a certain distance. The particles are able to provide an approximate 10 fold enhancement of the cyanine based dyes used in the work (Figure 8). The particles are bright and distinct enough to be able to distinguish single particles by microscopy; furthermore the metal cores scatter light so well as to make detection possible by darkfield microscopy. The neutravidin molecules allowed for easy, plug-and-play, conjugation of biotinylated homing peptides.

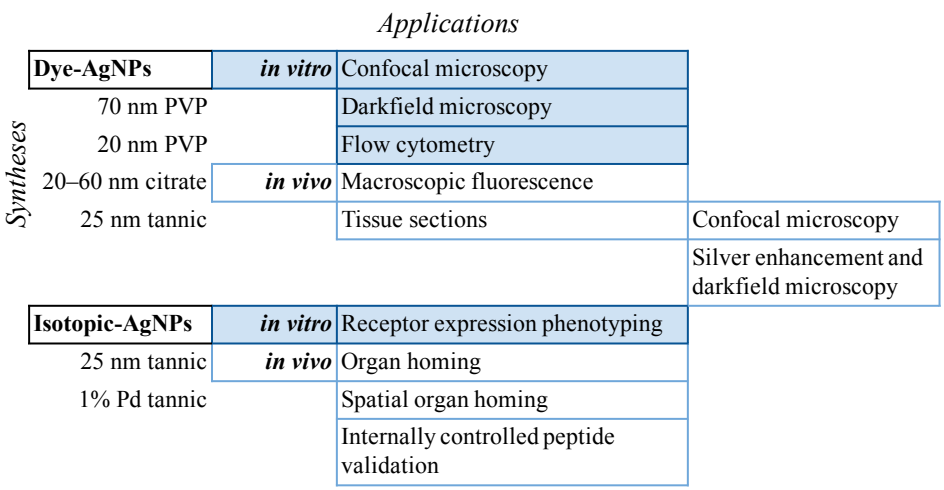

FIGURE 6: Summary of AgNPs and their applications. The AgNPs produced can be divided into two primary categories: either isotopic which are detectable by ICP-MS or those detectable by attached fluorescent dyes and the natural silver core.

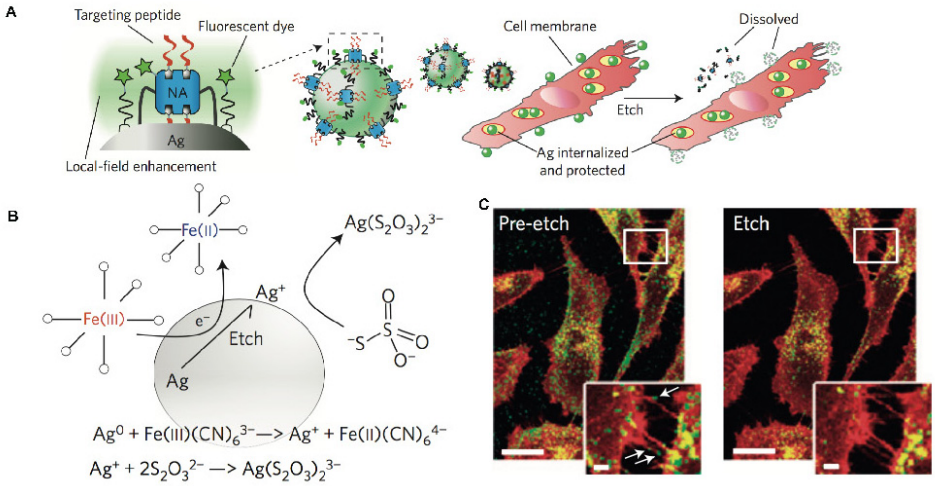

FIGURE 7: Dye-labeled, peptide functionalized silver nanoparticles (AgNPs) and their etching for cell internalization and tracking. (A) Scheme of AgNPs coated with NeutrAvidin-PEG-thiol (NA) and lipoic-PEG-amine, each having attached fluorescent dyes (stars) with brightness enhanced by the local plasmonic field. Attachment of biotinylated internalizing peptide RPARPAR forms the complete Ag nanoprobe (R-Ag-NA488). These bind to and are taken up by cells, which are treated with exposure to etchant solution to remove extracellular particles. Plasmonic enhancement is lost for etched particles. (B) Etching reagents hexacyanoferrate (HCF) and thiosulfate (TS) oxidize and stabilize silver ions, respectively, releasing components into solution and dissolving the core. (C) Fluorescence confocal microscopy of cells incubated with R-Ag-NA488 (green) and membrane stain (red) shows how R-Ag-NA488 is retained selectively in cells when etched (right). Endosomal membranes strongly overlap with nanoparticles, appearing as yellow in the overlay **(I)**.

5.1.1 Etching (I, II, III)

The exciting advancement brought out by these AgNPs *versus* other nanoprobes, is their ability to be "etched" or dissolved by a mild biocompatible solution (Figure 7). The etchant is made up of a hexacyanoferrate and thiosulfate redox solution that, due to its highly charged components, does not pass through cell membranes. This enables the elimination of particles that are not protected by a cell membrane. Conjugated dye is then released to be washed away, removing signal. Even if the dye is still adsorbed, its plasmonic enhancement is turned off by particle dissolution, leading to a reduction of background signal. Etching allows for the quantification of total bound nanoparticles or only those that have internalized.

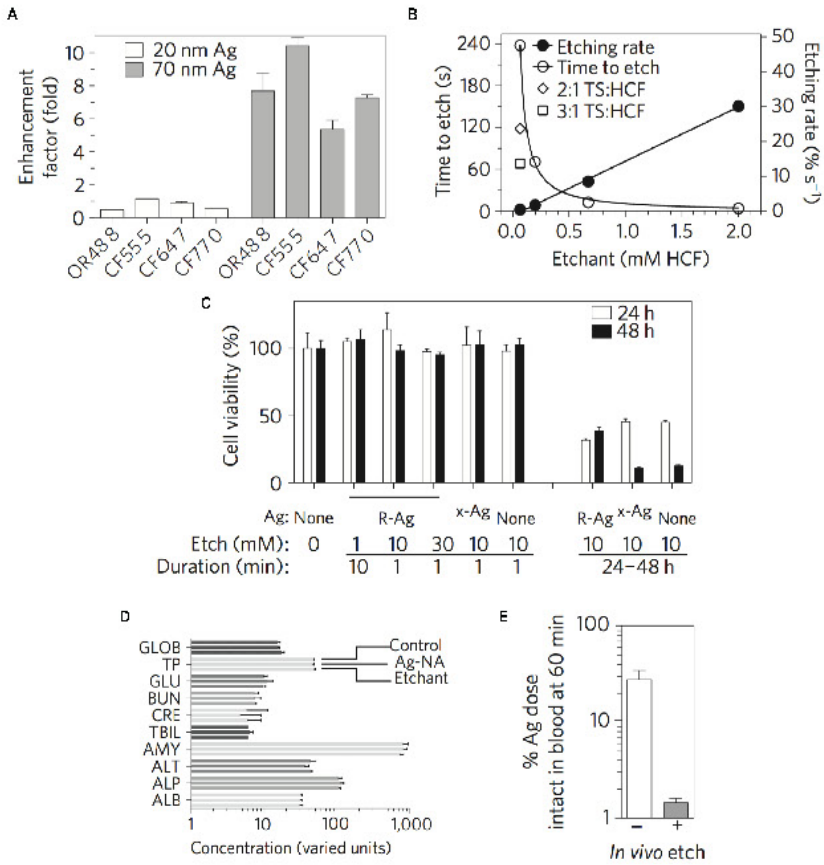

FIGURE 8: Nanoparticle characterization and toxicity screening. (A) Enhancement factor (EF) for several commonly used dyes shows a strong dependence for size of the Ag core. EF was calculated from the ratio of fluorescence for unetched/etched Ag-NA-dye conjugates. The approximate peak absorption value of the dye is on the x-axis. Error bars = S.D. from replicate wells. OR488, Oregon Green 488; CF dyes from Biotium. (B) Etching kinetics for Ag-NA depends linearly on the concentration and the molar ratio of the etchant components TS:HCF. The decrease in scattering intensity from the Ag plasmon band upon etching was used to calculate a rate, and the time to reach 10% of the initial value is plotted. 1:1 TS:HCF except where indicated, Ag-NA (70 nm core) concentration fixed in all conditions. (C) PPC-1 cells with RPARPAR Ag-NA (R-Ag) and etching showed no effect on 48 h viability (resazurin assay) for short-term exposures to etchant (n = 6). Values normalized to the condition of no Ag, no etchant. Ag-NA without peptide, x-Ag, does not internalize into cells. Etchant concentration and duration of contact with cells is indicated. (D) *In vivo* blood chemistry was evaluated 24 h after x-Ag-NA or etchant injection. Marker levels were not significantly different from those for a PBS control injection. Error bars = S.D. (n = 3–6 mice). (E) The etchant was capable of etching pre-injected Ag in mice. Ag was injected into the tail vein then 20 min later followed by either etchant or PBS injection, and blood was analyzed for fluorescence at 60 min. Values were normalized to % of fluorescence at 5 min. Ag had been labeled with CF555 and PEG for blood etching. Error bars = S.D. (n = 2). Terms and units for D: GLOB, globulin g/L; TP, total protein g/L; GLU, glucose mM; BUN, blood urea nitrogen mM; CRE, creatinine μM; TBIL, total bilirubin μM; AMY, amylase units/L; ALT, alanine transaminase units/L; ALP, alkaline phosphatase units/L; ALB, albumin g/L **(I)**.

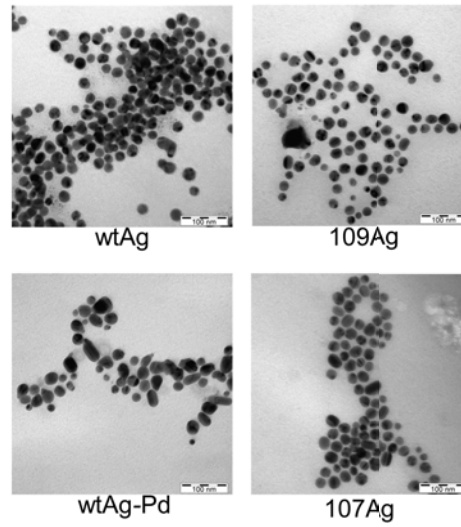

FIGURE 9: TEM images of AgNPs at 210k magnification. Samples were imaged on copper grids coated with holey formvar carbon film (Pacific Grid Tech). Similar AgNPs were produced despite core type with an average size of 24 ± 5 nm, although Pd-containing AgNPs were slightly more irregular in shape than non-doped AgNPs. Scale bar: 100 nm **(II)**.

5.1.2 Toxicity (I)

Toxicity testing indicated that short exposure to mild concentrations of etch and exposure to AgNPs had no impact on cell viability, while high concentrations of etch for over 24 hours became toxic (Figure 8 C). Clinical blood analysis on mice found normal liver and kidney function after exposure to AgNPs and etch indicating general safety (Figure 8 D), although more testing should be done.

5.1.3 Isotopic AgNPs (II, III)

Isotopic AgNPs (Figure 9) have ∼24 nm silver cores that are functionalized with PEG and NA molecules and are used with biotinylated peptides. Natural silver, wtAg, consists of 51.8% 107Ag and 48.2% 109Ag. Isotopic AgNPs were made out of only a single silver isotope or wtAg with an added 1% Pd doping. This isotopic difference in the silver cores is detectable by inductively coupled plasma mass spectrometry (ICP-MS), a very sensitive analytical method with a detection limit of 1 pg/g on average for Ag and Pd. Having three isotopically disinct particles (107Ag, 109Ag, and wtAg-Pd) allowed for the use of the AgNPs in a multiplexed format.

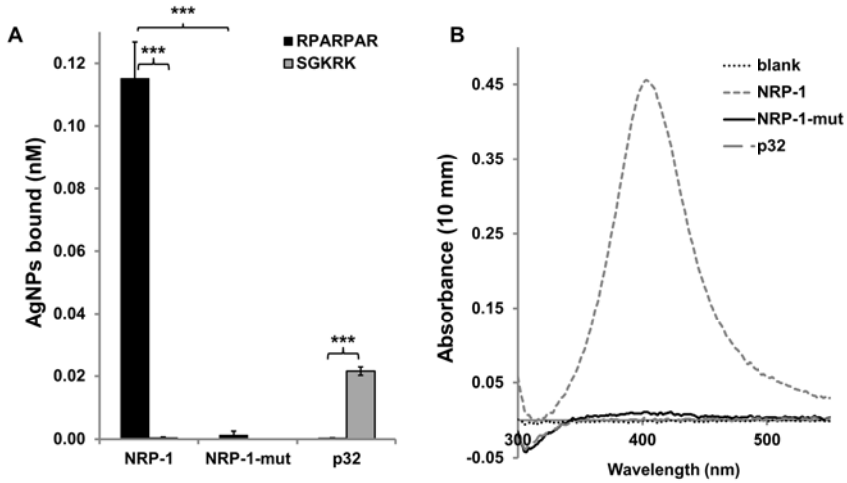

FIGURE 10: Binding of peptide particles to receptor proteins. (A) R-AgNPs bind to immobilized NRP-1-b1b2 domain but not to NRP-1-b1b2 protein with mutated CendR binding pocket [Teesalu et al., 2009] or to p32 protein; K-AgNPs bind to p32 and not to wt or mutant NRP-1-b1b2. Data represent mean values ± SD (n = 3); *** $p < 0.001$ by Student's t-test. (B) Representative raw data from UV-vis spectroscopy for R-AgNPs. AgNPs were eluted from protein-loaded Ni-NTA magnetic beads with 0.4 M imidazole-containing buffer and the UV-vis spectrum of the eluate was measured. The absorbance spectrum seen for NRP-1 binding is due to R-AgNPs; the peak absorbance was taken for calculations **(II)**.

5.2 *In vitro* applications

5.2.1 Immobilized protein binding (II)

Peptide-AgNPs should bind their target protein with low background binding. For proof of concept, known peptide/target combinations were chosen: CendR peptide RPARPAR (target NRP-1), SGKRK (target p32) a tumor homing peptide, and free biotin acted as control. NRP-1 with a mutated binding pocket that stops CendR peptide binding was also included. AgNPs with the above peptides were tested for binding to immobilized target proteins. The bound AgNPs were quantified by UV-Vis absorbance (Figure 10), taking advantage of the particles' high extinction coefficients and enabling dye-free detection. The AgNPs bound specifically to their targets, with very low background.

5.2.2 Flow cytometry and microscopy (I, II)

Specific binding to recombinant proteins was established. Next, peptide-AgNPs were tested for binding to cells which express the same proteins. The target proteins (NRP-1 and p32) are both expressed by PPC-1 prostate cancer cells, while

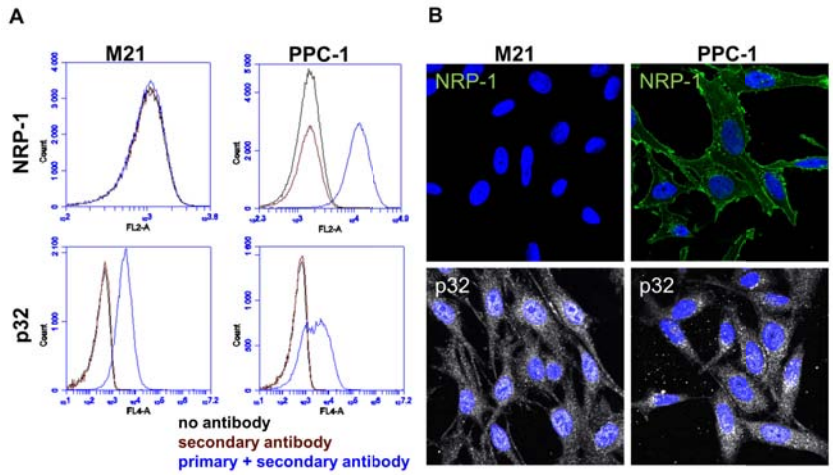

FIGURE 11: Expression of NRP-1 and p32 on the surface of cultured PPC-1 and M21 cells. M21 cells do not express NRP-1 as seen by flow cytometry (A) and confocal microscopy (B), but do express p32. PPC-1 cells express both NRP-1 and p32. For flow cytometry, cells were not permeabilized prior to antibody incubation thus only membrane staining was revealed; whereas microscopy shows both membrane and internal staining **(II)**.

M21 melanoma cells express p32 but not NRP-1 (Figure 11). For microscopy the R-AgNPs were found to work well as fluorescent probes (Figure 7 C), with non-internalized and non-specifically bound particles being removed from PPC-1 cells by etching. For flow cytometry (Figure 12), R-AgNPs bound specifically to NRP-1-expressing PPC-1 cells with ∼60 % of cells being positive for particle uptake, whereas control particles showed only a background level of uptake after etching. M21 cells took up negligible amounts of R-AgNPs but did take up K-AgNPs. The specific binding and uptake of peptide-AgNPs was demonstrated regardless of the core size being 70 nm or 25 nm (Figure 12 A and B respectively), and despite different fluorescent dyes being used. Due to the brighter dye (AF647 *vs.* CF555) and the dye enhancement by the larger core, there is a stronger overall fluorescence signal for the R-Ag-NA647 particles. There is also a higher level of background fluorescence, however this is removed when etch is applied. Additionally, AgNP uptake was found to alter cells' side scatter such that SSC readings could be used as read-out in a dye free assay.

5.2.3 Live cell imaging (I)

AgNPs were tested as probes for live cell imaging where brightness and photostability are paramount (Figure 13). R-AgNPs bound GFP-PC3 cells which express NRP-1 and membrane-bound *versus* internal particles were evaluated based on red (AgNPs) or yellow signal (colocalization of AgNPs and GFP), respectively. After etching (Figure 13 C), single particle tracking inside a cell was possible.

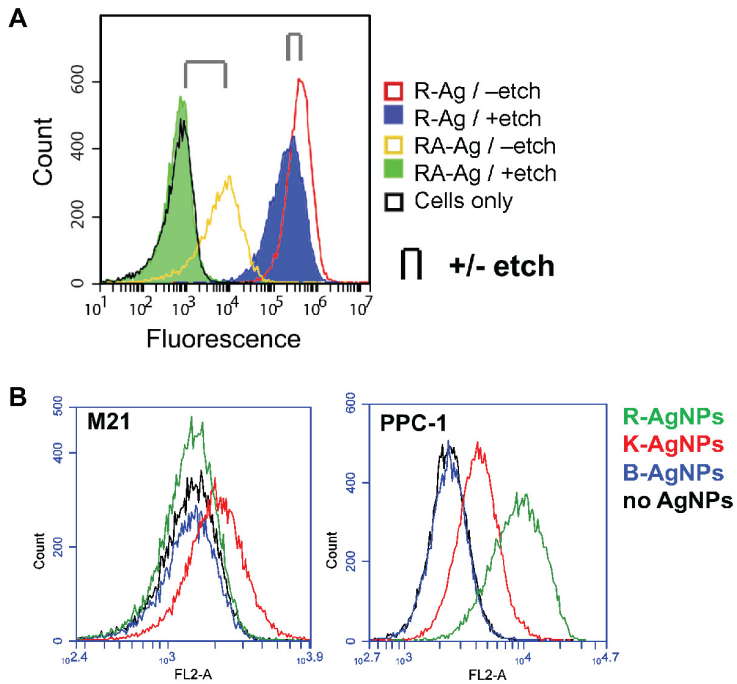

FIGURE 12: Receptor-dependent binding and uptake of nanoparticles as analyzed by flow cytometry. (A) Fluorescence histograms of cells with 70 nm Ag-NA647 carrying either of two peptides. Cell-gated plots of internalizing R-Ag-NA647 (red, -etch), and with etch (blue), *versus* non-internalizing control, RPARPARA (RA)-Ag-NA647 (yellow, -etch) and with etch (green). Cells without Ag were included as a control (black). Paired +/- etch is indicated in all panels by the clip icon. (B) Flow cytometry of M21 and PPC-1 cells incubated for 1 h with R-, K-, or B-AgNPs (25 nm), all labeled with CF555. Note that NRP-1-positive PPC-1 cells bind R-AgNPs (66 ± 1% positive), whereas M21 do not; both cell lines score positive for binding of K-AgNPs 7 ± 1% positive for M21 and 8 ± 1% for PPC-1 cells; etching was not used, (adapted from **I, II**).

The particles were presumed to be in endosomes and the combining of two AgNP signals into one was thought be an endosome fusion event. To further validate how etching works, cells were fixed with aldehyde and then etched (Figure 14). In nonpermeabilized, fixed cells the internalized particles were not affected. After application of Triton X-100 detergent, which disrupts membrane integrity, the etch was able to enter cells and dissolve particles. A limited test of multiplexing was conducted with two dyes and two peptides and distinguishing the two AgNP types binding to different targets was possible.

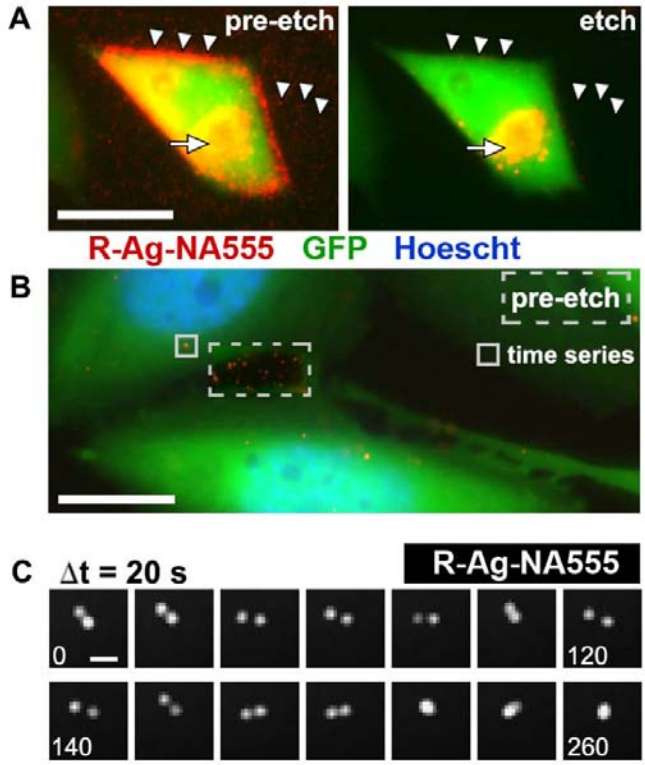

FIGURE 13: Tracking AgNPs within live cells. (A) Epifluorescence microscopy of GFP-expressing PC-3 cells after binding and endocytosing R-Ag-NA555. These cells express the NRP-1 receptor. R-Ag-NA555 appears red when not associated with the GFP in cells, and these were removed by etching (arrowheads). The yellow color represents cell-associated R-Ag-NA555, due to spatial overlap with the cells, indicated by the full arrow. (B) Intracellular tracking was possible by time-lapse epifluorescence imaging when a lower amount of R-Ag-NA555 was added with shorter incubation time. This post-etch image shows only a small number of red objects survived etching, and a pre-etch image of a region outside the cells (dashed box) is overlaid to show the representative intensity from R-Ag-NA555 that had adsorbed to the substrate. A region inside the cell body (solid box) was chosen for the time series presented in (C). (C) R-Ag-NA555 moved within the cell and relative to each other. Each frame advances forward by 20 s, with numbers in frames indicating the elapsed time. The two structures undergo an apparent fusion event at +220 s. Scale bars are 25 μm in (A), 10 μm in (B), 1 μm in (C) **(I)**.

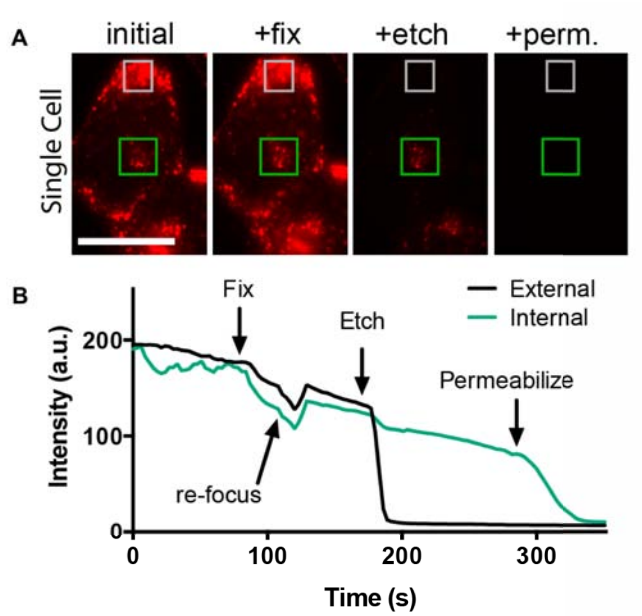

FIGURE 14: Etching AgNPs outside fixed cells and within permeabilized cells. (A) R-Ag-NA555 were incubated with PC-3-GFP cells and imaged during the sequential procedure of fixing (fix), etching, and permeabilization (perm.). Representative regions for R-Ag-NA555 that were internalized (green box), and a region of bound but external particles (gray box). (B) Time trace of the mean pixel intensity of the regions in (A) with each reagent added without washing. Rapid drops in intensity were due to etching of Ag and the gradual downward slope is due to fluorescence photobleaching. Two cells were averaged for this trace. Scale bar is 25 μm **(I)**.

5.3 *In vivo* applications (I, III, IV)

For many anti-cancer agents, such as nucleic acids, it is important to reach inside the cell to be effective. Etching of AgNPs after incubation with cultured cells was able to reveal the internalized fraction, the same was tested for tumor sections. iRGD-AgNPs were injected into 4T1 breast cancer bearing mice. When tumor sections were etched *ex vivo*, background signal was markedly reduced compared to control organs (Figure 15 A–C), an improvement on most contrast agents that cannot be turned off. The amount of AgNPs internalized by the tumor was $\sim$ 25% *vs.* $\sim$100% internalization for the liver, attributable to liver macrophages. The use of etch was also tested as an *in vivo* chaser, and was successful at clearing circulating AgNPs (Figure 8 E).

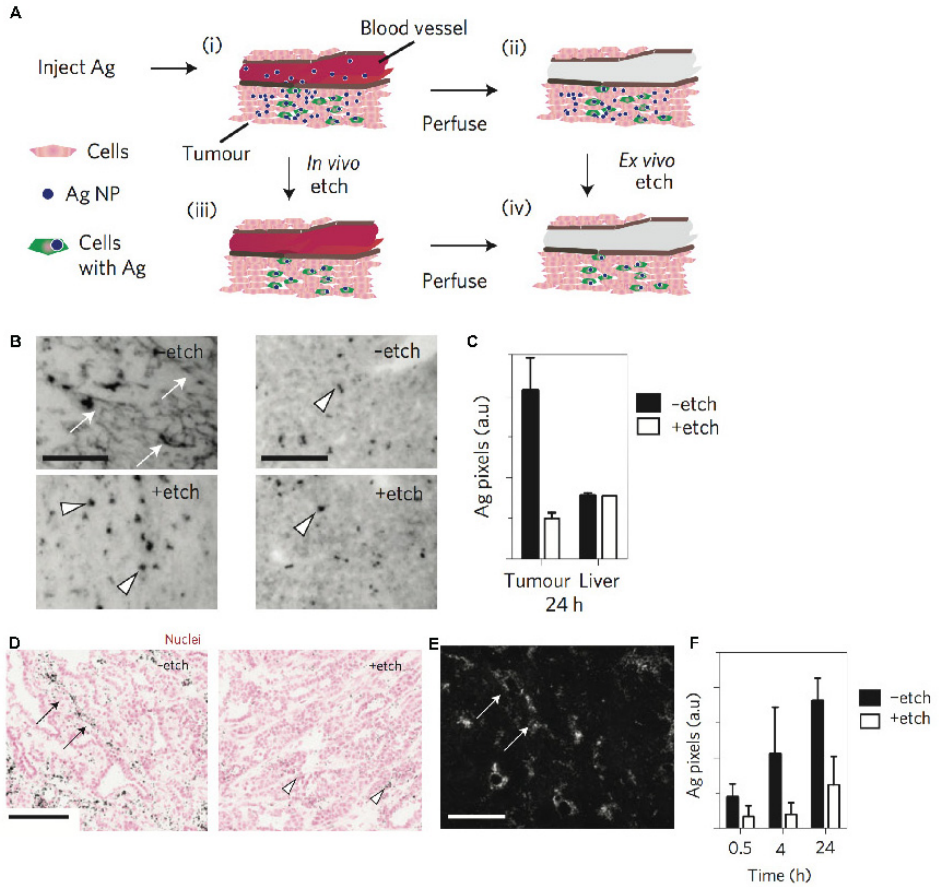

FIGURE 15: *In vivo* etching. (A) Schematic of *in vivo* tumor homing, *ex vivo* and *in vivo* etching. Stages are: (i) iRGD-Ag-NA homing and extravasation, (ii) tissue perfusion was followed by etching *ex vivo*, or instead, (iii) *in vivo* etching followed by perfusion, and (iv) tissue with Ag retained in cells. (B) Brightfield imaging of *ex vivo* 4T1 tumor and liver tissue sections are presented, −etch (upper), +etch (lower). Ag was amplified by autometallography and appeared as dark pixels. Diffuse dark pixels (full arrows) were attributed to extracellular Ag, arrowheads to endosomal Ag. (C) Samples from B were quantified for dark Ag pixels per field as a measure of iRGD-Ag-NA in the tissue. (D) *In vivo* etching with MMTV-PyMT tumors. Mice were perfused at 0.5, 4, or 24 h hours post injection of iRGD-Ag-PEG, and selected mice (+etch) were injected with etchant 10 min prior to perfusion. Shown are representative tumor tissue sections from 4 h −etch (left), +etch (right). (E) Darkfield imaging of Ag amplified section (4 h, −etch) shows strong signals (arrows) consistent with the pattern in brightfield, D. Note: this image has no nuclear counterstain and was taken from a separate section than D. (F) Tumor samples from D were quantified for dark Ag pixels per field, representing the amount of iRGD-Ag-PEG in the tissue for the indicated circulation times. Error bars = S.D. with $n > 2$ randomly chosen fields per condition in C, $n > 4$ in F. Scale bars are 100 μm in B, D, E **(I)**.

5.3.1 Biodistribution kinetics (I)

An *in vivo* etching strategy was developed to determine biodistribution kinetics in the MMTV-PyMT tumor mouse model (Figure 15 A, D–F). Time points were collected post iRGD-AgNP injection that either were or were not chased with etch. The signal was amplified with silver enhancement, which uses AgNPs as seeds and grows them into larger particles, for improved detection. This experiment enabled determination of homing *versus* uptake of nanoparticles as well as to find out how quickly homing leads to uptake. The easily tracked AgNPs worked well as a model nanosystem for targeted therapeutics.

5.3.2 Homing to healthy tissues (III)

Peptide-AgNPs were tested for homing to healthy tissues. Lung and brain, both with known homing peptides, RPARPAR [Teesalu et al., 2009] and CAGALCY [Fan et al., 2007] respectively, were chosen as target tissues. For these experiments, citrate particles with CF555 dye were used since their larger size makes them enhance the attached dye and eases detection. Balb/c mice were injected via tail vain with AgNPs and after five hours were perfused and sacrificed. Confocal imaging of tissue sections confirmed that RPARPAR-AgNPs accumulated in lung ∼9 fold more than control particles (Figure 16). Silver enhancement and imaging by darkfield produced similar results. CAGALCY-AgNPs were also found in brain tissue about 9-fold more than control particles (Figure 17).

5.3.3 Homing to peritoneal carcinomatosis (IV)

IP3 peptide was found using phage display and further studied as a free peptide and as conjugated to AgNPs (Figure 18). *Ex vivo* and *in vivo* phage display biopanning was conducted on MKN-45P peritoneal tumors in athymic nude mice. Peptide-phage binding was analyzed by high throughput sequencing (HTS) and custom bioinformatics software. Since biopanning conducted in the peritoneal cavity typically has problems with high background binding, emphasis was based on finding a peptide with high tumor and low kidney binding (high T/K ratio). This lead to the discovery of IP3 peptide, sequence [CKRDLSRRC]. IP3 peptide contains the motif LSRR, very similar to known LSRPR motif found in link protein which binds hyaluronic acid (HA). HA is a known tumor marker and is also found in the MKN-45P tumor model used. Fluorescently-labeled IP3 was found to bind immobilized HA ∼6 fold more than control heptaglycine peptide.

IP3 peptide was synthesized with a fluorescein label and tested for homing to intraperitoneal MKN-45P tumors. After washes, tumors were examined for macroscopic fluorescent signal as well as sectioned and imaged by confocal microscopy. FAM-IP3 was found in both large and small tumor nodules. Immunostaining revealed accumulation away from CD-31 stained blood vessels, and colocalization with CD11b positive areas rich in macrophages.

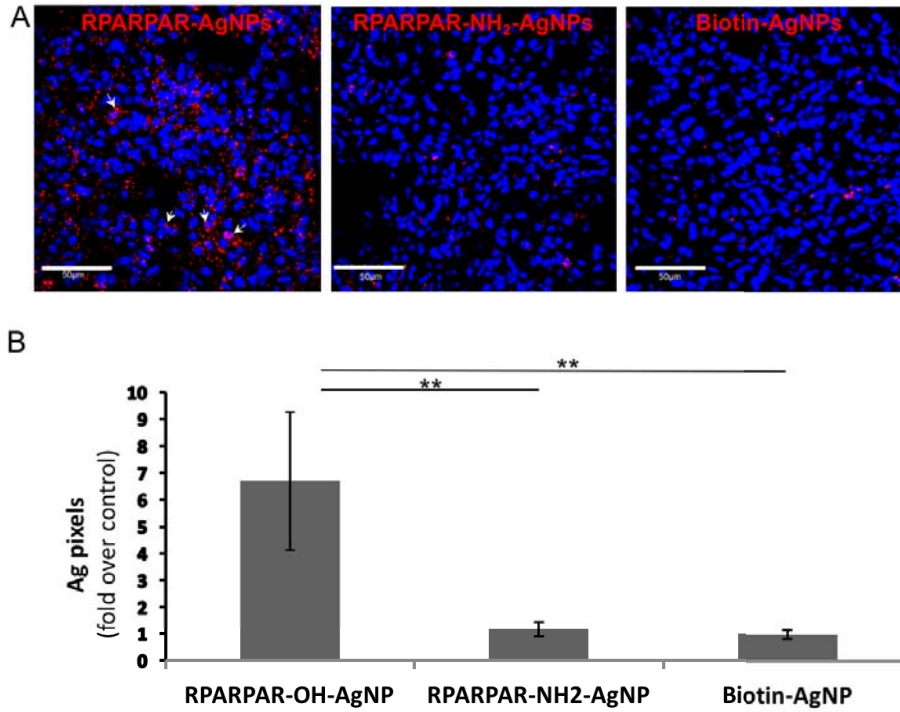

FIGURE 16: Systemic CF555-labeled RPARPAR-OH-AgNPs home to lung tissue. Balb/c mice were injected in the tail vein with CF555-labelled RPARPAR-OH and biotin-AgNPs in 200 μL PBS. After 1-h or 5-h circulation, the animals were perfused with 15 mL PBS to wash out blood and to remove unbound plasma AgNPs, and the organs of interest were snap-frozen. (A) Confocal imaging of lung cryosections from mice injected with CF555-AgNPs (red), nuclei stained with DAPI (blue), circulation time 5 h. Arrows point at areas of accumulation of CF555-positive RPARPAR-OH AgNPs (n = 3); scale bars = 50 μm. (B) Quantification of the CF555 fluorescence in tissue sections. AgNP signal (red in panel A) expressed as percent of pixels with intensity above threshold. Five randomly chosen fields from each of 3 animals/group were analyzed. Data represent mean ± SD, ** $p < 0.01$, (adapted from **III**).

AgNPs were functionalized with biotinylated IP3 peptide to test its utility as a homing peptide for guiding nanoscale pharmaceuticals or imaging agents. In addition to the MKN-45P gastric cancer model, the CT26 colon cancer model was also tested for IP3-AgNP homing. Microscopy showed strong peripheral binding to both tumor types, with some deeper penetration as well. The limited penetration of IP3-AgNPs *versus* free peptide can be attributed to strong, irreversible binding to HA at the tumor surface due to the multimeric display of the peptide on the nanoparticle.

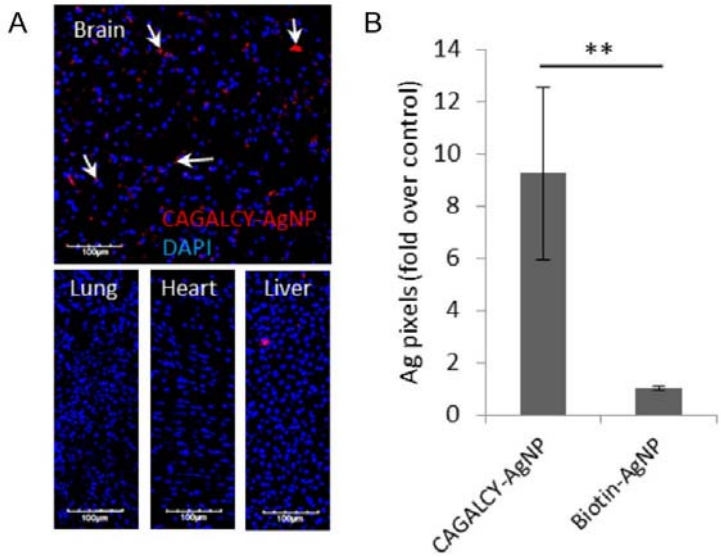

FIGURE 17: Biodistribution of systemically administered CF555-CAGALCY-AgNPs. (A) Confocal imaging of tissues from mice injected with CAGALCY-functionalized AgNPs labeled with CF555 fluorescent dye, circulation time 5 h. Arrows point at areas of accumulation of CAGALCY AgNPs (red). Scale bars = 100 μm. (B) Quantification of CF555 fluorescence in tissue sections. Ag pixels/field were plotted for each type of nanoparticle as fold over control (n = 3); 5 fields were analyzed per tissue. Data represent mean ± SD **(III)**.

5.4 *Ex vivo* applications (I, IV)

AgNPs coated with iRGD, sequence [CRGDKGPDC], a known tumor homing peptide with integrin binding motif and cryptic CendR motif, were tested for binding to freshly excised living tumor tissue. Microscopy of the tissue showed a high degree of binding by the iRGD-AgNPs as compared to control (Figure 19). This is a useful model since it can be used on clinical samples and its inclusion of both stromal and epithelial cells and other tumor connective tissue more closely approximates *in vivo* tumors than cultured cells. The tissue was etched to reveal internalized AgNPs, an important insight when it comes to drug delivery since most drugs must get inside the cell to be effective. IP3-AgNPs were also tested for binding to freshly excised colon tumors and some binding was observed while control particles did not bind (Figure 19).

5.5 Phenotyping cells using isotopic AgNPs (II)

The specific binding of RPARPAR- and SGKRK-AgNPs to cultured PPC-1 and M21 cells was established by microscopy and flow cytometry. This same cell

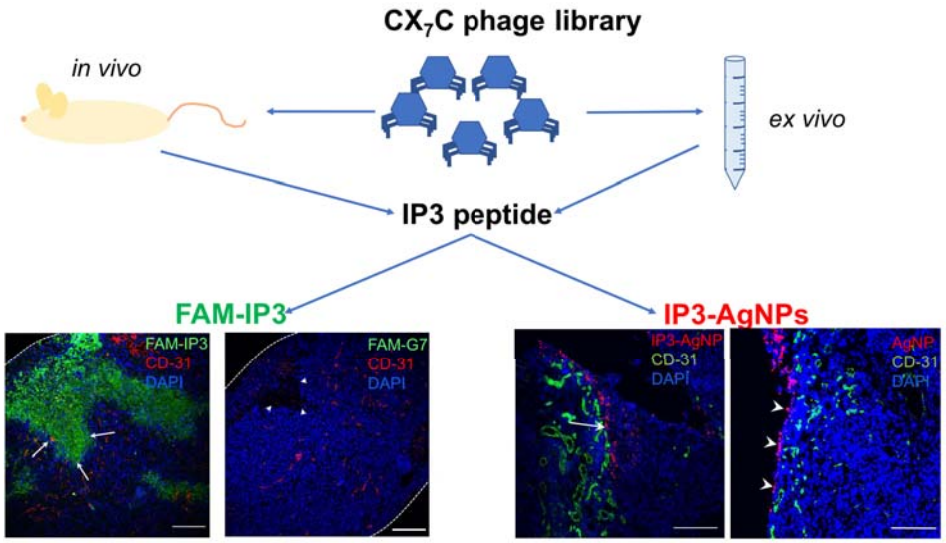

FIGURE 18: IP3 discovery and validation scheme. IP3 peptide, sequence [CKRDLSRRC], was discovered through phage display using the CX_7C library and doing *in vivo* screens on MKN-45 tumor bearing mice as well as *ex vivo* screening on excised tumors. IP3 peptide synthesized with fluorescent label (FAM) or with biotin, for use with AgNPs, homed to MKN-45P tumors, while free peptide penetrated deeper (adapted from **IV**).

binding was then analyzed using inductively coupled plasma mass spectrometry (ICP-MS). At first only R-AgNPs were used as coupled to the three different isotopic cores (107Ag, 109Ag, wtAg-Pd), and tested for binding to PPC-1 and M21 cells. The AgNPs bound the PPC-1 cells and not the M21 cells as expected, indicating that the nanoparticle core did not impact binding. ICP-MS not only identified the presence of AgNPs, but also measured the correct isotope(s) (Figure 20). When samples were etched, to dissolve non-internalized AgNPs, the quantity of silver measured was reduced as expected. For example, in PPC-1 cells incubated with R-107AgNPs, the etched 107Ag signal was 25.7 ± 1.5 ng/g *versus* 61.0 ± 5.6 ng/g for non-etched cells.

With ICP-MS measurement of the isotopic AgNPs established, the platform was tested in multiplexed format to phenotype cells (Figure 21). The three unique cores were each coupled with either RPARPAR, SGKRK, or free biotin. The three types of particles were mixed together and applied to PPC-1 or M21 cells. The samples were etched and internalized particles were measured. The results showed that PPC-1 cells took up mostly RPARPAR-AgNPs (75% ± 5%) and some SGKRK-AgNPs (25% ± 2%) (Figure 22). The M21 cells contained mostly SGKRK-AgNPs (89% ± 9%) with a small amount of RPARPAR-AgNPs. The cell lines can be phenotyped as: PPC-1 mainly NRP-1 positive and M21 as only p32 positive. The amount of internalized control particles was below the limit of detection. This is expected based on previously found low-background binding,

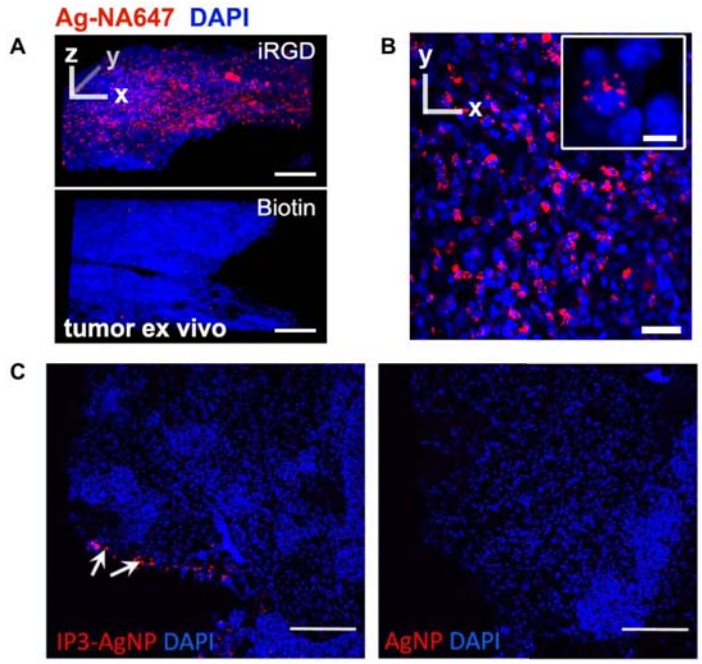

FIGURE 19: AgNPs used in *ex vivo* applications. (A) MCF10CA1a (human breast) tumors were developed in nude female mice. Living tumor slices of 200 μm thickness were prepared from resected tumors and cultured in media. Confocal laser microscopy was performed after incubation and etching of (top) iRGD-Ag-NA647 or (bottom) biotin Ag-NA647 as a non-peptide control. Strong internalization was seen with iRGD. Z-stacks were collected through 60 μm total thickness, step size 2 μm, 20x objective. (B) 2D slice from A, top, for iRGD-Ag-NA647. Inset shows the perinuclear localization in red, 40x objective. (C) IP3-AgNPs accumulate in a surgically excised peritoneal tumor explant. Arrows point to IP3-AgNPs bound on the edge of the tumor. Red, IP3-AgNPs or AgNPs; blue, DAPI. Scale bars are: (A) 100 μm, (B) 25 μm, (B)-inset 5 μm, (C) 200 μm. CF647 dye was used in (A) and (B), CF555 in (C), (adapted from **I, IV**).

especially when extracellular particles are etched. These results showed the potential of isotopic AgNPs for detecting multiple cell surface-expressed receptors at one time. Multiplexing in this way is also useful because it avoids dye-related effects due to non-specific binding, variable brightness, bleaching, and overlapping signals.

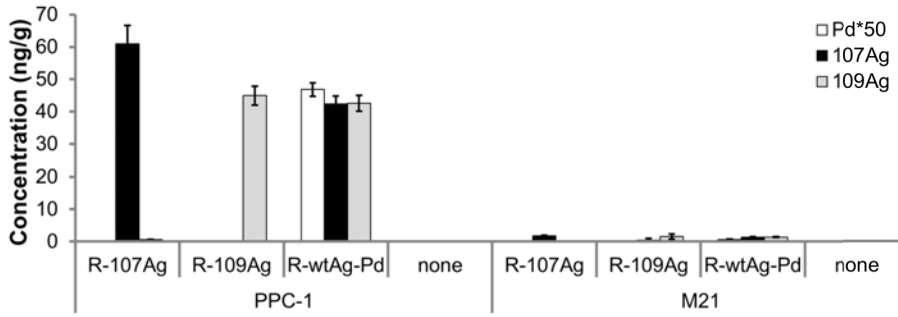

FIGURE 20: Isotopic R-AgNP binding and internalization into M21 and PPC-1 cells. Three isotope-tagged RPARPAR-coupled silver cores were incubated with PPC-1 or M21 cells for 1 h and total bound AgNPs were quantified by ICP-MS. Each of the three silver cores functionalized with RPARPAR peptide showed robust PPC-1 binding and low M21 binding. The Pd concentration is multiplied by 50 to visualize more clearly; the R-wt-Ag-Pd sample's Pd content of 0.94 ± 0.04 ng/g is 100 times above the detection limit. Data represent mean values ± SD (n = 3) **(II)**.

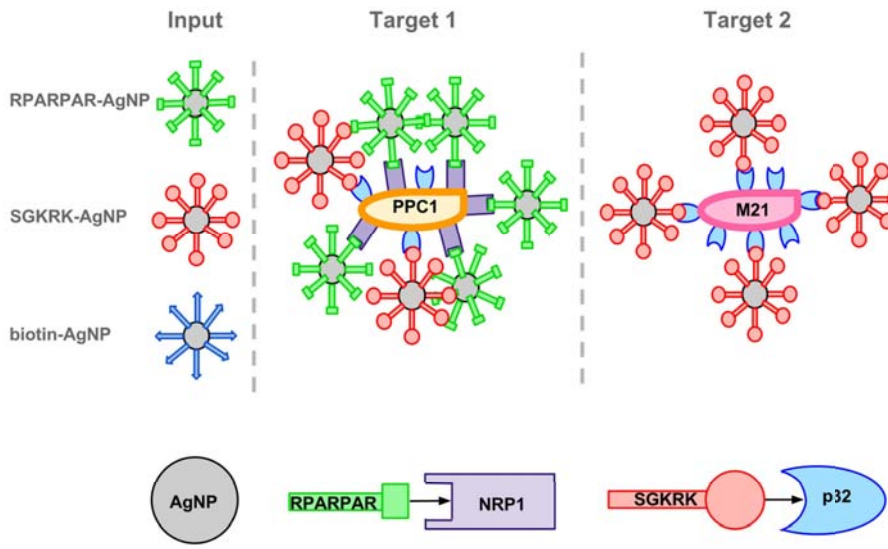

FIGURE 21: Multiplexed ratiometric AgNP test system. The triplex system shown here is based on two targeting peptides: RPARPAR and SGKRK, and two biological targets: NRP-1 and p32. M21 cells express cell surface p32, whereas PPC-1 cells express both p32 and NRP-1 on the cell surface. Control biotin-AgNPs do not bind to either cell line and serve as a negative control. When an input of three different AgNPs is applied to the cells, their cell binding and uptake pattern will correlate with accessible cell surface receptor expression **(II)**.

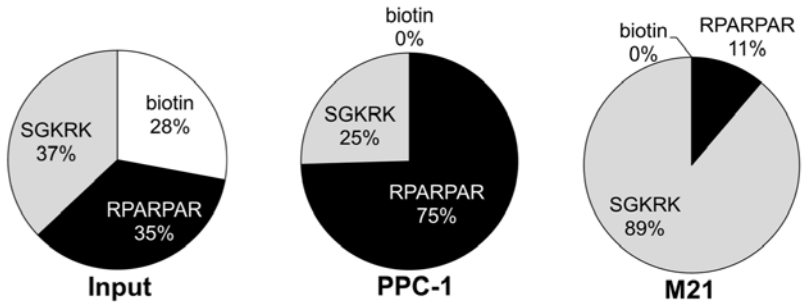

FIGURE 22: Isotopic multiplexing of AgNP binding and internalization into M21 and PPC-1 cells. Cells incubated with isotopically coded AgNPs (R-107AgNPs, K-109AgNPs, B-wtAg-PdNPs), followed by etching to remove the extracellular nanoparticles and quantification of the internalized nanoparticles by ICP-MS. PPC-1 cells demonstrated preferential uptake of R-AgNPs and M21 cells took up mainly K-AgNPs (n = 3) **(II)**.

5.6 *In vivo* application of isotopic targeted silver nanoparticles (III)

To test the application of isotopic AgNPs *in vivo*, two targets were chosen: healthy lung and brain. Both targets have a known homing peptide: RPARPAR [Teesalu et al., 2009] and CAGALCY [Fan et al., 2007] respectively. RPARPAR homes to NRP-1 expressing areas in the vascular bed of the lungs, whereas the receptor for CAGALCY is not yet known. The AgNPs were used in a duplex fashion with 107Ag particles being conjugated with the biotinylated peptide of interest, and 109Ag particles serving as an internal control.

5.6.1 Homing analyzed by ICP-MS of whole organs (III)

Mice were injected with an equimolar mixture of peptide-107Ag and control-109Ag particles and, after 1 or 5 hours of circulation, tissues were analyzed by ICP-MS. RPARPAR-AgNPs were found in ∼9 fold greater quantity in the lungs, at the one hour time point, as compared to control, as calculated from the ratio of 107Ag to 109Ag (Figure 23 A). By five hours that difference had been reduced to ∼5 fold. CAGALCY-AgNPs were also found in greater quantity in the brain than control particles (Figure 23 B). The difference was statistically significant although not as great as seen by microscopic analysis. This is likely due to heterogeneous accumulation patterns, and inadvertent bias in imaging areas with larger accumulation of CAGALCY-AgNPs, *versus* taking an average of a whole brain lysate.

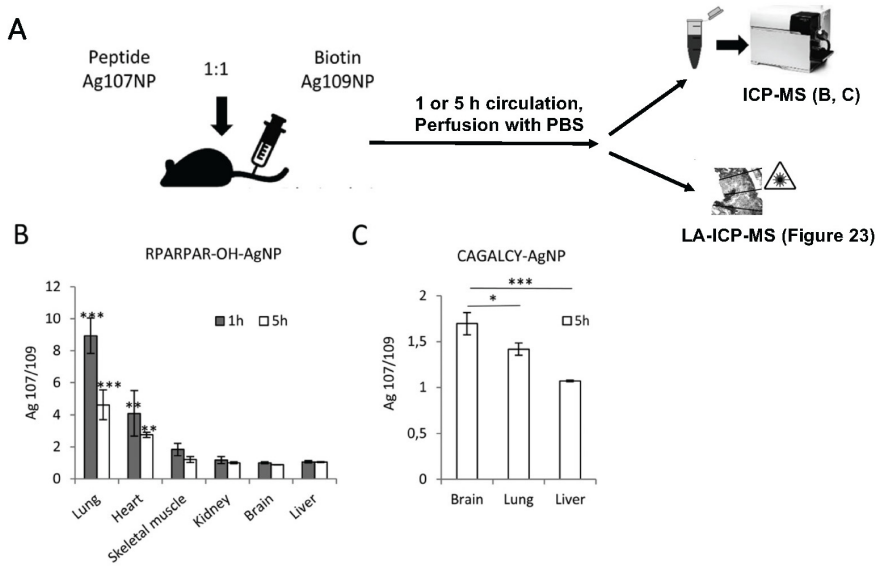

FIGURE 23: ICP-MS analysis of tissue distribution of homing peptide-functionalized AgNPs. (A) Outline of the ICP-MS ratiometric homing experiments. Balb/c mice were injected in tail vein with an equimolar mix of peptide-AgNPs (Ag107) and biotin-AgNPs (Ag109) in 200 μL PBS. 1 h or 5 h post *i.v.* administration, the animals were perfused with 15 mL PBS to remove free plasma AgNPs, and the organs of interest were snap-frozen. Tissues were subjected to a HNO_3/ H_2O_2 extraction protocol for ICP-MS, or cryosectioned for laser ablation ICP-MS (LA-ICP-MS). (B) ICP-MS analysis of tissue distribution of RPARPAR-OH-AgNPs after 1 or 5 h of circulation. Data represent mean values ± SD (n = 3). (C) ICP-MS-based analysis of tissue distribution of CAGALCY AgNPs. Balb/c mice were intravenously injected with an equimolar mixture of targeted CAGALCY AgNPs and biotin-AgNPs. After 5-h circulation the animals were perfused with PBS, and the extracts of organs were subjected to ICP-MS to for relative quantification of silver isotopes. Data represent mean ± SD (n = 3), *** $p < 0.001$, ** $p < 0.01$, * $p < 0.05$, (adapted from **III**).

5.6.2 Spatial homing analyzed by LA-ICP-MS (III)

Laser ablation (LA) ICP-MS was tested next to study heterogeneous accumulation patterns in target tissues. Experimental conditions were the same as previously, except instead of producing a whole tissue lysate, 30 μm sections were cut. The results showed heterogenous accumulation of RPARPAR-AgNPs: more in vascularized areas than non-vascular (Figure 24). When liver sections were analyzed, no heterogeneity was found. Quantifying an avarage of ablation paths showed a ∼6-fold greater RPARPAR-AgNP accumulation in the lung, similar to the 9-fold number found for whole tissue lysate. The liver had a ratio of ∼1 for both types of analysis as expected from non-targeted accumulation. The combination of the two

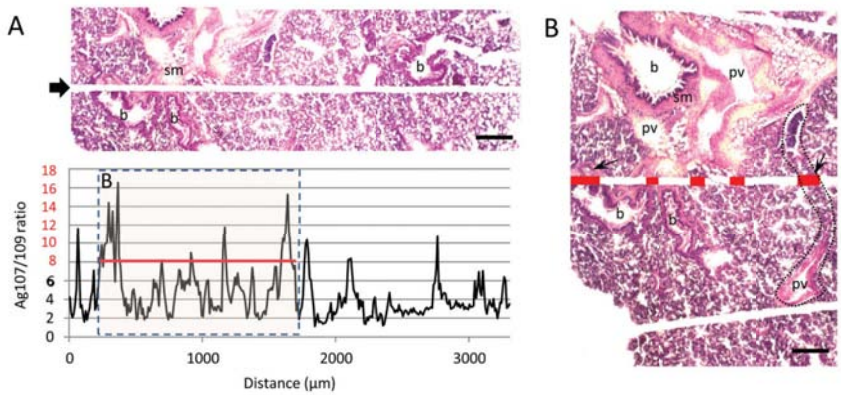

FIGURE 24: Ratiometric LA-ICP-MS profiling on sections of lung. (A) Balb/c mice were injected *i.v.* with 200 μL of a mixture of RPARPAR-OH-107AgNPs and control biotin-109AgNPs. At 5-h time point, tissues were snap-frozen, sectioned at 30 μm, and subjected to 40 μm line scans using a Cetac LSX-213 G2+ laser ablation system. Hematoxylin-eosin staining of a lung cryosection used for LA-ICP-MS. The laser ablation path is indicated by arrow. Note the microanatomical heterogenity of the lung section. The region of the graph indicated by the dashed box and pink shading correspond to the inset showing the laser ablation path in panel B. (B) Areas along the ablation path with 107Ag/109Ag $>$ 9 are indicated in red. Elevated 107Ag/109Ag ratios are associated with vascular and bronchial structures: b = bronchiole; sm = smooth muscle; pv = pulmonary vein. Data are representative of 16 laser ablation paths. Scale bars: A, 200 μm; B, 100 μm **(III)**.

types of ICP-MS allows for versatility in studying AgNP targeting for an entire tissue or discrete regions in the tissue.

5.7 Therapeutic nanoparticles (V)

The end goal of peptide-targeted nanoparticles is to treat cancer in patients. To that end, AgNPs have been developed further (in unpublished work) to carry the drug monomethyl auristatin E (MMAE), a very potent substance used clinically only in antibody-drug-conjugate form. So far, *in vitro* results show a selective killing of targeted PPC-1 cells by MMAE-RPARPAR-AgNPs *versus* untargeted M21 cells. While these results are preliminary they are promising enough to warrant further studies and *in vivo* development.

An example of therapeutic nanoparticles already working in cancer treatment is found in paper V [Simón Gracia et al., 2016a]. Polymer NPs, polymersomes, were loaded with paclitaxel to treat MKN-45P peritoneal cancer in mice and found to be

more effective than paclitaxel alone or paclitaxel in clinically approved nanoparticle formulation (Abraxane^{TM}). The polymersome platform has since been developed further to include peptide targeting as well, to improved effect [Simón Gracia et al., 2016b].

6. Summary and conclusions

This thesis describes the development of a silver nanoparticle (AgNP) platform for use in cancer research. The nanoparticles were intended to function as synthetic alternatives to the bacteriophages used in the phage display discovery of targeting peptides. The AgNPs would also model cancer nanotherapeutics and have potential applications as cancer imaging agents and drug delivery vehicles. The goals were to synthesize silver cores of various size and composition and to coat them in a biocompatible way. The polymer and protein coating was intended to enable the conjugation of dyes and of the targeting peptides. The AgNPs would work as nanoprobes: trackable by microscopy and flow cytometry. The AgNPs should work *in vitro* as well as *in vivo*. Used *in vivo* they should be able to home to target organs or tumors and be visualized in tissue sections. Ideally the AgNPs could be dissolved to enable distinction between particles inside or outside a cell, something that is lacking in most nanoprobes. A further goal of the research was to develop the AgNPs beyond optical detection techniques, which are only semi-quantitative, into probes that can be quantified by mass spectrometry.

AgNPs were synthesized and conjugated with targeting peptides and fluorescent dyes. Their silver cores enhance fluorescent dyes and effectively scatter light for darkfield microscopy as well as having a high extinction coefficient for UV-vis detection. A biocompatible *etch* solution was developed, to dissolve the AgNPs, to facilitate distinction between internalized *versus* extracellular particles. A set of isotopically distinguishable AgNPs was developed for use with quantitative inductively coupled plasma mass spectrometry (ICP-MS). These AgNPs were used in multiplexed format to evaluate surface expression of targeting receptors in order to phenotype cancer cells. They were also used in duplex to evaluate peptide-AgNP homing *in vivo* in an internally controlled manner. In addition to platform development, a new tumor homing peptide was evaluated using the silver nanoparticles.

The accomplished goals were as follows:

1. AgNPs of different sizes (20–70 nm) were synthesized and functionalized with a biocompatible coating for dye and peptide conjugation.

2. AgNPs with isotopically unique cores were developed. The nanoparticles could be distinguished and quantified by ICP-MS.

3. AgNPs were coupled with dyes and targeting peptides to bind and internalize into targeted cells. The nanoprobes were detectable with fluorescence microscopy and flow cytometry. The extracellular fraction of particles was

dissolved by a novel etching solution that does not pass through the cell membrane.

4. AgNPs were used with fluorescent dyes and homing peptides to target organs and tumors *in vivo*. AgNP detection was eased by their enhancement of fluorescent dyes and their visualization by silver staining of sections. AgNPs remaining in circulation were successfully etched.

5. Isotopic AgNPs were used with two targeting peptides (RPARPAR target NRP-1, GKRK target p32) and an untargeted control to bind to and internalize into cancer cells. ICP-MS analysis was successfully able to detect the expected AgNPs based on cell surface receptor expression, proving the applicability of the AgNPs for cell phenotyping.

6. A duplex system of isotopic AgNPs was used to demonstrate internally controlled peptide-targeted AgNP homing *in vivo*. Lung and brain were targeted with RPARPAR and CAGALCY peptide-AgNPs respectively. ICP-MS was able to quantify homing in target organ lysate and spatial homing by LA-ICP-MS.

Bibliography

Abraxane website [2017]. `abraxane.com`. Accessed: 2017-08-17.

Agemy, L., Friedmann-Morvinski, D., Kotamraju, V. R., Roth, L., Sugahara, K. N., Girard, O. M., Mattrey, R. F., Verma, I. M. and Ruoslahti, E. [2011]. Targeted nanoparticle enhanced proapoptotic peptide as potential therapy for glioblastoma, *Proceedings of the National Academy of Sciences* **108**(42): 17450–17455.

Agemy, L., Kotamraju, V. R., Friedmann-Morvinski, D., Sharma, S., Sugahara, K. N. and Ruoslahti, E. [2013]. Proapoptotic peptide-mediated cancer therapy targeted to cell surface p32, *Molecular Therapy* **21**(12): 2195–2204.

Agilent [2015]. *Agilent 8800 ICP-QQQ Application Handbook*, 2nd edn, Agilent.

Ahamed, M., AlSalhi, M. S. and Siddiqui, M. [2010]. Silver nanoparticle applications and human health, *Clinica Chimica Acta* **411**(23): 1841 – 1848.

Albanese, A., Tang, P. S. and Chan, W. C. [2012]. The effect of nanoparticle size, shape, and surface chemistry on biological systems, *Annual Review of Biomedical Engineering* **14**(1): 1–16.

Alberici, L., Roth, L., Sugahara, K. N., Agemy, L., Kotamraju, V. R., Teesalu, T., Bordignon, C., Traversari, C., Rizzardi, G.-P. and Ruoslahti, E. [2013]. De novo design of a tumor-penetrating peptide, *Cancer Research* **73**(2): 804–812.

Amamoto, R., Yagi, M., Song, Y., Oda, Y., Tsuneyoshi, M., Naito, S., Yokomizo, A., Kuroiwa, K., Tokunaga, S., Kato, S., Hiura, H., Samori, T., Kang, D. and Uchiumi, T. [2011]. Mitochondrial p32/C1QBP is highly expressed in prostate cancer and is associated with shorter prostate-specific antigen relapse time after radical prostatectomy, *Cancer Science* **102**(3): 639–647.

Arap, W., Haedicke, W., Bernasconi, M., Kain, R., Rajotte, D., Krajewski, S., Ellerby, H. M., Bredesen, D. E., Pasqualini, R. and Ruoslahti, E. [2002]. Targeting the prostate for destruction through a vascular address, *Proceedings of the National Academy of Sciences* **99**(3): 1527–1531.

Arap, W., Pasqualini, R. and Ruoslahti, E. [1998]. Cancer treatment by targeted drug delivery to tumor vasculature in a mouse model, *Science* **279**(5349): 377–380.

Bastos, V., de Oliveira, J. F., Brown, D., Jonhston, H., Malheiro, E., da Silva, A. D., Duarte, I., Santos, C. and Oliveira, H. [2016]. The influence of citrate or PEG coating on silver nanoparticle toxicity to a human keratinocyte cell line, *Toxicology Letters* **249**: 29 – 41.

Bastos, V., de Oliveira, J. M. F., Carrola, J., da Silva, A. L. D., Duarte, I. F., Santos, C. and Oliveira, H. [2017]. Coating independent cytotoxicity of citrate- and peg-coated silver nanoparticles on a human hepatoma cell line, *Journal of Environmental Sciences* **51**: 191 – 201.

Beer, C., Foldbjerg, R., Hayashi, Y., Sutherland, D. S. and Autrup, H. [2012]. Toxicity of silver nanoparticles – Nanoparticle or silver ion?, *Toxicology Letters* **208**(3): 286 – 292.

Brattain, M. G., Strobel-Stevens, J., Fine, D., Webb, M. and Sarrif, A. M. [1980]. Establishment of mouse colonic carcinoma cell lines with different metastatic properties, *Cancer Research* **40**(7): 2142–2146.

Braun, G. B., Friman, T., Pang, H.-B., Pallaoro, A., de Mendoza, T. H., Willmore, A.-M. A., Kotamraju, V. R., Mann, A. P., She, Z.-G., Sugahara, K. N., Reich, N. O., Teesalu, T. and Ruoslahti, E. [2014]. Etchable plasmonic nanoparticle probes to image and quantify cellular internalization, *Nature Materials* **13**(9): 904–911.

Braun, G. B., Lee, S. J., Laurence, T., Fera, N., Fabris, L., Bazan, G. C., Moskovits, M. and Reich, N. O. [2009]. Generalized approach to sers-active nanomaterials via controlled nanoparticle linking, polymer encapsulation, and small-molecule infusion, *The Journal of Physical Chemistry C* **113**(31): 13622–13629.

Braun, G. B., Sugahara, K. N., Yu, O. M., Kotamraju, V. R., Mölder, T., Lowy, A. M., Ruoslahti, E. and Teesalu, T. [2016]. Urokinase-controlled tumor penetrating peptide, *Journal of Controlled Release* **232**: 188 – 195.

Brown, D. M. and Ruoslahti, E. [2004]. Metadherin, a cell surface protein in breast tumors that mediates lung metastasis, *Cancer Cell* **5**(4): 365 – 374.

Caballero-Díaz, E., Pfeiffer, C., Kastl, L., Rivera-Gil, P., Simonet, B., Valcárcel, M., Jiménez-Lamana, J., Laborda, F. and Parak, W. J. [2013]. The toxicity of silver nanoparticles depends on their uptake by cells and thus on their surface chemistry, *Particle & Particle Systems Characterization* **30**(12): 1079–1085.

Chaudhary, B., Khaled, Y., Ammori, B. and Elkord, E. [2014]. Neuropilin 1: Function and therapeutic potential in cancer, *Cancer Immunology, Immunotherapy* **63**(2): 81 – 99.

Chauhan, V. P., Popovi , Z., Chen, O., Cui, J., Fukumura, D., Bawendi, M. G. and Jain, R. K. [2011]. Fluorescent nanorods and nanospheres for real-time in vivo probing of nanoparticle shape-dependent tumor penetration, *Angewandte Chemie International Edition* **50**(48): 11417–11420.

Choi, K. Y., Liu, G., Lee, S. and Chen, X. [2012]. Theranostic nanoplatforms for simultaneous cancer imaging and therapy: current approaches and future perspectives, *Nanoscale* **4**: 330–342.

Commissioner of Food and Drugs [2007]. Nanotechnology task force report 2007, *Technical report*, U.S. Food and Drug Administration.

CovaChem [2017]. Sulfo-NHS and NHS Esters in Protein Chemistry, `covachem.com`. Accessed: 2017-08-17.

Dadosh, T. [2009]. Synthesis of uniform silver nanoparticles with a controllable size, *Materials Letters* **63**(26): 2236 – 2238.

Doxil website [2017]. `doxil.com`. Accessed: 2017-08-17.

Dubree, N. J. P., Artis, D. R., Castanedo, G., Marsters, J., Sutherlin, D., Caris, L., Clark, K., Keating, S. M., Beresini, M. H., Chiu, H., Fong, S., Lowman, H. B., Skelton, N. J. and Jackson, D. Y. [2002]. Selective $\alpha 4\beta 7$ integrin antagonists and their potential as antiinflammatory agents, *Journal of Medicinal Chemistry* **45**(16): 3451–3457.

Fan, X., Venegas, R., Fey, R., van der Heyde, H., Bernard, M. A., Lazarides, E. and Woods, C. M. [2007]. An in vivo approach to structure activity relationship analysis of peptide ligands, *Pharmaceutical Research* **24**(5): 868–879.

Fogal, V., Richardson, A. D., Karmali, P. P., Sche er, I. E., Smith, J. W. and Ruoslahti, E. [2010]. Mitochondrial p32 protein is a critical regulator of tumor metabolism via maintenance of oxidative phosphorylation, *Molecular and Cellular Biology* **30**(6): 1303–1318.

Fogal, V., Zhang, L., Krajewski, S. and Ruoslahti, E. [2008]. Mitochondrial/Cell-Surface Protein p32/gC1qR as a Molecular Target in Tumor Cells and Tumor Stroma, *Cancer Research* **68**(17): 7210–7218.

Gabizon, A., Catane, R., Uziely, B., Kaufman, B., Safra, T., Cohen, R., Martin, F., Huang, A. and Barenholz, Y. [1994]. Prolonged circulation time and enhanced accumulation in malignant exudates of doxorubicin encapsulated in polyethylene-glycol coated liposomes, *Cancer Research* **54**(4): 987–992.

Garay, R. P., El-Gewely, R., Armstrong, J. K., Garratty, G. and Richette, P. [2012]. Antibodies against polyethylene glycol in healthy subjects and in patients treated with peg-conjugated agents, *Expert Opinion on Drug Delivery* **9**(11): 1319–1323.

Ghebrehiwet, B., Lim, B. L., Peerschke, E. I., Willis, A. C. and Reid, K. B. [1994]. Isolation, cDNA cloning, and overexpression of a 33-kD cell surface glycoprotein that binds to the globular "heads" of C1q, *Journal of Experimental Medicine* **179**(6): 1809–1821.

Ghebrehiwet, B. and Peerschke, E. I. [2004]. cC1q-R (calreticulin) and gC1q-R/p33: ubiquitously expressed multi-ligand binding cellular proteins involved in inflammation and infection, *Molecular Immunology* **41**(2–3): 173 – 183.

Gradishar, W. J., Tjulandin, S., Davidson, N., Shaw, H., Desai, N., Bhar, P., Hawkins, M. and O'Shaughnessy, J. [2005]. Phase III Trial of Nanoparticle Albumin-Bound Paclitaxel Compared With Polyethylated Castor Oil-Based Paclitaxel in Women With Breast Cancer, *Journal of Clinical Oncology* **23**(31): 7794–7803.

Green, M. R., Manikhas, G. M., Orlov, S., Afanasyev, B., Makhson, A. M., Bhar, P. and Hawkins, M. J. [2006]. Abraxane®, a novel cremophor®-free, albumin-bound particle form of paclitaxel for the treatment of advanced non-small-cell lung cancer, *Annals of Oncology* **17**(8): 1263–1268.

Guo, W.-X., Ghebrehiwet, B., Weksler, B., Schweitzer, K. and Peerschke, E. I. [1999]. Up-regulation of endothelial cell binding proteins/receptors for complement component {C1q} by inflammatory cytokines, *Journal of Laboratory and Clinical Medicine* **133**(6): 541 – 550.

Gurrath, M., Müller, G., Kessler, H., Aumailley, M. and Timpl, R. [1992]. Conformation/activity studies of rationally designed potent anti-adhesive RGD peptides, *European Journal of Biochemistry* **210**(3): 911–921.

Guy, C. T., Cardiff, R. D. and Muller, W. J. [1992]. Induction of mammary tumors by expression of polyomavirus middle t oncogene: a transgenic mouse model for metastatic disease., *Mol Cell Biol* **12**(3): 954–961.

Hamzah, J., Kotamraju, V. R., Seo, J. W., Agemy, L., Fogal, V., Mahakian, L. M., Peters, D., Roth, L., Gagnon, M. K. J., Ferrara, K. W. and Ruoslahti, E. [2011]. Specific penetration and accumulation of a homing peptide within atherosclerotic plaques of apolipoprotein e-deficient mice, *Proceedings of the National Academy of Sciences* **108**(17): 7154–7159.

Hoffman, J. A., Giraudo, E., Singh, M., Zhang, L., Inoue, M., Porkka, K., Hanahan, D. and Ruoslahti, E. [2003]. Progressive vascular changes in a transgenic mouse model of squamous cell carcinoma, *Cancer Cell* **4**(5): 383 – 391.

Hong, T.-M., Chen, Y.-L., Wu, Y.-Y., Yuan, A., Chao, Y.-C., Chung, Y.-C., Wu, M.-H., Yang, S.-C., Pan, S.-H., Shih, J.-Y., Chan, W.-K. and Yang, P.-C. [2007]. Targeting neuropilin 1 as an antitumor strategy in lung cancer, *Clinical Cancer Research* **13**(16): 4759–4768.

Hu, C.-M. J., Zhang, L., Aryal, S., Cheung, C., Fang, R. H. and Zhang, L. [2011]. Erythrocyte membrane-camouflaged polymeric nanoparticles as a biomimetic delivery platform, *Proceedings of the National Academy of Sciences* **108**(27): 10980–10985.

Hunt, H., Simón-Gracia, L., Tobi, A., Kotamraju, V. R., Sharma, S., Nigul, M., Sugahara, K. N., Ruoslahti, E. and Teesalu, T. [2017]. Targeting of p32 in peritoneal carcinomatosis with intraperitoneal linTT1 peptide-guided pro-apoptotic nanoparticles, *Journal of Controlled Release* **260**: 142 – 153.

Ikemoto, H., Lingasamy, P., Willmore, A.-M. A., Hunt, H., Kurm, K., Tammik, O., Scodeller, P., Simón Gracia, L., Kotamraju, V. R., Lowy, A. M., Sugahara, K. N. and Teesalu, T. [2017]. Hyaluronan-binding peptide for targeting peritoneal carcinomatosis, *Tumor Biology* **39**(5).

Jokerst, J. V., Lobovkina, T., Zare, R. N. and Gambhir, S. S. [2011]. Nanoparticle pegylation for imaging and therapy, *Nanomedicine* **6**(4): 715–728.

Järvinen, T. A. and Ruoslahti, E. [2007]. Molecular changes in the vasculature of injured tissues, *The American Journal of Pathology* **171**(2): 702 – 711.

Karjalainen, K., Jaalouk, D. E., Bueso-Ramos, C. E., Zurita, A. J., Kuniyasu, A., Eckhardt, B. L., Marini, F. C., Lichtiger, B., O'Brien, S., Kantarjian, H. M., Cortes, J. E., Koivunen, E., Arap, W. and Pasqualini, R. [2011]. Targeting neuropilin-1 in human leukemia and lymphoma, *Blood* **117**(3): 920–927.

Karmali, P. P., Kotamraju, V. R., Kastantin, M., Black, M., Missirlis, D., Tirrell, M. and Ruoslahti, E. [2009]. Targeting of albumin-embedded paclitaxel nanoparticles to tumors, *Nanomedicine: Nanotechnology, Biology and Medicine* **5**(1): 73 – 82.

King, A., Ndifon, C., Lui, S., Widdows, K., Kotamraju, V. R., Agemy, L., Teesalu, T., Glazier, J. D., Cellesi, F., Tirelli, N., Aplin, J. D., Ruoslahti, E. and Harris, L. K. [2016]. Tumor-homing peptides as tools for targeted delivery of payloads to the placenta, *Science Advances* **2**(5).

Koivunen, E., Arap, W., Valtanen, H., Rainisalo, A., Medina, O. P., Heikkila, P., Kantor, C., Gahmberg, C. G., Salo, T., Konttinen, Y. T., Sorsa, T., Ruoslahti, E. and Pasqualini, R. [1999]. Tumor targeting with a selective gelatinase inhibitor, *Nat Biotech* **17**(8): 768–774.

Koivunen, E., Wang, B. and Ruoslahti, E. [1994]. Isolation of a highly specific ligand for the alpha 5 beta 1 integrin from a phage display library, *The Journal of Cell Biology* **124**(3): 373–380.

Laakkonen, P., Porkka, K., Hoffman, J. A. and Ruoslahti, E. [2002]. A tumor-homing peptide with a targeting specificity related to lymphatic vessels, *Nat Med* **8**(7): 751–755.

Lakowicz, J. R. [2005]. Radiative decay engineering 5: metal-enhanced fluorescence and plasmon emission, *Analytical Biochemistry* **337**(2): 171 – 194.

Lambert, S., Bouttier, M., Vassy, R., Seigneuret, M., Petrow-Sadowski, C., Janvier, S., Heveker, N., Ruscetti, F. W., Perret, G., Jones, K. S. and Pique, C. [2009]. Htlv-1 uses hspg and neuropilin-1 for entry by molecular mimicry of vegf165, *Blood* **113**(21): 5176–5185.

Latil, A., Bièche, I., Pesche, S., Valéri, A., Fournier, G., Cussenot, O. and Lidereau, R. [2000]. Vegf overexpression in clinically localized prostate tumors and neuropilin-1 overexpression in metastatic forms, *International Journal of Cancer* **89**(2): 167–171.

Lee, P. C. and Meisel, D. [1982]. Adsorption and surface-enhanced Raman of dyes on silver and gold sols, *The Journal of Physical Chemistry* **86**(17): 3391–3395.

Liu, R., Li, X., Xiao, W. and Lam, K. S. [2017]. Tumor-targeting peptides from combinatorial libraries, *Advanced Drug Delivery Reviews* **110**: 13 – 37. Peptides and Peptide Conjugates in Medicine.

Longmire, M., Choyke, P. L. and Kobayashi, H. [2008]. Clearance properties of nano-sized particles and molecules as imaging agents: Considerations and caveats, *Nanomedicine (Lond)* **3**(5): 703–717.

Lynch, I. and Dawson, K. A. [2008]. Protein-nanoparticle interactions, *Nano Today* **3**(1-2): 40–47.

Mahmoudi, M., Lynch, I., Ejtehadi, M. R., Monopoli, M. P., Bombelli, F. B. and Laurent, S. [2011]. Protein-nanoparticle interactions: Opportunities and challenges, *Chemical Reviews* **111**(9): 5610–5637.

Mann, A. P., Scodeller, P., Hussain, S., Joo, J., Kwon, E., Braun, G. B., Mölder, T., She, Z.-G., Kotamraju, V. R., Ranscht, B., Krajewski, S., Teesalu, T., Bhatia, S., Sailor, M. J. and Ruoslahti, E. [2016]. A peptide for targeted, systemic delivery of imaging and therapeutic compounds into acute brain injuries, *Nature Communications* **7**: 11980.

Matsumura, Y. and Maeda, H. [1986]. A new concept for macromolecular therapeutics in cancer chemotherapy: Mechanism of tumoritropic accumulation of proteins and the antitumor agent smancs, *Cancer Research* **46**(12 Part 1): 6387–6392.

Miyagi, M., Aoyagi, K., Kato, S. and Shirouzu, K. [2007]. The timp-1 gene transferred through adenovirus mediation shows a suppressive effect on peritoneal metastases from gastric cancer, *International Journal of Clinical Oncology* **12**(1): 17–24.

Mutch, S. and University of Washington [2009]. *Method for Quanti cation of Low Copy Number Proteins Using Single Molecule Spectroscopy Applied to Synaptic Vesicle Membrane Proteins*, University of Washington.

Nasarre, C., Roth, M., Jacob, L., Roth, L., Koncina, E., Thien, A., Labourdette, G., Poulet, P., Hubert, P., Cremel, G., Roussel, G., Aunis, D. and Bagnard, D. [2010]. Peptide-based interference of the transmembrane domain of neuropilin-1 inhibits glioma growth in vivo, *Oncogene* **29**(16): 2381–2392.

O'Brien, M. E. R., Wigler, N., Inbar, M., Rosso, R., Grischke, E., Santoro, A., Catane, R., Kieback, D. G., Tomczak, P., Ackland, S. P., Orlandi, F., Mellars, L., Alland, L. and Tendler, C. [2004]. Reduced cardiotoxicity and comparable efficacy in a phase III trial of pegylated liposomal doxorubicin HCl (CAELYX /Doxil) versus conventional doxorubicin for first-line treatment of metastatic breast cancer, *Annals of Oncology* **15**(3): 440–449.

Ong, C., Lim, J., Ng, C.-T., Li, J., Yung, L.-Y. and Bay, B.-H. [2013]. Silver nanoparticles in cancer: Therapeutic efficacy and toxicity, *Current Medicinal Chemistry* **20**(6): 772–781.

Paasonen, L., Sharma, S., Braun, G. B., Kotamraju, V. R., Chung, T. D. Y., She, Z.-G., Sugahara, K. N., Yliperttula, M., Wu, B., Pellecchia, M., Ruoslahti, E. and Teesalu, T. [2016]. New p32/gC1qR ligands for targeted tumor drug delivery, *ChemBioChem* **17**(7): 570–575.

Pang, H.-B., Braun, G. B., Friman, T., Aza-Blanc, P., Ruidiaz, M. E., Sugahara, K. N., Teesalu, T. and Ruoslahti, E. [2014b]. An endocytosis pathway initiated through neuropilin-1 and regulated by nutrient availability, *Nature Communications* **5**: 4904.

Pang, H.-B., Braun, G. B., She, Z.-G., Kotamraju, V. R., Sugahara, K. N., Teesalu, T. and Ruoslahti, E. [2014a]. A free cysteine prolongs the half-life of a homing peptide and improves its tumor-penetrating activity, *J Control Release* **175**: 48–53.

Park, J.-H., von Maltzahn, G., Zhang, L., Schwartz, M. P., Ruoslahti, E., Bhatia, S. N. and Sailor, M. J. [2008]. Magnetic iron oxide nanoworms for tumor targeting and imaging, *Advanced Materials* **20**(9): 1630–1635.

Parodi, A., Quattrocchi, N., van de Ven, A. L., Chiappini, C., Evangelopoulos, M., Martinez, J. O., Brown, B. S., Khaled, S. Z., Yazdi, I. K., Enzo, M. V., Isenhart, L., Ferrari, M. and Tasciotti, E. [2013]. Synthetic nanoparticles functionalized with biomimetic leukocyte membranes possess cell-like functions, *Nat Nano* **8**(1): 61–68.

Pasqualini, R. and Ruoslahti, E. [1996]. Organ targeting *in vivo* using phage display peptide libraries, *Nature* **380**: 364–366.

Petersen, G. H., Alzghari, S. K., Chee, W., Sankari, S. S. and La-Beck, N. M. [2016]. Meta-analysis of clinical and preclinical studies comparing the anticancer efficacy of liposomal versus conventional non-liposomal doxorubicin, *Journal of Controlled Release* **232**: 255 – 264.

Pierce Biotechnology [2013]. *NeutrAvidin Biotin-Binding Protein*, 0443.6 edn, Pierce Biotechnology, 3747 N. Meridian Road Rockford, lL 61105 USA.

Pierschbacher, M. and Ruoslahti, E. [1984]. Cell attachment activity of fibronectin can be duplicated by small synthetic fragments of the molecule, *Nature* **309**(5963): 30–33.

Pilch, J., Brown, D. M., Komatsu, M., Järvinen, T. A. H., Yang, M., Peters, D., Hoffman, R. M. and Ruoslahti, E. [2006]. Peptides selected for binding to clotted plasma accumulate in tumor stroma and wounds, *Proceedings of the National Academy of Sciences of the United States of America* **103**(8): 2800–2804.

Prud'homme, G. and Glinka, Y. [2012]. Neuropilins are multifunctional coreceptors involved in tumor initiation, growth, metastasis and immunity, *Oncotarget* **3**(9).

Pulaski, B. A. and Ostrand-Rosenberg, S. [2001]. *Mouse 4T1 Breast Tumor Model*, John Wiley & Sons, Inc.

Ramanathan, R. K., Korn, R. L., Sachdev, J. C., Fetterly, G. J., Marceau, K., Marsh, V., Neil, J. M., Newbold, R. G., Raghunand, N., Prey, J., Klinz, S. G., Bayever, E. and Fitzgerald, J. B. [2014]. Abstract CT224: Pilot study in patients with advanced solid tumors to evaluate feasibility of ferumoxytol (FMX) as tumor imaging agent prior to MM-398, a nanoliposomal irinotecan (nal-IRI), *Cancer Research* **74**(19 Supplement): CT224–CT224.

Roth, L., Agemy, L., Kotamraju, V. R., Braun, G., Teesalu, T., Sugahara, K. N., Hamzah, J. and Ruoslahti, E. [2012]. Transtumoral targeting enabled by a novel neuropilin-binding peptide, *Oncogene* **31**(33): 3754–3763.

Roth, L., Prahst, C., Ruckdeschel, T., Savant, S., Weström, S., Fantin, A., Riedel, M., Héroult, M., Ruhrberg, C. and Augustin, H. G. [2016]. Neuropilin-1 mediates vascular permeability independently of vascular endothelial growth factor receptor-2 activation, *Science Signaling* **9**(425): ra42–ra42.

Ruoslahti, E. [2002]. Specialization of tumour vasculature, *Nat Rev Cancer* **2**(2): 83–90.

Ruoslahti, E. [2004]. Vascular zip codes in angiogenesis and metastasis, *Biochemical Society Transactions* **32**(3): 397–402.

Shi, J., Kantoff, P. W., Wooster, R. and Farokhzad, O. C. [2017]. Cancer nanomedicine: progress, challenges and opportunities, *Nat Rev Cancer* **17**(1): 20–37.

Simberg, D., Duza, T., Park, J. H., Essler, M., Pilch, J., Zhang, L., Derfus, A. M., Yang, M., Hoffman, R. M., Bhatia, S., Sailor, M. J. and Ruoslahti, E. [2007]. Biomimetic amplification of nanoparticle homing to tumors, *Proceedings of the National Academy of Sciences* **104**(3): 932–936.

Simón Gracia, L., Hunt, H., Scodeller, P. D., Gaitzsch, J., Braun, G. B., Willmore, A.-M. A., Ruoslahti, E., Battaglia, G. and Teesalu, T. [2016a]. Paclitaxel-loaded polymersomes for enhanced intraperitoneal chemotherapy, *Molecular Cancer Therapeutics* **15**(4): 670–679.

Simón Gracia, L., Hunt, H., Scodeller, P., Gaitzsch, J., Kotamraju, V. R., Sugahara, K. N., Tammik, O., Ruoslahti, E., Battaglia, G. and Teesalu, T. [2016b]. iRGD peptide conjugation potentiates intraperitoneal tumor delivery of paclitaxel with polymersomes, *Biomaterials* **104**: 247 – 257.

Skrabalak, S. E., Au, L., Li, X. and Xia, Y. [2007]. Facile synthesis of Ag nanocubes and Au nanocages, *Nat. Protocols* **2**(9): 2182–2190.

Smith, G. P. and Petrenko, V. A. [1997]. Phage display, *Chemical Reviews* **97**(2): 391–410.

Sperling, R. A. and Parak, W. J. [2010]. Surface modification, functionalization and bioconjugation of colloidal inorganic nanoparticles, *Philosophical Transactions of the Royal Society of London A: Mathematical, Physical and Engineering Sciences* **368**(1915): 1333–1383.

Stephenson, J. M., Banerjee, S., Saxena, N. K., Cherian, R. and Banerjee, S. K. [2002]. Neuropilin-1 is differentially expressed in myoepithelial cells and vascular smooth muscle cells in preneoplastic and neoplastic human breast: A possible marker for the progression of breast cancer, *International Journal of Cancer* **101**(5): 409–414.

Storz, P., Hausser, A., Link, G., Dedio, J., Ghebrehiwet, B., Pfizenmaier, K. and Johannes, F.-J. [2000]. Protein kinase c μ is regulated by the multifunctional chaperon protein p32, *Journal of Biological Chemistry* **275**(32): 24601–24607.

Straume, O. and Akslen, L. A. [2003]. Increased expression of VEGF-receptors (FLT-1, KDR, NRP-1) and thrombospondin-1 is associated with glomeruloid microvascular proliferation, an aggressive angiogenic phenotype, in malignant melanoma, *Angiogenesis* **6**(4): 295–301.

Sugahara, K. N., Teesalu, T., Karmali, P. P., Kotamraju, V. R., Agemy, L., Girard, O. M., Hanahan, D., Mattrey, R. F. and Ruoslahti, E. [2009]. Tissue-penetrating delivery of compounds and nanoparticles into tumors., *Cancer Cell* **16**(6): 510–520.

Sugahara, K. N., Teesalu, T., Karmali, P. P., Kotamraju, V. R., Agemy, L., Greenwald, D. R. and Ruoslahti, E. [2010]. Coadministration of a tumor-penetrating peptide enhances the efficacy of cancer drugs., *Science* **328**(5981): 1031–1035.

Sun, Y. and Xia, Y. [2003]. Gold and silver nanoparticles: A class of chromophores with colors tunable in the range from 400 to 750 nm, *Analyst* **128**: 686–691.

Teesalu, T., Sugahara, K. N., Kotamraju, V. R. and Ruoslahti, E. [2009]. C-end rule peptides mediate neuropilin-1-dependent cell, vascular, and tissue penetration., *Proc. Natl. Acad. Sci. USA* **106**(38): 16157–16162.

Teesalu, T., Sugahara, K. N. and Ruoslahti, E. [2012]. Chapter two - mapping of vascular ZIP codes by phage display, *in* K. D. Wittrup and G. L. Verdine (eds), *Protein Engineering for Therapeutics, Part B*, Vol. 503 of *Methods in Enzymology*, Academic Press, pp. 35 – 56.

Tian, J., Wong, K. K., Ho, C.-M., Lok, C.-N., Yu, W.-Y., Che, C.-M., Chiu, J.-F. and Tam, P. K. H. [2007]. Topical delivery of silver nanoparticles promotes wound healing, *ChemMedChem* **2**(1): 129–136.

Toome, K., Willmore, A.-M. A., Paiste, P., Tobi, A., Sugahara, K. N., Kirsimäe, K., Ruoslahti, E., Braun, G. B. and Teesalu, T. [2017]. Ratiometric in vivo auditioning of targeted silver nanoparticles, *Nanoscale* **9**: 10094–10100.

Uchida, M., Kosuge, H., Terashima, M., Willits, D. A., Liepold, L. O., Young, M. J., McConnell, M. V. and Douglas, T. [2011]. Protein cage nanoparticles bearing the lyp-1 peptide for enhanced imaging of macrophage-rich vascular lesions, *ACS Nano* **5**(4): 2493–2502.

van Vlerken, L. E., Vyas, T. K. and Amiji, M. M. [2007]. Poly(ethylene glycol)-modified nanocarriers for tumor-targeted and intracellular delivery, *Pharmaceutical Research* **24**(8): 1405–1414.

von Maltzahn, G., Ren, Y., Park, J.-H., Min, D.-H., Kotamraju, V. R., Jayakumar, J., Fogal, V., Sailor, M. J., Ruoslahti, E. and Bhatia, S. N. [2008]. In vivo tumor cell targeting with "click nanoparticles, *Bioconjugate Chemistry* **19**(8): 1570–1578.

Wiley, B., Sun, Y., Mayers, B. and Xia, Y. [2005]. Shape-controlled synthesis of metal nanostructures: The case of silver, *Chemistry A European Journal* **11**(2): 454–463.

Willmore, A.-M. A., Simón Gracia, L., Toome, K., Paiste, P., Kotamraju, V. R., Mölder, T., Sugahara, K. N., Ruoslahti, E., Braun, G. B. and Teesalu, T. [2016]. Targeted silver nanoparticles for ratiometric cell phenotyping, *Nanoscale* **8**: 9096–9101.

Yaqoob, U., Cao, S., Shergill, U., Jagavelu, K., Geng, Z., Yin, M., de Assuncao, T. M., Cao, Y., Szabolcs, A., Thorgeirsson, S., Schwartz, M., Yang, J. D., Ehman, R., Roberts, L., Mukhopadhyay, D. and Shah, V. H. [2012]. Neuropilin-1 stimulates tumor growth by increasing fibronectin fibril assembly in the tumor microenvironment, *Cancer Research* **72**(16): 4047–4059.

Yokoi, K., Tanei, T., Godin, B., van de Ven, A. L., Hanibuchi, M., Matsunoki, A., Alexander, J. and Ferrari, M. [2014]. Serum biomarkers for personalization of nanotherapeutics-based therapy in different tumor and organ microenvironments, *Cancer Letters* **345**(1): 48 – 55.

Zhang, F., Braun, G. B., Shi, Y., Zhang, Y., Sun, X., Reich, N. O., Zhao, D. and Stucky, G. [2010]. Fabrication of Ag@SiO2@Y2O3:Er nanostructures for bioimaging: Tuning of the upconversion fluorescence with silver nanoparticles, *Journal of the American Chemical Society* **132**(9): 2850–2851.

Zhang, L., Giraudo, E., Hoffman, J. A., Hanahan, D. and Ruoslahti, E. [2006]. Lymphatic zip codes in premalignant lesions and tumors, *Cancer Research* **66**(11): 5696–5706.

Zhang, L., Hoffman, J. A. and Ruoslahti, E. [2005]. Molecular profiling of heart endothelial cells, *Circulation* **112**(11): 1601–1611.

Zhang, P., Wang, T. and Gong, J. [2015]. Mechanistic understanding of the plasmonic enhancement for solar water splitting, *Advanced Materials* **27**(36): 5328–5342.

Summary in Estonian

Hõbeda nanoosakesed vähiuuringutes

Sissejuhatus

Vähktõve efektiivse ravi tagamine on kaasaegsele meditsiinile jätkuvalt suureks väljakutseks. Kuigi nanoravimitega on viimase 20 aasta jooksul saavutatud mõningast edu vähiravi kõrvaltoimete vähendamisel, ei ole see ravimiklass osutunud loodetud imerohuks ega suurendanud patsientide elumust. Praegu kliinilises kasutuses olevad nanoravimid akumuleeruvad kasvajalistes kudedes passiivselt. Vähirakke selektiivselt ära tundvaid nanoosakesi testitakse arvukates prekliinilistes ja kliinilistes uuringutes. Vähirakke ära tundvate moodulite lisamine terapeutilistele nanoosakestele võimaldab parandada akumulatsiooni vähikoes ning seeläbi võimaldada efektiivsemat ravi ning vähendada kõrvaltoimeid. Üks võimalus nanoosakeste suunamiseks on kasutada *in vivo* faagidisplei meetodi abil avastatud kullerpeptiidide. Selliste peptiidide avastamiseks süstitakse vähi-hiiri bakteriofaagi kattevalgul kuvatud peptiidi-raamatukogudega. Kasvajakoes üle-esindatud peptiidi-faagide sekveneerimine aitab seejärel tuvastada koeselektiivsed kullerpeptiidid. Kullerpeptiidide ja teiste nanoosakeste pinnamodifikatsioonide mõju hindamiseks oleks palju abi mudel-nanoosakeste platvormist, mida on lihtne kasutada, mikroskoopiliselt uurida ja kvantifitseerida. Kuna enamik ravimeid peavad ravitoime avaldumiseks sisenema rakku, võiks üks nanoosakeste platvormi kasulik omadus olla võimalus eristada intra- ja ekstratsellulaarseid osakesi. Hõbeda nanoosakestel (AgNP) on olemas kõik eelpool soovitud omadused. AgNP võimendavad neile kinnitatud värvainete fluorestsentsi, neil on optilisel tuvastamisel kõrge ekstinktsioonikoefitsient ning nendega on võimalik siduda lühikesi peptiide. Veelgi enam, AgNP lahustuvad kiiresti ja täielikult mittetoksilises metalse hõbeda söövituslahustis; see võimaldab rakuväliste osakeste lahustamist, mõjutamata rakusiseseid osakesi. AgNP on võimalik valmistada hõbeda puhastest isotoopidest, võimaldamaks osakeste isotoopset tuvastamist ja kvantifitseerimist massispektromeetria abil.

Töö eesmärgid

Käesoleva doktoritöö eesmärgiks oli AgNP mudel-platvormi optimiseerimine vähiuuringuteks. Uuriti AgNP rakendatavust kvantifitseeritava meetodina kullerpeptiidide koeselektiivsuse ja rakku sisenemise hindamiseks.

Töö eesmärgid olid:

1. Optimiseerida protokollid AgNP sünteesimiseks, funktsionaliseerimiseks ja analüüsiks.
2. Töötada välja meetodid AgNP sünteesimiseks puhastest hõbeda isotoopidest ning isotoopselt-kodeeritud osakeste kvantitatiivseks analüüsiks.
3. Välja töötada protokollid peptiididega suunatud fluorestseeruvate AgNP rakku sisenemise katseteks.
4. Kasutada peptiididega suunatud fluorestseeruvaid AgNP organite ja kasvajatega seondumiseks *in vivo*.
5. Kasutada kullerpeptiididega suunatud isotoopseid AgNP vähirakkude fenotüpiseerimiseks.
6. Rakendada kullerpeptiididega suunatud isotoopseid AgNP kullerpeptiidide *in vivo* valideerimiseks.

Meetodid

Töö käigus valmistati AgNP kõrge puhtusastmega komponentidest kasutades erinevaid sünteesiradu saavutamaks vajaliku suuruse ja kujuga osakesi. AgNP iseloomustamiseks kasutati nende UV-vis neeldumisspektri analüüsi ja transmissioonelektronmikroskoopiat. AgNP funktsionaliseeriti PEG-kattega ja neutravidiiniga. Osakeste pinnaga seotud neutravidiin võimaldab siduda biotinüleeritud peptiide, samas kui PEG'i vabu amiinrühmasid saab rakendada värvainete sidumiseks. Kullerpeptiididest kasutasime peamiselt NRP1-seonduvat peptiidi aminohappejärjestusega RPARPAR. Seda peptiidi kasutasime kvaliteedikontrolliks ja uute osakeste välja töötamiseks. Lisaks kasutasime p32-suunatud kullerpeptiide ja negatiivse kontrollina ilma kullerpeptiidita osakesi. Rakukatseteks kasutasime mudelina NRP1-positiivset PPC-1 eesnäärmekartsinoomi rakuliini ning NRP1-negatiivseid M21 melanoomirakke. Ekstratsellulaarsete AgNP-de lahustamiseks töötasime välja biosobiva söövituslahuse. AgNP seondumise ja rakku sisenemise hindamiseks kasutati epifluorestsents- ja konfokaal-mikroskoopiat ning voolutsütomeetriat. Fluorestsentsmärgist kandvate AgNP koedistributsiooni uuringuteks kasutati konfokaalmikroskoopiat külmlõikudel. Isotoopselt kodeeritud AgNP rakkudega seondumist ja internalisatsiooni kultiveeritud rakkudel ja distributsiooni koeproovides hinnati kvantitatiivselt kasutades induktiivsidestatud plasma massispektromeetria meetodit(ICP-MS).

Tulemused ja järeldused

1. Töötati välja tingimused 20–70 nm diameetriga, värvainete ja peptiididega funktsionaliseeritud biosobiva kattega AgNP sünteesiks.

2. Optimiseeriti tingimused isotoopselt kodeeritud AgNP sünteesiks ja ICP-MS meetodil põhinevaks kvantitatiivseks analüüsiks.

3. Töötati välja protokollid AgNP funktsionaliseerimiseks värvainete ja sihtrakke ära tundvate kullerpeptiididega, et osakesi rakendada fluorestsentsmikroskoopial ja voolutsütomeetrial põhinevates analüüsides. Töötati välja ja optimiseeriti protokollid rakuväliste AgNP lahustamiseks kasutades uudset rakumembraani mitteläbivat söövituslahust.

4. Rakendati fluorestseeruvate värvainete ja kullerpeptiididega funktsionaliseeritud AgNP *in vivo* koedistributsiooni uuringuteks.

5. Isotoopseid AgNP koos kahe sihtrakke ära tundva peptiidiga (RPARPAR seondub NRP1, GKRK p32 valguga) ja kontrollpeptiidiga kasutati *in vitro* rakukatseteks. Näitasime kasutades ICP-MS meetodit, et pinnaretseptorite ekspressiooni vastab kullerpeptiididega suunatud osakeste seondumisprofiilidele, näidates nii, et AgNP platvorm on rakendatav rakkude *in vitro* fenotüpiseerimiseks.

6. Isotoopseid AgNP kasutati koos kahe sihtmärk-kudesid ära tundva peptiidiga (RPARPAR seondub kopsukoega, GAGALCY seondub ajukoega) ja kontrollpeptiidiga. ICP-MS meetodil kvantifitseeriti kullerpeptiididega funktsionaliseeritud osakeste seondumine märklaudorgani lüsaadis ning LA-ICP-MS meetodit kasutades hinnati osakeste ruumilist jaotuvust koelõikudel

Meie töö tulemuseks on AgNP platvormi kui mudel-nanoplatvormi igakülgne optimiseerimine ja valideerimine uuringuteks kultiveeritud rakkudel ja kudedes. Selle platvormi rakendamine muudab võimalikuks afiinsus-suunatud nanoosakeste senisest efektiivsema väljatöötamise.

Acknowledgements

This work was supported by the European Union through the European Regional Development Fund (Project No. 2014-2020.4.01.15-0012), by EMBO Installation grant #2344, European Research Council starting grant GLIOMADDS from the European Regional Development Fund, Wellcome Trust International Fellowship WT095077MA, and the Valda and Bernard Õuna memorial fund.

I would like to thank my surpervisor, Tambet Teesalu, for giving me the opportunity to conduct research in the exciting, cross-disciplinary field of nanomedicine. He came to Tartu at just the right time and started the lab of cancer biology, which has been a great place to work for the past five years. Tambet has been a supportive and calm presence, guiding me to the finish line. I am grateful to my other supervisor, Gary B. Braun, who taught me everything I know about silver nanoparticles. Gary is a brilliant scientist and has been incredibly helpful even from very far away. Many thanks to Erkki Ruoslahti, and his lab members, for providing the opportunity to learn nanoparticle work at both UCSB, my *alma mater*, and in La Jolla. Erkki has given valuable feedback on ongoing research and article drafts.

Thanks to all cancer biology lab members, past and present, for making going to work a pleasure. Special thanks to Lorena for being my nanoparticle support group in Tartu; to Tarmo for teaching me cell culture and for translating; to Pille for many useful discussions on microscopy etc; and to Kadri for boldly jumping into nanoparticle work. Thanks to Päärn for being a great collaborator and making all my isotope-nanoparticle work possible; and Prof. Kirsimäe for allowing him to do it. Thanks to Rein Laiverik for teaching me TEM, and thanks to Prof. Pooga's group for the use of their TEM as well.

I would like to dedicate this work to my parents, Rein and Aino Anton, who have supported me in higher education for 16 years. My father has always emphasized education above all else and my mother flew 10 000 km back and forth to help take care of my kids so I could write. Thanks also to aunt Mare and to Krista for keeping the kids happy while mom was busy. Thanks to my family: Chris, Toomas, and Aivi for supporting me in their own ways, and for helping me keep life in perspective. Finally, I would like to thank my dear french bulldog, Tibu, who left us during the writing of this thesis. She was a great friend, unconditionally loving and crazy, and kept me company the many months that I spent stuck at home writing. She will be sorely missed.

Publications

Curriculum Vitae

Name: Anne-Mari Anton Willmore
Date of birth: 21.04.1983
Citizenship: Estonian, USA
Address: Ravila 14B, Tartu, 51014
Telephone: 737 4268
E-mail: annemw@ut.ee

Education

2011–...	University of Tartu, PhD student
2009–2010	M.Sc. *with distinction* Chemical Engineering, University College London, UK
2003–2004	Georg August Universität, Göttingen, Germany
2001–2006	B.S. Chemical Engineering, University of California, Santa Barbara, USA

Scienti c awards

2016	Valda and Bernard Õuna memorial stipend
2014	National research award for university students, 1st place

Professional employment

2012–...	University of Tartu, lab of cancer biology, lab specialist
2010–2012	Icosagen Cell Factory OÜ, protein purification process development, scientist
2008	Genentech Inc., late stage purification, intern
2007–2008	Gilead Sciences Inc., pharmaceutical release, QC analyst
2005	Genentech Inc., manufacturing science and technology, intern
2004	Henkel KGaA, phosphating process development, intern

Publications

1. Braun, G. B., Friman, T., Pang, H.-B., Pallaoro, A., de Mendoza, T. H., **Willmore, A.-M. A.**, Kotamraju, V. R., Mann, A. P., She, Z.-G., Sugahara, K. N., Reich, N. O., Teesalu, T. and Ruoslahti, E. [2014]. Etchable plasmonic nanoparticle probes to image and quantify cellular internalization, *Nature Materials*, **13**(9): 904–911.

2. Simón Gracia, L., Hunt, H., Scodeller, P. D., Gaitzsch, J., Braun, G. B., **Willmore, A.-M. A.**, Ruoslahti, E., Battaglia, G. and Teesalu, T. [2016]. Paclitaxel-loaded polymersomes for enhanced intraperitoneal chemotherapy, *Molecular Cancer Therapeutics* **15**(4): 670–679.

3. **Willmore, A.-M. A.**, Simón Gracia, L., Toome, K., Paiste, P., Kotamraju, V. R., Mölder, T., Sugahara, K. N., Ruoslahti, E., Braun, G. B. and Teesalu, T. [2016]. Targeted silver nanoparticles for ratiometric cell phenotyping, *Nanoscale* **8**: 9096–9101.

4. Ikemoto, H., Lingasamy, P., **Willmore, A.-M. A.**, Hunt, H., Kurm, K., Tammik, O., Scodeller, P., Simón Gracia, L., Kotamraju, V. R., Lowy, A. M., Sugahara, K. N. and Teesalu, T. [2017]. Hyaluronan-binding peptide for targeting peritoneal carcinomatosis, *Tumor biology* **39**(5).

5. Toome, K., **Willmore, A.-M. A.**, Paiste, P., Tobi, A., Sugahara, K. N., Kirsimäe, K., Ruoslahti, E., Braun, G. B. and Teesalu, T. [2017]. Ratiometric in vivo auditioning of targeted silver nanoparticles, *Nanoscale* **9**: 10094–10100.

Elulookirjeldus

Nimi: Anne-Mari Anton Willmore
Sünniaeg: 21.04.1983
Kodakondsus: Eesti, USA
Aadress: Ravila 14B, Tartu, 51014
Telefon: 737 4268
E-post: annemw@ut.ee

Haridustee

2011–...	Tartu Ülikool, Doktorant
2009–2010	M.Sc. Keemiatehnoloogias, University College London, UK
2003–2004	Georg August Universität, Göttingen, Saksamaa
2001–2006	B.S. Keemiatehnoloogias, Kalifornia Ülikool, Santa Barbara, USA

Teaduspreemiad ja tunnustused

2016	Valda ja Bernard Õuna mälestusstipendium
2014	Eesti üliõpilaste teadustööde konkurss, I preemia

Töökohad ja ametid

2012–...	Tartu Ülikool, vähibioloogia labor, laborispetsialist
2010–2012	Icosagen Cell Factory OÜ, valkude puhastamise tehnoloogia arendus, teadur
2008	Genentech Inc., valkude puhastamise tehnoloogia arendus, praktikant
2007–2008	Gilead Sciences Inc., ravimite kvaliteet, analüütik
2005	Genentech Inc., tootmis teadus ja tehnoloogia, praktikant
2004	Henkel KGaA, fosfaateerimis tehnoloogia arendus, praktikant

Publikatsioonid

1. Braun, G. B., Friman, T., Pang, H.-B., Pallaoro, A., de Mendoza, T. H., **Willmore, A.-M. A.**, Kotamraju, V. R., Mann, A. P., She, Z.-G., Sugahara, K. N., Reich, N. O., Teesalu, T. and Ruoslahti, E. [2014]. Etchable plasmonic nanoparticle probes to image and quantify cellular internalization, *Nature Materials*, **13**(9): 904–911.

2. Simón Gracia, L., Hunt, H., Scodeller, P. D., Gaitzsch, J., Braun, G. B., **Willmore, A.-M. A.**, Ruoslahti, E., Battaglia, G. and Teesalu, T. [2016]. Paclitaxel-loaded polymersomes for enhanced intraperitoneal chemotherapy, *Molecular Cancer Therapeutics* **15**(4): 670–679.

3. **Willmore, A.-M. A.**, Simón Gracia, L., Toome, K., Paiste, P., Kotamraju, V. R., Mölder, T., Sugahara, K. N., Ruoslahti, E., Braun, G. B. and Teesalu, T. [2016]. Targeted silver nanoparticles for ratiometric cell phenotyping, *Nanoscale* **8**: 9096–9101.

4. Ikemoto, H., Lingasamy, P., **Willmore, A.-M. A.**, Hunt, H., Kurm, K., Tammik, O., Scodeller, P., Simón Gracia, L., Kotamraju, V. R., Lowy, A. M., Sugahara, K. N. and Teesalu, T. [2017]. Hyaluronan-binding peptide for targeting peritoneal carcinomatosis, *Tumor biology* **39**(5).

5. Toome, K., **Willmore, A.-M. A.**, Paiste, P., Tobi, A., Sugahara, K. N., Kirsimäe, K., Ruoslahti, E., Braun, G. B. and Teesalu, T. [2017]. Ratiometric in vivo auditioning of targeted silver nanoparticles, *Nanoscale* **9**: 10094–10100.

DISSERTATIONES MEDICINAE UNIVERSITATIS TARTUENSIS

1. **Heidi-Ingrid Maaroos**. The natural course of gastric ulcer in connection with chronic gastritis and *Helicobacter pylori*. Tartu, 1991.
2. **Mihkel Zilmer**. Na-pump in normal and tumorous brain tissues: Structural, functional and tumorigenesis aspects. Tartu, 1991.
3. **Eero Vasar**. Role of cholecystokinin receptors in the regulation of behaviour and in the action of haloperidol and diazepam. Tartu, 1992.
4. **Tiina Talvik**. Hypoxic-ischaemic brain damage in neonates (clinical, biochemical and brain computed tomographical investigation). Tartu, 1992.
5. **Ants Peetsalu**. Vagotomy in duodenal ulcer disease: A study of gastric acidity, serum pepsinogen I, gastric mucosal histology and *Helicobacter pylori*. Tartu, 1992.
6. **Marika Mikelsaar**. Evaluation of the gastrointestinal microbial ecosystem in health and disease. Tartu, 1992.
7. **Hele Everaus**. Immuno-hormonal interactions in chronic lymphocytic leukaemia and multiple myeloma. Tartu, 1993.
8. **Ruth Mikelsaar**. Etiological factors of diseases in genetically consulted children and newborn screening: dissertation for the commencement of the degree of doctor of medical sciences. Tartu, 1993.
9. **Agu Tamm**. On metabolic action of intestinal microflora: clinical aspects. Tartu, 1993.
10. **Katrin Gross**. Multiple sclerosis in South-Estonia (epidemiological and computed tomographical investigations). Tartu, 1993.
11. **Oivi Uibo**. Childhood coeliac disease in Estonia: occurrence, screening, diagnosis and clinical characterization. Tartu, 1994.
12. **Viiu Tuulik**. The functional disorders of central nervous system of chemistry workers. Tartu, 1994.
13. **Margus Viigimaa**. Primary haemostasis, antiaggregative and anticoagulant treatment of acute myocardial infarction. Tartu, 1994.
14. **Rein Kolk**. Atrial versus ventricular pacing in patients with sick sinus syndrome. Tartu, 1994.
15. **Toomas Podar**. Incidence of childhood onset type 1 diabetes mellitus in Estonia. Tartu, 1994.
16. **Kiira Subi**. The laboratory surveillance of the acute respiratory viral infections in Estonia. Tartu, 1995.
17. **Irja Lutsar**. Infections of the central nervous system in children (epidemiologic, diagnostic and therapeutic aspects, long term outcome). Tartu, 1995.
18. **Aavo Lang**. The role of dopamine, 5-hydroxytryptamine, sigma and NMDA receptors in the action of antipsychotic drugs. Tartu, 1995.
19. **Andrus Arak**. Factors influencing the survival of patients after radical surgery for gastric cancer. Tartu, 1996.

20. **Tõnis Karki**. Quantitative composition of the human lactoflora and method for its examination. Tartu, 1996.
21. **Reet Mändar**. Vaginal microflora during pregnancy and its transmission to newborn. Tartu, 1996.
22. **Triin Remmel**. Primary biliary cirrhosis in Estonia: epidemiology, clinical characterization and prognostication of the course of the disease. Tartu, 1996.
23. **Toomas Kivastik**. Mechanisms of drug addiction: focus on positive reinforcing properties of morphine. Tartu, 1996.
24. **Paavo Pokk**. Stress due to sleep deprivation: focus on $GABA_A$ receptor-chloride ionophore complex. Tartu, 1996.
25. **Kristina Allikmets**. Renin system activity in essential hypertension. Associations with atherothrombogenic cardiovascular risk factors and with the efficacy of calcium antagonist treatment. Tartu, 1996.
26. **Triin Parik**. Oxidative stress in essential hypertension: Associations with metabolic disturbances and the effects of calcium antagonist treatment. Tartu, 1996.
27. **Svetlana Päi**. Factors promoting heterogeneity of the course of rheumatoid arthritis. Tartu, 1997.
28. **Maarike Sallo**. Studies on habitual physical activity and aerobic fitness in 4 to 10 years old children. Tartu, 1997.
29. **Paul Naaber**. *Clostridium difficile* infection and intestinal microbial ecology. Tartu, 1997.
30. **Rein Pähkla**. Studies in pinoline pharmacology. Tartu, 1997.
31. **Andrus Juhan Voitk**. Outpatient laparoscopic cholecystectomy. Tartu, 1997.
32. **Joel Starkopf**. Oxidative stress and ischaemia-reperfusion of the heart. Tartu, 1997.
33. **Janika Kõrv**. Incidence, case-fatality and outcome of stroke. Tartu, 1998.
34. **Ülla Linnamägi**. Changes in local cerebral blood flow and lipid peroxidation following lead exposure in experiment. Tartu, 1998.
35. **Ave Minajeva**. Sarcoplasmic reticulum function: comparison of atrial and ventricular myocardium. Tartu, 1998.
36. **Oleg Milenin**. Reconstruction of cervical part of esophagus by revascularised ileal autografts in dogs. A new complex multistage method. Tartu, 1998.
37. **Sergei Pakriev**. Prevalence of depression, harmful use of alcohol and alcohol dependence among rural population in Udmurtia. Tartu, 1998.
38. **Allen Kaasik**. Thyroid hormone control over β-adrenergic signalling system in rat atria. Tartu, 1998.
39. **Vallo Matto**. Pharmacological studies on anxiogenic and antiaggressive properties of antidepressants. Tartu, 1998.
40. **Maire Vasar**. Allergic diseases and bronchial hyperreactivity in Estonian children in relation to environmental influences. Tartu, 1998.
41. **Kaja Julge**. Humoral immune responses to allergens in early childhood. Tartu, 1998.

42. **Heli Grünberg**. The cardiovascular risk of Estonian schoolchildren. A cross-sectional study of 9-, 12- and 15-year-old children. Tartu, 1998.
43. **Epp Sepp**. Formation of intestinal microbial ecosystem in children. Tartu, 1998.
44. **Mai Ots**. Characteristics of the progression of human and experimental glomerulopathies. Tartu, 1998.
45. **Tiina Ristimäe**. Heart rate variability in patients with coronary artery disease. Tartu, 1998.
46. **Leho Kõiv**. Reaction of the sympatho-adrenal and hypothalamo-pituitary-adrenocortical system in the acute stage of head injury. Tartu, 1998.
47. **Bela Adojaan**. Immune and genetic factors of childhood onset IDDM in Estonia. An epidemiological study. Tartu, 1999.
48. **Jakov Shlik**. Psychophysiological effects of cholecystokinin in humans. Tartu, 1999.
49. **Kai Kisand**. Autoantibodies against dehydrogenases of α-ketoacids. Tartu, 1999.
50. **Toomas Marandi**. Drug treatment of depression in Estonia. Tartu, 1999.
51. **Ants Kask**. Behavioural studies on neuropeptide Y. Tartu, 1999.
52. **Ello-Rahel Karelson**. Modulation of adenylate cyclase activity in the rat hippocampus by neuropeptide galanin and its chimeric analogs. Tartu, 1999.
53. **Tanel Laisaar**. Treatment of pleural empyema — special reference to intrapleural therapy with streptokinase and surgical treatment modalities. Tartu, 1999.
54. **Eve Pihl**. Cardiovascular risk factors in middle-aged former athletes. Tartu, 1999.
55. **Katrin Õunap**. Phenylketonuria in Estonia: incidence, newborn screening, diagnosis, clinical characterization and genotype/phenotype correlation. Tartu, 1999.
56. **Siiri Kõljalg**. *Acinetobacter* – an important nosocomial pathogen. Tartu, 1999.
57. **Helle Karro**. Reproductive health and pregnancy outcome in Estonia: association with different factors. Tartu, 1999.
58. **Heili Varendi**. Behavioral effects observed in human newborns during exposure to naturally occurring odors. Tartu, 1999.
59. **Anneli Beilmann**. Epidemiology of epilepsy in children and adolescents in Estonia. Prevalence, incidence, and clinical characteristics. Tartu, 1999.
60. **Vallo Volke**. Pharmacological and biochemical studies on nitric oxide in the regulation of behaviour. Tartu, 1999.
61. **Pilvi Ilves**. Hypoxic-ischaemic encephalopathy in asphyxiated term infants. A prospective clinical, biochemical, ultrasonographical study. Tartu, 1999.
62. **Anti Kalda**. Oxygen-glucose deprivation-induced neuronal death and its pharmacological prevention in cerebellar granule cells. Tartu, 1999.
63. **Eve-Irene Lepist**. Oral peptide prodrugs – studies on stability and absorption. Tartu, 2000.

64. **Jana Kivastik**. Lung function in Estonian schoolchildren: relationship with anthropometric indices and respiratory symptomas, reference values for dynamic spirometry. Tartu, 2000.
65. **Karin Kull**. Inflammatory bowel disease: an immunogenetic study. Tartu, 2000.
66. **Kaire Innos**. Epidemiological resources in Estonia: data sources, their quality and feasibility of cohort studies. Tartu, 2000.
67. **Tamara Vorobjova**. Immune response to *Helicobacter pylori* and its association with dynamics of chronic gastritis and epithelial cell turnover in antrum and corpus. Tartu, 2001.
68. **Ruth Kalda**. Structure and outcome of family practice quality in the changing health care system of Estonia. Tartu, 2001.
69. **Annika Krüüner**. *Mycobacterium tuberculosis* – spread and drug resistance in Estonia. Tartu, 2001.
70. **Marlit Veldi**. Obstructive Sleep Apnoea: Computerized Endopharyngeal Myotonometry of the Soft Palate and Lingual Musculature. Tartu, 2001.
71. **Anneli Uusküla**. Epidemiology of sexually transmitted diseases in Estonia in 1990–2000. Tartu, 2001.
72. **Ade Kallas**. Characterization of antibodies to coagulation factor VIII. Tartu, 2002.
73. **Heidi Annuk**. Selection of medicinal plants and intestinal lactobacilli as antimicrobil components for functional foods. Tartu, 2002.
74. **Aet Lukmann**. Early rehabilitation of patients with ischaemic heart disease after surgical revascularization of the myocardium: assessment of health-related quality of life, cardiopulmonary reserve and oxidative stress. A clinical study. Tartu, 2002.
75. **Maigi Eisen**. Pathogenesis of Contact Dermatitis: participation of Oxidative Stress. A clinical – biochemical study. Tartu, 2002.
76. **Piret Hussar**. Histology of the post-traumatic bone repair in rats. Elaboration and use of a new standardized experimental model – bicortical perforation of tibia compared to internal fracture and resection osteotomy. Tartu, 2002.
77. **Tõnu Rätsep**. Aneurysmal subarachnoid haemorrhage: Noninvasive monitoring of cerebral haemodynamics. Tartu, 2002.
78. **Marju Herodes**. Quality of life of people with epilepsy in Estonia. Tartu, 2003.
79. **Katre Maasalu**. Changes in bone quality due to age and genetic disorders and their clinical expressions in Estonia. Tartu, 2003.
80. **Toomas Sillakivi**. Perforated peptic ulcer in Estonia: epidemiology, risk factors and relations with *Helicobacter pylori*. Tartu, 2003.
81. **Leena Puksa**. Late responses in motor nerve conduction studies. F and A waves in normal subjects and patients with neuropathies. Tartu, 2003.
82. **Krista Lõivukene**. *Helicobacter pylori* in gastric microbial ecology and its antimicrobial susceptibility pattern. Tartu, 2003.

83. **Helgi Kolk**. Dyspepsia and *Helicobacter pylori* infection: the diagnostic value of symptoms, treatment and follow-up of patients referred for upper gastrointestinal endoscopy by family physicians. Tartu, 2003.
84. **Helena Soomer**. Validation of identification and age estimation methods in forensic odontology. Tartu, 2003.
85. **Kersti Oselin**. Studies on the human MDR1, MRP1, and MRP2 ABC transporters: functional relevance of the genetic polymorphisms in the *MDR1* and *MRP1* gene. Tartu, 2003.
86. **Jaan Soplepmann**. Peptic ulcer haemorrhage in Estonia: epidemiology, prognostic factors, treatment and outcome. Tartu, 2003.
87. **Margot Peetsalu**. Long-term follow-up after vagotomy in duodenal ulcer disease: recurrent ulcer, changes in the function, morphology and *Helicobacter pylori* colonisation of the gastric mucosa. Tartu, 2003.
88. **Kersti Klaamas**. Humoral immune response to *Helicobacter pylori* a study of host-dependent and microbial factors. Tartu, 2003.
89. **Pille Taba**. Epidemiology of Parkinson's disease in Tartu, Estonia. Prevalence, incidence, clinical characteristics, and pharmacoepidemiology. Tartu, 2003.
90. **Alar Veraksitš**. Characterization of behavioural and biochemical phenotype of cholecystokinin-2 receptor deficient mice: changes in the function of the dopamine and endopioidergic system. Tartu, 2003.
91. **Ingrid Kalev**. CC-chemokine receptor 5 (CCR5) gene polymorphism in Estonians and in patients with Type I and Type II diabetes mellitus. Tartu, 2003.
92. **Lumme Kadaja**. Molecular approach to the regulation of mitochondrial function in oxidative muscle cells. Tartu, 2003.
93. **Aive Liigant**. Epidemiology of primary central nervous system tumours in Estonia from 1986 to 1996. Clinical characteristics, incidence, survival and prognostic factors. Tartu, 2004.
94. **Andres, Kulla**. Molecular characteristics of mesenchymal stroma in human astrocytic gliomas. Tartu, 2004.
95. **Mari Järvelaid**. Health damaging risk behaviours in adolescence. Tartu, 2004.
96. **Ülle Pechter**. Progression prevention strategies in chronic renal failure and hypertension. An experimental and clinical study. Tartu, 2004.
97. **Gunnar Tasa**. Polymorphic glutathione S-transferases – biology and role in modifying genetic susceptibility to senile cataract and primary open angle glaucoma. Tartu, 2004.
98. **Tuuli Käämbre**. Intracellular energetic unit: structural and functional aspects. Tartu, 2004.
99. **Vitali Vassiljev**. Influence of nitric oxide syntase inhibitors on the effects of ethanol after acute and chronic ethanol administration and withdrawal. Tartu, 2004.

100. **Aune Rehema**. Assessment of nonhaem ferrous iron and glutathione redox ratio as markers of pathogeneticity of oxidative stress in different clinical groups. Tartu, 2004.
101. **Evelin Seppet**. Interaction of mitochondria and ATPases in oxidative muscle cells in normal and pathological conditions. Tartu, 2004.
102. **Eduard Maron**. Serotonin function in panic disorder: from clinical experiments to brain imaging and genetics. Tartu, 2004.
103. **Marje Oona**. *Helicobacter pylori* infection in children: epidemiological and therapeutic aspects. Tartu, 2004.
104. **Kersti Kokk**. Regulation of active and passive molecular transport in the testis. Tartu, 2005.
105. **Vladimir Järv**. Cross-sectional imaging for pretreatment evaluation and follow-up of pelvic malignant tumours. Tartu, 2005.
106. **Andre Õun**. Epidemiology of adult epilepsy in Tartu, Estonia. Incidence, prevalence and medical treatment. Tartu, 2005.
107. **Piibe Muda**. Homocysteine and hypertension: associations between homocysteine and essential hypertension in treated and untreated hypertensive patients with and without coronary artery disease. Tartu, 2005.
108. **Külli Kingo**. The interleukin-10 family cytokines gene polymorphisms in plaque psoriasis. Tartu, 2005.
109. **Mati Merila**. Anatomy and clinical relevance of the glenohumeral joint capsule and ligaments. Tartu, 2005.
110. **Epp Songisepp**. Evaluation of technological and functional properties of the new probiotic *Lactobacillus fermentum* ME-3. Tartu, 2005.
111. **Tiia Ainla**. Acute myocardial infarction in Estonia: clinical characteristics, management and outcome. Tartu, 2005.
112. **Andres Sell**. Determining the minimum local anaesthetic requirements for hip replacement surgery under spinal anaesthesia – a study employing a spinal catheter. Tartu, 2005.
113. **Tiia Tamme**. Epidemiology of odontogenic tumours in Estonia. Pathogenesis and clinical behaviour of ameloblastoma. Tartu, 2005.
114. **Triine Annus**. Allergy in Estonian schoolchildren: time trends and characteristics. Tartu, 2005.
115. **Tiia Voor**. Microorganisms in infancy and development of allergy: comparison of Estonian and Swedish children. Tartu, 2005.
116. **Priit Kasenõmm**. Indicators for tonsillectomy in adults with recurrent tonsillitis – clinical, microbiological and pathomorphological investigations. Tartu, 2005.
117. **Eva Zusinaite**. Hepatitis C virus: genotype identification and interactions between viral proteases. Tartu, 2005.
118. **Piret Kõll**. Oral lactoflora in chronic periodontitis and periodontal health. Tartu, 2006.
119. **Tiina Stelmach**. Epidemiology of cerebral palsy and unfavourable neurodevelopmental outcome in child population of Tartu city and county, Estonia Prevalence, clinical features and risk factors. Tartu, 2006.

120. **Katrin Pudersell**. Tropane alkaloid production and riboflavine excretion in the field and tissue cultures of henbane (*Hyoscyamus niger* L.). Tartu, 2006.
121. **Külli Jaako**. Studies on the role of neurogenesis in brain plasticity. Tartu, 2006.
122. **Aare Märtson**. Lower limb lengthening: experimental studies of bone regeneration and long-term clinical results. Tartu, 2006.
123. **Heli Tähepõld**. Patient consultation in family medicine. Tartu, 2006.
124. **Stanislav Liskmann**. Peri-implant disease: pathogenesis, diagnosis and treatment in view of both inflammation and oxidative stress profiling. Tartu, 2006.
125. **Ruth Rudissaar**. Neuropharmacology of atypical antipsychotics and an animal model of psychosis. Tartu, 2006.
126. **Helena Andreson**. Diversity of *Helicobacter pylori* genotypes in Estonian patients with chronic inflammatory gastric diseases. Tartu, 2006.
127. **Katrin Pruus**. Mechanism of action of antidepressants: aspects of serotoninergic system and its interaction with glutamate. Tartu, 2006.
128. **Priit Põder**. Clinical and experimental investigation: relationship of ischaemia/reperfusion injury with oxidative stress in abdominal aortic aneurysm repair and in extracranial brain artery endarterectomy and possibilities of protection against ischaemia using a glutathione analogue in a rat model of global brain ischaemia. Tartu, 2006.
129. **Marika Tammaru**. Patient-reported outcome measurement in rheumatoid arthritis. Tartu, 2006.
130. **Tiia Reimand**. Down syndrome in Estonia. Tartu, 2006.
131. **Diva Eensoo**. Risk-taking in traffic and Markers of Risk-Taking Behaviour in Schoolchildren and Car Drivers. Tartu, 2007.
132. **Riina Vibo**. The third stroke registry in Tartu, Estonia from 2001 to 2003: incidence, case-fatality, risk factors and long-term outcome. Tartu, 2007.
133. **Chris Pruunsild**. Juvenile idiopathic arthritis in children in Estonia. Tartu, 2007.
134. **Eve Õiglane-Šlik**. Angelman and Prader-Willi syndromes in Estonia. Tartu, 2007.
135. **Kadri Haller**. Antibodies to follicle stimulating hormone. Significance in female infertility. Tartu, 2007.
136. **Pille Ööpik**. Management of depression in family medicine. Tartu, 2007.
137. **Jaak Kals**. Endothelial function and arterial stiffness in patients with atherosclerosis and in healthy subjects. Tartu, 2007.
138. **Priit Kampus**. Impact of inflammation, oxidative stress and age on arterial stiffness and carotid artery intima-media thickness. Tartu, 2007.
139. **Margus Punab**. Male fertility and its risk factors in Estonia. Tartu, 2007.
140. **Alar Toom**. Heterotopic ossification after total hip arthroplasty: clinical and pathogenetic investigation. Tartu, 2007.

141. **Lea Pehme**. Epidemiology of tuberculosis in Estonia 1991–2003 with special regard to extrapulmonary tuberculosis and delay in diagnosis of pulmonary tuberculosis. Tartu, 2007.
142. **Juri Karjagin**. The pharmacokinetics of metronidazole and meropenem in septic shock. Tartu, 2007.
143. **Inga Talvik**. Inflicted traumatic brain injury shaken baby syndrome in Estonia – epidemiology and outcome. Tartu, 2007.
144. **Tarvo Rajasalu**. Autoimmune diabetes: an immunological study of type 1 diabetes in humans and in a model of experimental diabetes (in RIP-B7.1 mice). Tartu, 2007.
145. **Inga Karu**. Ischaemia-reperfusion injury of the heart during coronary surgery: a clinical study investigating the effect of hyperoxia. Tartu, 2007.
146. **Peeter Padrik**. Renal cell carcinoma: Changes in natural history and treatment of metastatic disease. Tartu, 2007.
147. **Neve Vendt**. Iron deficiency and iron deficiency anaemia in infants aged 9 to 12 months in Estonia. Tartu, 2008.
148. **Lenne-Triin Heidmets**. The effects of neurotoxins on brain plasticity: focus on neural Cell Adhesion Molecule. Tartu, 2008.
149. **Paul Korrovits**. Asymptomatic inflammatory prostatitis: prevalence, etiological factors, diagnostic tools. Tartu, 2008.
150. **Annika Reintam**. Gastrointestinal failure in intensive care patients. Tartu, 2008.
151. **Kristiina Roots**. Cationic regulation of Na-pump in the normal, Alzheimer's and CCK_2 receptor-deficient brain. Tartu, 2008.
152. **Helen Puusepp**. The genetic causes of mental retardation in Estonia: fragile X syndrome and creatine transporter defect. Tartu, 2009.
153. **Kristiina Rull**. Human chorionic gonadotropin beta genes and recurrent miscarriage: expression and variation study. Tartu, 2009.
154. **Margus Eimre**. Organization of energy transfer and feedback regulation in oxidative muscle cells. Tartu, 2009.
155. **Maire Link**. Transcription factors FoxP3 and AIRE: autoantibody associations. Tartu, 2009.
156. **Kai Haldre**. Sexual health and behaviour of young women in Estonia. Tartu, 2009.
157. **Kaur Liivak**. Classical form of congenital adrenal hyperplasia due to 21-hydroxylase deficiency in Estonia: incidence, genotype and phenotype with special attention to short-term growth and 24-hour blood pressure. Tartu, 2009.
158. **Kersti Ehrlich**. Antioxidative glutathione analogues (UPF peptides) – molecular design, structure-activity relationships and testing the protective properties. Tartu, 2009.
159. **Anneli Rätsep**. Type 2 diabetes care in family medicine. Tartu, 2009.
160. **Silver Türk**. Etiopathogenetic aspects of chronic prostatitis: role of mycoplasmas, coryneform bacteria and oxidative stress. Tartu, 2009.

161. **Kaire Heilman**. Risk markers for cardiovascular disease and low bone mineral density in children with type 1 diabetes. Tartu, 2009.
162. **Kristi Rüütel**. HIV-epidemic in Estonia: injecting drug use and quality of life of people living with HIV. Tartu, 2009.
163. **Triin Eller**. Immune markers in major depression and in antidepressive treatment. Tartu, 2009.
164. **Siim Suutre**. The role of TGF-β isoforms and osteoprogenitor cells in the pathogenesis of heterotopic ossification. An experimental and clinical study of hip arthroplasty. Tartu, 2010.
165. **Kai Kliiman**. Highly drug-resistant tuberculosis in Estonia: Risk factors and predictors of poor treatment outcome. Tartu, 2010.
166. **Inga Villa**. Cardiovascular health-related nutrition, physical activity and fitness in Estonia. Tartu, 2010.
167. **Tõnis Org**. Molecular function of the first PHD finger domain of Autoimmune Regulator protein. Tartu, 2010.
168. **Tuuli Metsvaht**. Optimal antibacterial therapy of neonates at risk of early onset sepsis. Tartu, 2010.
169. **Jaanus Kahu**. Kidney transplantation: Studies on donor risk factors and mycophenolate mofetil. Tartu, 2010.
170. **Koit Reimand**. Autoimmunity in reproductive failure: A study on associated autoantibodies and autoantigens. Tartu, 2010.
171. **Mart Kull**. Impact of vitamin D and hypolactasia on bone mineral density: a population based study in Estonia. Tartu, 2010.
172. **Rael Laugesaar**. Stroke in children – epidemiology and risk factors. Tartu, 2010.
173. **Mark Braschinsky**. Epidemiology and quality of life issues of hereditary spastic paraplegia in Estonia and implemention of genetic analysis in everyday neurologic practice. Tartu, 2010.
174. **Kadri Suija**. Major depression in family medicine: associated factors, recurrence and possible intervention. Tartu, 2010.
175. **Jarno Habicht**. Health care utilisation in Estonia: socioeconomic determinants and financial burden of out-of-pocket payments. Tartu, 2010.
176. **Kristi Abram**. The prevalence and risk factors of rosacea. Subjective disease perception of rosacea patients. Tartu, 2010.
177. **Malle Kuum**. Mitochondrial and endoplasmic reticulum cation fluxes: Novel roles in cellular physiology. Tartu, 2010.
178. **Rita Teek**. The genetic causes of early onset hearing loss in Estonian children. Tartu, 2010.
179. **Daisy Volmer**. The development of community pharmacy services in Estonia – public and professional perceptions 1993–2006. Tartu, 2010.
180. **Jelena Lissitsina**. Cytogenetic causes in male infertility. Tartu, 2011.
181. **Delia Lepik**. Comparison of gunshot injuries caused from Tokarev, Makarov and Glock 19 pistols at different firing distances. Tartu, 2011.
182. **Ene-Renate Pähkla**. Factors related to the efficiency of treatment of advanced periodontitis. Tartu, 2011.

183. **Maarja Krass**. L-Arginine pathways and antidepressant action. Tartu, 2011.
184. **Taavi Lai**. Population health measures to support evidence-based health policy in Estonia. Tartu, 2011.
185. **Tiit Salum**. Similarity and difference of temperature-dependence of the brain sodium pump in normal, different neuropathological, and aberrant conditions and its possible reasons. Tartu, 2011.
186. **Tõnu Vooder**. Molecular differences and similarities between histological subtypes of non-small cell lung cancer. Tartu, 2011.
187. **Jelena Štšepetova**. The characterisation of intestinal lactic acid bacteria using bacteriological, biochemical and molecular approaches. Tartu, 2011.
188. **Radko Avi**. Natural polymorphisms and transmitted drug resistance in Estonian HIV-1 CRF06_cpx and its recombinant viruses. Tartu, 2011, 116 p.
189. **Edward Laane**. Multiparameter flow cytometry in haematological malignancies. Tartu, 2011, 152 p.
190. **Triin Jagomägi**. A study of the genetic etiology of nonsyndromic cleft lip and palate. Tartu, 2011, 158 p.
191. **Ivo Laidmäe**. Fibrin glue of fish (*Salmo salar*) origin: immunological study and development of new pharmaceutical preparation. Tartu, 2012, 150 p.
192. **Ülle Parm**. Early mucosal colonisation and its role in prediction of invasive infection in neonates at risk of early onset sepsis. Tartu, 2012, 168 p.
193. **Kaupo Teesalu**. Autoantibodies against desmin and transglutaminase 2 in celiac disease: diagnostic and functional significance. Tartu, 2012, 142 p.
194. **Maksim Zagura**. Biochemical, functional and structural profiling of arterial damage in atherosclerosis. Tartu, 2012, 162 p.
195. **Vivian Kont**. Autoimmune regulator: characterization of thymic gene regulation and promoter methylation. Tartu, 2012, 134 p.
196. **Pirje Hütt**. Functional properties, persistence, safety and efficacy of potential probiotic lactobacilli. Tartu, 2012, 246 p.
197. **Innar Tõru**. Serotonergic modulation of CCK-4- induced panic. Tartu, 2012, 132 p.
198. **Sigrid Vorobjov**. Drug use, related risk behaviour and harm reduction interventions utilization among injecting drug users in Estonia: implications for drug policy. Tartu, 2012, 120 p.
199. **Martin Serg**. Therapeutic aspects of central haemodynamics, arterial stiffness and oxidative stress in hypertension. Tartu, 2012, 156 p.
200. **Jaanika Kumm**. Molecular markers of articular tissues in early knee osteoarthritis: a population-based longitudinal study in middle-aged subjects. Tartu, 2012, 159 p.
201. **Kertu Rünkorg**. Functional changes of dopamine, endopioid and endocannabinoid systems in CCK2 receptor deficient mice. Tartu, 2012, 125 p.
202. **Mai Blöndal**. Changes in the baseline characteristics, management and outcomes of acute myocardial infarction in Estonia. Tartu, 2012, 127 p.

203. **Jana Lass**. Epidemiological and clinical aspects of medicines use in children in Estonia. Tartu, 2012, 170 p.
204. **Kai Truusalu**. Probiotic lactobacilli in experimental persistent *Salmonella* infection. Tartu, 2013, 139 p.
205. **Oksana Jagur**. Temporomandibular joint diagnostic imaging in relation to pain and bone characteristics. Long-term results of arthroscopic treatment. Tartu, 2013, 126 p.
206. **Katrin Sikk**. Manganese-ephedrone intoxication – pathogenesis of neurological damage and clinical symptomatology. Tartu, 2013, 125 p.
207. **Kai Blöndal**. Tuberculosis in Estonia with special emphasis on drug-resistant tuberculosis: Notification rate, disease recurrence and mortality. Tartu, 2013, 151 p.
208. **Marju Puurand**. Oxidative phosphorylation in different diseases of gastric mucosa. Tartu, 2013, 123 p.
209. **Aili Tagoma**. Immune activation in female infertility: Significance of autoantibodies and inflammatory mediators. Tartu, 2013, 135 p.
210. **Liis Sabre**. Epidemiology of traumatic spinal cord injury in Estonia. Brain activation in the acute phase of traumatic spinal cord injury. Tartu, 2013, 135 p.
211. **Merit Lamp**. Genetic susceptibility factors in endometriosis. Tartu, 2013, 125 p.
212. **Erik Salum**. Beneficial effects of vitamin D and angiotensin II receptor blocker on arterial damage. Tartu, 2013, 167 p.
213. **Maire Karelson**. Vitiligo: clinical aspects, quality of life and the role of melanocortin system in pathogenesis. Tartu, 2013, 153 p.
214. **Kuldar Kaljurand**. Prevalence of exfoliation syndrome in Estonia and its clinical significance. Tartu, 2013, 113 p.
215. **Raido Paasma**. Clinical study of methanol poisoning: handling large outbreaks, treatment with antidotes, and long-term outcomes. Tartu, 2013, 96 p.
216. **Anne Kleinberg**. Major depression in Estonia: prevalence, associated factors, and use of health services. Tartu, 2013, 129 p.
217. **Triin Eglit**. Obesity, impaired glucose regulation, metabolic syndrome and their associations with high-molecular-weight adiponectin levels. Tartu, 2014, 115 p.
218. **Kristo Ausmees**. Reproductive function in middle-aged males: Associations with prostate, lifestyle and couple infertility status. Tartu, 2014, 125 p.
219. **Kristi Huik**. The influence of host genetic factors on the susceptibility to HIV and HCV infections among intravenous drug users. Tartu, 2014, 144 p.
220. **Liina Tserel**. Epigenetic profiles of monocytes, monocyte-derived macrophages and dendritic cells. Tartu, 2014, 143 p.
221. **Irina Kerna**. The contribution of *ADAM12* and *CILP* genes to the development of knee osteoarthritis. Tartu, 2014, 152 p.

222. **Ingrid Liiv**. Autoimmune regulator protein interaction with DNA-dependent protein kinase and its role in apoptosis. Tartu, 2014, 143 p.
223. **Liivi Maddison**. Tissue perfusion and metabolism during intra-abdominal hypertension. Tartu, 2014, 103 p.
224. **Krista Ress**. Childhood coeliac disease in Estonia, prevalence in atopic dermatitis and immunological characterisation of coexistence. Tartu, 2014, 124 p.
225. **Kai Muru**. Prenatal screening strategies, long-term outcome of children with marked changes in maternal screening tests and the most common syndromic heart anomalies in Estonia. Tartu, 2014, 189 p.
226. **Kaja Rahu**. Morbidity and mortality among Baltic Chernobyl cleanup workers: a register-based cohort study. Tartu, 2014, 155 p.
227. **Klari Noormets**. The development of diabetes mellitus, fertility and energy metabolism disturbances in a Wfs1-deficient mouse model of Wolfram syndrome. Tartu, 2014, 132 p.
228. **Liis Toome**. Very low gestational age infants in Estonia. Tartu, 2014, 183 p.
229. **Ceith Nikkolo**. Impact of different mesh parameters on chronic pain and foreign body feeling after open inguinal hernia repair. Tartu, 2014, 132 p.
230. **Vadim Brjalin**. Chronic hepatitis C: predictors of treatment response in Estonian patients. Tartu, 2014, 122 p.
231. **Vahur Metsna**. Anterior knee pain in patients following total knee arthroplasty: the prevalence, correlation with patellar cartilage impairment and aspects of patellofemoral congruence. Tartu, 2014, 130 p.
232. **Marju Kase**. Glioblastoma multiforme: possibilities to improve treatment efficacy. Tartu, 2015, 137 p.
233. **Riina Runnel**. Oral health among elementary school children and the effects of polyol candies on the prevention of dental caries. Tartu, 2015, 112 p.
234. **Made Laanpere**. Factors influencing women's sexual health and reproductive choices in Estonia. Tartu, 2015, 176 p.
235. **Andres Lust**. Water mediated solid state transformations of a polymorphic drug – effect on pharmaceutical product performance. Tartu, 2015, 134 p.
236. **Anna Klugman**. Functionality related characterization of pretreated wood lignin, cellulose and polyvinylpyrrolidone for pharmaceutical applications. Tartu, 2015, 156 p.
237. **Triin Laisk-Podar**. Genetic variation as a modulator of susceptibility to female infertility and a source for potential biomarkers. Tartu, 2015, 155 p.
238. **Mailis Tõnisson**. Clinical picture and biochemical changes in blood in children with acute alcohol intoxication. Tartu, 2015, 100 p.
239. **Kadri Tamme**. High volume haemodiafiltration in treatment of severe sepsis – impact on pharmacokinetics of antibiotics and inflammatory response. Tartu, 2015, 133 p.

240. **Kai Part**. Sexual health of young people in Estonia in a social context: the role of school-based sexuality education and youth-friendly counseling services. Tartu, 2015, 203 p.
241. **Urve Paaver**. New perspectives for the amorphization and physical stabilization of poorly water-soluble drugs and understanding their dissolution behavior. Tartu, 2015, 139 p.
242. **Aleksandr Peet**. Intrauterine and postnatal growth in children with HLA-conferred susceptibility to type 1 diabetes. Tartu. 2015, 146 p.
243. **Piret Mitt**. Healthcare-associated infections in Estonia – epidemiology and surveillance of bloodstream and surgical site infections. Tartu, 2015, 145 p.
244. **Merli Saare**. Molecular Profiling of Endometriotic Lesions and Endometria of Endometriosis Patients. Tartu, 2016, 129 p.
245. **Kaja-Triin Laisaar**. People living with HIV in Estonia: Engagement in medical care and methods of increasing adherence to antiretroviral therapy and safe sexual behavior. Tartu, 2016, 132 p.
246. **Eero Merilind**. Primary health care performance: impact of payment and practice-based characteristics. Tartu, 2016, 120 p.
247. **Jaanika Kärner**. Cytokine-specific autoantibodies in AIRE deficiency. Tartu, 2016, 182 p.
248. **Kaido Paapstel**. Metabolomic profile of arterial stiffness and early biomarkers of renal damage in atherosclerosis. Tartu, 2016, 173 p.
249. **Liidia Kiisk.** Long-term nutritional study: anthropometrical and clinico-laboratory assessments in renal replacement therapy patients after intensive nutritional counselling. Tartu, 2016, 207 p.
250. **Georgi Nellis**. The use of excipients in medicines administered to neonates in Europe. Tartu, 2017, 159 p.
251. **Aleksei Rakitin**. Metabolic effects of acute and chronic treatment with valproic acid in people with epilepsy. Tartu, 2017, 125 p.
252. **Eveli Kallas**. The influence of immunological markers to susceptibility to HIV, HBV, and HCV infections among persons who inject drugs. Tartu, 2017, 138 p.
253. **Tiina Freimann.** Musculoskeletal pain among nurses: prevalence, risk factors, and intervention. Tartu, 2017, 125 p.
254. **Evelyn Aaviksoo.** Sickness absence in Estonia: determinants and influence of the sick-pay cut reform. Tartu, 2017, 121 p.
255. **Kalev Nõupuu.** Autosomal-recessive Stargardt disease: phenotypic heterogeneity and genotype-phenotype associations. Tartu, 2017, 131 p.
256. **Ho Duy Binh.** Osteogenesis imperfecta in Vietnam. Tartu, 2017, 125 p.
257. **Uku Haljasorg.** Transcriptional mechanisms in thymic central tolerance. Tartu, 2017, 147 p.
258. **Živile Riispere.** IgA Nephropathy study according to the Oxford Classification: IgA Nephropathy clinical-morphological correlations, disease progression and the effect of renoprotective therapy. Tartu, 2017, 129 p.

259. **Hiie Soeorg**. Coagulase-negative staphylococci in gut of preterm neonates and in breast milk of their mothers. Tartu, 2017, 216 p.